Modeling strategies for multiple scenarios and fast simulations in large systems: applications to fire safety and energy engineering

GUELPA ELISA

TUTORS:
VITTORIO VERDA
ADRIANO SCIACOVELLI
ROMANO BORCHIELLINI

Thesis submitted for the degree of Doctor of Philosophy
Politecnico di Torino, Energy Department.
May 2016

TABLE OF CONTENT

1

Introduction

1.1 Introduction

The use of computational modeling has become very popular and important in many engineering and physical fields, as it is considered a fast and inexpensive technique to support and often substitute experimental analysis. In fact system design and analysis can be carried out through computational studies instead of experiments, that are typically demanding in terms of cost and technical resources; sometimes the systems characteristics and the technical problems make the experiments impossible to perform and the use of computational tools is the only feasible option.
Demand of resources for realistic simulation is increasing due to the interest in studying complex and large systems. Many systems with these characteristics, involving different phenomena, are modeled and studied through computational tools. It is possible for example to think to the weather forecast, the prediction of wave surge in areas below the sea levels (Figure 1.1b) (Verlaan 1998; Booij *et al* 1999), the crowd dynamic simulation for the achievement of effective evacuation strategies (Figure 1.1a) (Helbing *et al* 2002 ; Schadschneider *et al* 2009), and air quality model aimed at evaluating the pollutant concentration in the atmosphere when a specific scenario takes place (Figure 1.1c) (Horowitz *et al*. 2003, Seaman 2000). All these examples show that sometimes systems involving large spaces have to be studied with a sufficient level of detail,

trough the use of simulation. Clearly to perform these kinds of studies large computational resources are required. Not only large systems model require high computational cost, but also small domain systems that require an high level of detail. Molecular dynamics studies for the analysis of proteins (Figure 1.1d) (Romo *et al* 1995) and the design of LCI circuits for processor unit (Antoulas 2005) are some examples.

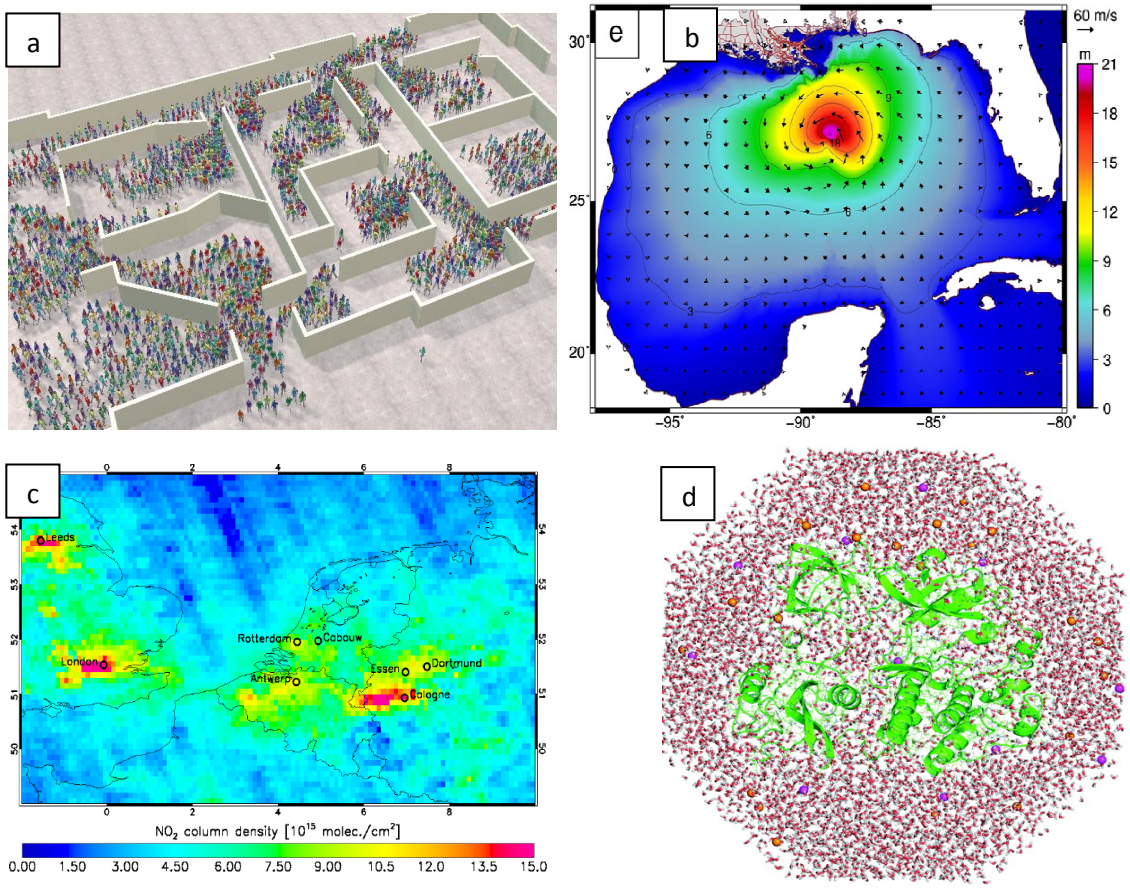

Figure 1.1. Examples of complex systems modeling.
a) Crowd dynamic Analysis (Narain et al 2009) b) Waves surge Prediction (Dietrich et al 2011), c) Air Quality Analysis (Piters et al. 2012) d) Molecular dynamics studies (Karplus and Kuriyan 2005)

In these framework smart modeling approaches and model reduction techniques play a crucial role for making complex and large system suitable for simulations. Moreover, it should be considered that often more than one simulation is requested in order to perform an analysis. For instance, if a heuristic method is applied to the optimization of a component, the model has to be run a certain number of times. The same problem arises when a certain level of uncertainty affect the system parameters; in this case also many simulation are required for obtaining the desired information. This is the reason why the use of technique that allows to obtain compact model is an interesting topic nowadays. Many of the system previously reported, by way of example, are

modeled using approaches or reduction techniques able to simplify the used model in order to reduce the needed computational resources. In this thesis, three large systems involving heat transfer are modeled and reduced in order to obtain fast tools for operational purpose.

1.2 Compact model achievement

By technique for compact model achievement it is intended a problem resolution method which consists in simplifying the full initial model with the goal of performing simulations within an acceptable amount of time and limited computational resources, but with reliable results (Schilders 2008). This allows to facilitate or enable simulations for design, control and optimization of the physical systems modeled (Benner, Faßbender 2015). The most common techniques to obtain compact model can be, in the author opinion, gathered in the following three groups: 1) the approaches for model simplification and multi-level approach, 2) the model approximation techniques and 3) the physical model reduction techniques (Figure 1.2).

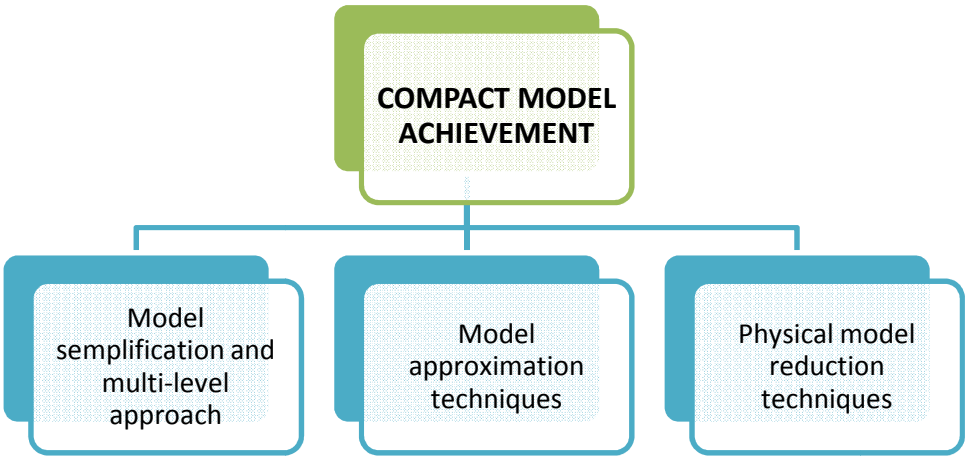

Figure 1.2. Compact model achievement techniques

The simplest reduction approach to avoid high computational complexity consists in choosing the sufficient level of detail that is necessary for the analysis of a particular system, or to chose different levels of detail for analyzing the different parts of the studied system. Often, when a system is modeled trough the governing equations expressing the physical phenomena, some of the aspects are negligible in terms of effects on the main results which are of interest. Therefore, it is often possible to simplify the model excluding some contributions that do not actually affect the results. This approach can be applied to the entire system or only in some parts of it. In the first case a simplification of the overall system is performed, in the second case, a multi-level or multi-scale approach is obtained. The multi-level modeling approach analyzes the different parts of the system with different levels of detail. An interesting example is that of simulating what

happens in a tunnel where a fire takes place, as reported in Colella *et al* 2011 (Figure 1.3a). In the part in the vicinity of operating jet fans or close to the fire source the flow field has a complex 3D behaviour with large transversal and longitudinal temperature and velocity differences. In these areas a 3D-model has been used. Contrarily at high distances from these regions, temperature and velocity gradients become smaller and therefore the flow behaviour can be analyzed trough a 1D model. Clearly the main advantages of these kind of approach is mainly related to the considerable reduction of computational time compared to the use of a 3D model for the entire system. Another example (Quarteroni *et al* 2003) regards the simulation of the blood flow (Figure 1.3b). In this work a full 3D model description of blood flow through Navier– Stokes equations is used in a particular area of an arterial. The other parts of the circulation system are analyzed trough a 1D model. The full 3D model and the 1D model are coupled with the aim of obtaining a multi-level model. Results of these studies show that it may not be necessary to calculate all details for obtaining an accurate simulation of the considered phenomena.

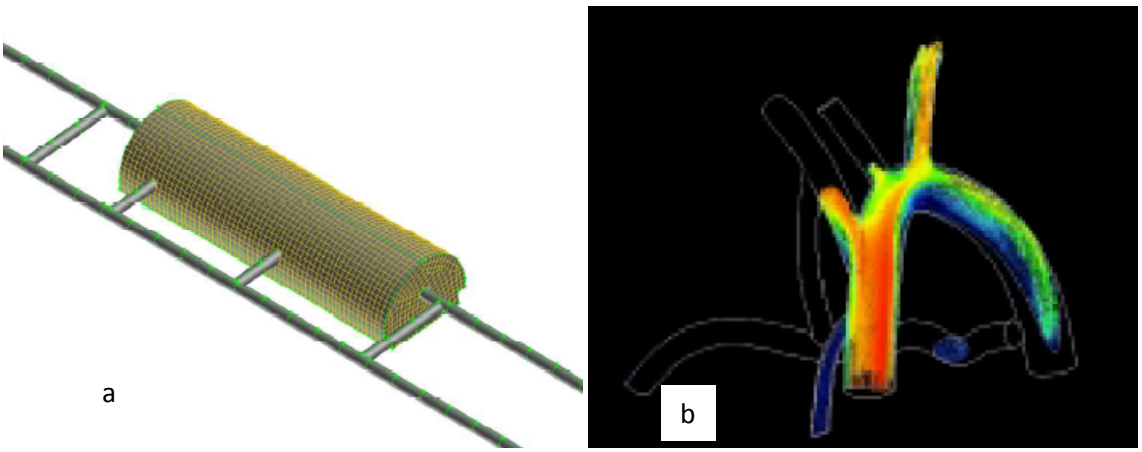

Figure 1.3. Multi-level approach applied to: a) tunnel ventilation (Colella et al 2011)
b) blood circulation (Quarteroni and Veneziani et al 2003)

Another approach to obtain fast simulations consists in using compact models obtained through functions able to approximate the system behaviour. In this case a series of experimental data or full model results can be used in order to build the compact model. As an example neural networks are a modeling tool able to estimate or approximate functions; it has been used in different fields, such as system control (Irwin *et al* 1995), geotechnical engineering (Shahin *et al* 2001), medical imaging (Miller and Blott 1992), business analysis (Wong *et al* 1997).
A very effective method for fast fitting is the use Radial Basis Functions (RBFs). RBFs are not used only for data fitting, as for mappings of two- or three-dimensional images (Figure 1.4) (Arad T AL 1994) and for fire detection (Angayarkkani and Radhakrishnan 2010) but also to for the local reconstruction of solutions of algorithms which solve numerically the conservation laws (Iske and Sonar 1996, Pollandt 1997).

Figure 1.4.Interpolation approach:RBF for image detection and reduction (Samozino et al 2006)

Another opportunity consists in using some mathematical techniques for capturing the main features of the analyzed system. The modeling of physical dynamical systems usually leads to a set of partial differential equations (PDEs) or ordinary differential equations (ODEs). However after the discretization it is common to obtain a set of ODEs and algebraic equations. In this case, model reduction approach consists in finding a smaller set of ODEs that is able to well describe the system evolution. The two main families of such model reduction techniques are the Krylov methods and SVD related methods. Krylov methods are mainly used in applications such as the electronic circuits, when the system complexity becomes really high (Antoulas 2005). Instead, SVD methods are characterized by several features that make them suitable to be used in the area of computational fluid-dynamic (Schilders 2008).Among these features, it is worth reporting the fact that these methods are able to preserve model stability; in addition some of them can be also applied to non-linear models.

A very effective SVD method that can be used for both linear and non-linear system reduction is Proper Orthogonal Decomposition (POD). The possibility of using POD for studying non-linear partial differential equations is a very powerful option. This method is the most common in the area of computational fluid-dynamic.

In the Chapter 2 an accurate description of the POD technique is provided. In Figure 1.5 the use of POD technique for evaluating the main problem eigenfunctions is applied to reactors physics (Buchan *et al*. 2013).

Further developments of the POD have been obtained through proper generalized decomposition (PGD), a technique that allows one to compute a priori, by means of successive enrichment, a representation of the unknown field (Chinesta *et al* 2011). In PGD the obtained model is solved once for life, in order to obtain a general solution including the solution for all the possible parameter values (Chinesta, *et al* 2013).

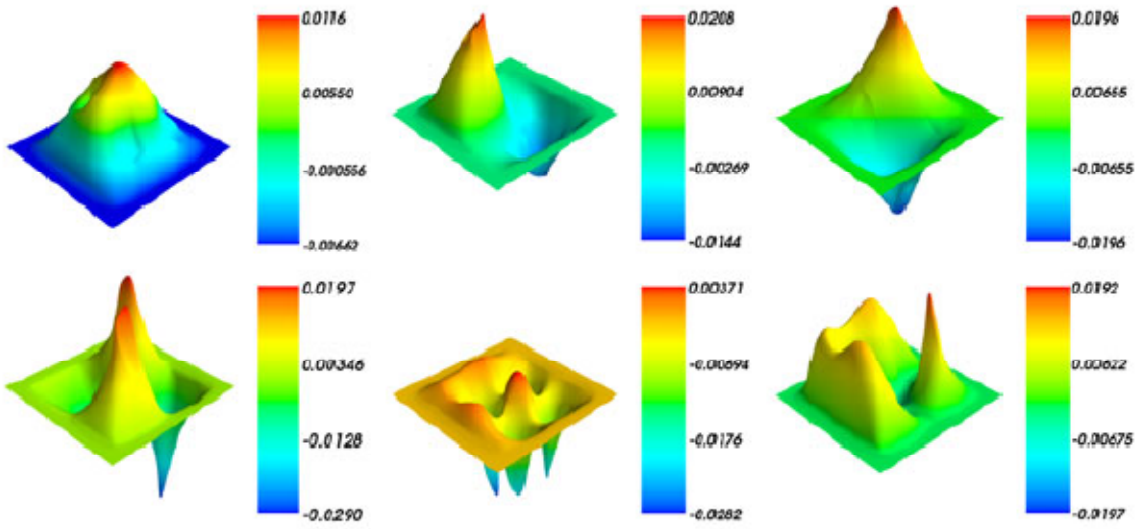

Figure 1.5. Model reduction technique: POD eigenfunctions of a reactor analysis (Buchan et al. 2013)

In this work the different reduction approaches and strategies have been used in order to analyze three energetic systems involving large domain and long time, one for each reduction approach categories.

- The first topic analyzed is the analysis of groundwater temperature perturbations due to geothermal heat pump installations.
- The second system analyzed is the district heating network (DHN), studied from both the fluid-dynamic and thermal point of view and applied to the Turin district heating system (DHS)
- The third topic is included in the fire safety field and it is the wildfire propagation simulation.

In all the topic considered, a smart model has been adopted and, when data were available, tested using experimental data. All the model are characterized by large domain and the time involved in the analysis are high in all the cases, therefore a method for compact model achievement is used in all the cases. In the next paragraphs the developed tools are presented and then they are analyzed in details in the next Chapters.

1.3 Applications

For each of the systems analyzed a suitable method for speeding up the model is selected.

- As regards the ***groundwater application*** the system can be easily considered as made up of two parts: the first part is the area near the wells where the temperature gradients are

larger and fluid flow occurs with three dimensional features; the second part is composed by the areas far from the wells, where the occurring gradients are smaller. Therefore a multi-level approach is used for the model computational cost reduction.

- As regards the ***DHS modeling***, the aim is at first obtaining a physical model to be applied generically to the network and secondly to produce a fast tool for the operational optimization of the Turin DHN. Interpolation method is a good option due to the fact that tool has to be applied always to the same network and it has to be sufficiently fast.
- As regard the ***wildfire system,*** the aim is to carry out a physical model to be used for different landscape propagations, in different situations, like different meteorological conditions, fuel type, orography, landscape dimension, etc. In order to take in account all these characteristics and the possibility of using fire retardants and extinguishing substances a physical model has been used. The model should be fast even if the phenomenon taking place in the system are very complex, and it has to run many times for take into account the parameters uncertainty. A multi-level model by itself it is not-sufficient in order to reduce the computational cost due to the high complexity of the system where the combustion takes place; furthermore the use of interpolation approaches is less robust then a physical model reduction and it could interfere with the possibility to use the model in different landscape. In order to solve this problem, a physical model reduction technique is the natural choice for the current system.

1.3.1 Groundwater analysis

Geothermal heat pump is a technology that is expected to play a major role in future energy scenarios. In the case of groundwater flow, open loop heat pumps can be applied. Their main advantage is the very high efficiency that can be reached through the use of groundwater which is typically at a temperatures of 15 °C. On the other hand, the proliferation of such systems in urban areas may generate problems related to environmental impact on water basins and interactions between the various installations. Both these issues are associated with the thermal plume produced by the heat pump during operation. This effect is particularly evident in the case of open loop systems, because of the large advective heat transfer. The impact of an installation has to be calculated through thermo-fluid dynamic models of the subsurface. The groundwater area affected to the thermal plume is very wide. The simulation domain has therefore to be large enough to include all the involved groundwater area, especially downstream the various heat pump installations that are analyzed. Furthermore an unsteady model has to be used because of the changes in heat pump operating conditions during the different seasons considered. In fact the groundwater velocity is very low (about 10^{-4} m/s) and therefore a very long time should be considered to obtain complete information on the groundwater thermal plume. These are the

reasons why a full 3D model may become too time consuming for achieving results in a reasonable wait.

In this work, due to the potential large extension of the area which can be affected and the long time period to be simulated, a multi-level approach, combining CFD 3D and a 1D models, is proposed. This model is coupled with the thermal request of the users and the heat pump performances through appropriate boundary conditions imposed at the wells. Various scenarios corresponding to different operating modes of the heat pump are considered. This part of the work is described in the Chapter 3 of the thesis.

1.3.2 District heating system applications

District heating (DH) is considered a very efficient option for providing heating and domestic hot water to buildings, particularly when they are located in densely populated areas (Lund *et al*. 2010). The main advantage of DH systems consists in the possibility of utilizing the waste heat from industries or waste-to-energy plants or the heat generated by a number of efficient/low carbon thermal plants, such as cogeneration plants, and biomass (Roos *et al*. 2003) , solar (Lindenberger *et al* 2000) and geothermal (Østergaard *et al* 2010) systems.

An important aspect to achieve high efficiency in DH is the optimization of the operating conditions that the system has to face in order to comply with the household thermal request. In the literature, various works deal with the analysis of supply temperature during daily (Benonysson *et al* 1995) and seasonal operations (Pirouti *et al* 2012) or with the selection of the optimal supply and return temperatures (Laajalehto *et al*. 2014). In (Gustafsson *et al* 2010) a control approach is proposed in order to increase the temperature difference across the substations with a consequent increase of overall performances. In (Jiang *et al*. 2014), the operating conditions of a district heating system are optimized acting both on the set-point temperature of the boilers and on the water flow of the pumps; the total fuel consumption is considered as the objective function to be minimized. In (Verda and Baccino 2014) and (Jokinen *et al* 2014) the opportunities to modify the thermal request profile of some users are investigated to maximize the heat production from cogeneration or renewable plants.

In order to improve the network performances and select optimal operations and management (Aringhieri and Malucelli 2003), network analysis in different working conditions are important subjects. This necessity is related to technical, economical and environmental reasons. In particular, investigation on systems responses to configuration variations or user request variation, aiming at achieving primary energy reduction, can be achieved using models and simulation tools. This is the reason why DHS modeling have been applied in both design (Ancona *et al*. 2014) and management stages (Bojic and Trifunovic 2000). An important detail that DH system model aiming at real time operations have to posses is the rapidity. In fact if a model is used for

obtaining information on the best operation in a particular operating condition (of malfunctioning or not), results have to be provided as quickly as possible. Low computational cost becomes more important when the DHN analyzed involve large spaces. In this case, the use of strategies for obtaining fast models is crucial.

In this work the minimization of the primary energy consumption in a DHN is pursued analyzing two different aspects (Figure 1.6). In the first part of the DHS analysis the pumping cost connected with the water distribution along the network is minimized selecting the optimal operating strategy. The second part is instead connected to the minimization of the morning thermal peak, since peak reduction allows a better exploitation of the cogenerating systems.

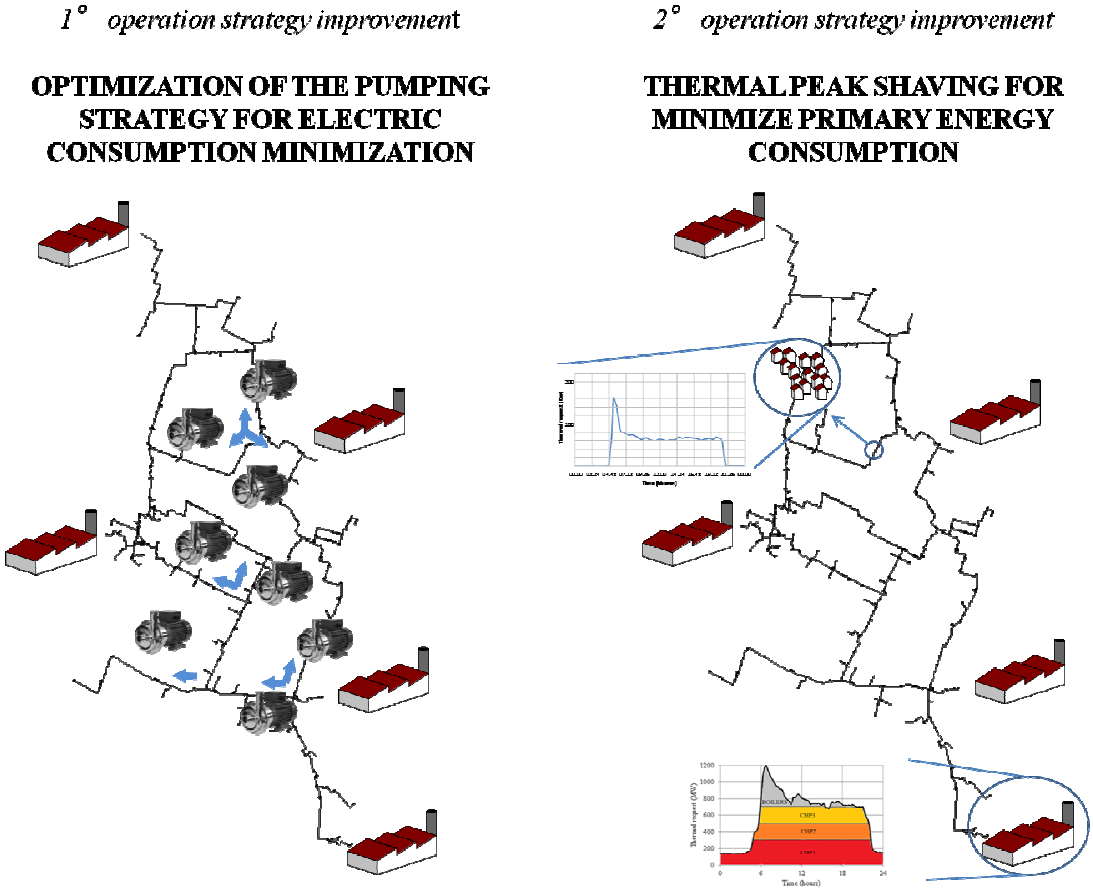

Figure 1.6. DHS operation strategy improvement analysis

1.3.2.1 District heating system modeling for pumping cost minimization

In DHSs the energy consumption for pumping operation is not negligible because of the significant pressure drops that may be registered and the large number of operating hours. This is particularly important for large extension networks and for network operating with small

temperatures. Modeling and simulation of DHS pumping system is of a great importance for implementing operational improvements. The aim of this part of the work is to find the set of pumping pressures that should be applied to the pumps located along the network in order to minimize the total electricity consumption for a given operating scenario. In order to perform the minimization a physical model has to be used in order to evaluate mass flow rates and pressures along the network. Simulation and optimization of DHNs may involve large computational resources, particularly in the case of large DHNs and when the number of scenarios to be examined is high. This is the reason why optimization is carried out through two different model approaches. The first model is a fluid-dynamic model based on mass and momentum conservation equations which considers the network topology through a graph approach. The second method is a reduced model, which has been derived from the fluid-dynamic model. Model reduction is obtained through the combination of proper orthogonal decomposition (POD) and radial basis functions (RBF). Both the full physical model and the POD-RBF model are used in order to find the optimal set of pumping pressures that minimizes the mechanical power that should be applied to the working fluid (i.e. the efficiency of the pump and the efficiency in the overall energy supply chain from primary energy to electricity production have not been considered) to fulfill the thermal requests of the various users, once the heat production of each plant is fixed. In the following, this objective function has been indicated as pumping cost, which should be intended as a cost expressed in energy units. An analysis with different thermal loads has been performed because of the peculiar characteristics of district heating networks which operate for a large number of operating hours in off-design conditions because of request variations, possible malfunctions, etc. Therefore a careful analysis of optimal operating conditions is necessary to achieve high levels of the annual efficiency. The heat flow supplied by each thermal plant is provided as an input of the model by setting the water mass flow rates exiting the various plants. The optimization of the pumping strategy is deeply analyzed in Chapter 4.

1.3.2.2 District heating system modeling for thermal peak shaving

The large amount of thermal power required to the DHS between 5 am and 7 am leads an high quantity of heat produced through boilers. In fact only a fraction of the thermal peak request is supplied using cogeneration groups with a consequent decrease of the overall system performances. In order to reduce this problem, different managements changes can be considered. Two of possible options are the installation of storage systems and the variation of user behavioral constraints in order to obtain a more flat thermal load profile. The analysis of the effects produced by the systems and the operation changes can be studied through proper network modeling. With this aim, a method for solving both thermal and hydraulic DHN problems for the analysis of large district heating systems (also involving loops) is presented. The model capability to reproduce network behavior is tested through some experimental data collected in the Turin district heating

system. This is the largest network in Italy as it connects more than 5000 buildings and large users. The model predicts the evolution of heat power required during the daily transient. Results are compared with real data. The model is reduced in order to obtain a faster tool for the operations managements and then it is applied for analyzing possible techniques intended for shaving morning peak, with the aim of reducing primary energy consumption. Details about the thermal peak shaving analysis are presented in Chapter 5.

1.3.3 Wildfire fast modeling applications

Wildfire propagation models have been widely applied to the prediction of fire front evolution, in order to obtain useful information for evacuation plans and fire management. A major difficulty in treating wildland fires is related to the complexity of the phenomena that are involved. In addition, it is difficult to obtain accurate input data for the models, especially in the case of on-going fire events. Results obtained from models are therefore affected by errors.

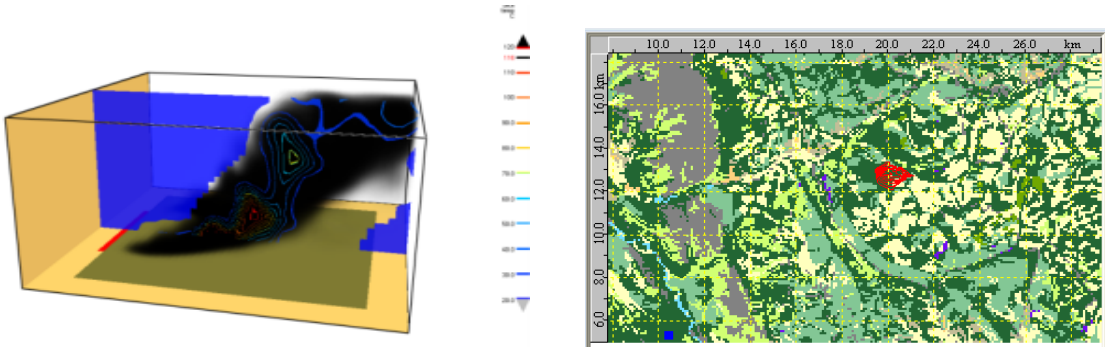

Figure 1.7. Wildfire propagation prediction models
a) Physical model (WFDS, Mell at al. *2007)*
b) Empirical model (Behave, Burgan and Rothermel 1984),

Over the last decades, empirical and physical based models have been proposed (Figure 1.7). Physical models of wildfires are of particular interest in fire behaviour research as well as for applications to firefighting, rescue and evacuation. They are able to provide information and details about the fire propagation which can be used for fire safety management. Furthermore, physical models allow one to analyze possible approaches for fire extinction or for fire propagation delaying. Nevertheless, physical models present a drawback related to the large computational resources that are often necessary, with respect to empirical models. The latter models treat the interaction between the physical phenomena in a oversimplified manner but very fast.

The computational time requested by fire propagation models computational time is a very important characteristics, for many reasons. At first because the results obtained are used for the

rescue operations and they have to be provided a fast as possible. A second reason is related to the fact that a large number of fire propagation simulations is required when risk analysis are carried out. In particular, two main important actions in fire safety analysis are the estimation of the real time risk analysis and the preventive evaluation of risk.

- The ***real time risk analysis*** covers a primary role when fire is spreading and a prediction of the future propagation is required for planning safety measures and rescue actions. In this case multiple simulations are requested; it is mainly due to the uncertainties related to the input data, such as wind and weather data, available from meteorological stations, fuel characteristics and orographic characteristics data, that are often inaccurate. Furthermore, predictions related to the change of the input data during the fire event and the effectiveness of firefighting actions are necessary. Results obtained from models are therefore affected by errors. Multi-simulation approaches are useful in order to determine risk probabilities for critical areas, but this requires the use of suitable models in order to perform large number of simulations.
- The ***preventive risk analysis*** has the aims to evaluate the risk related to the occurrence of a fire event in a certain area. This kind of analysis allows one to estimate the risk level in the various areas, for the following period. This is crucial in order to have troops and means prepared to intervene. In order to estimate the preventive risk not only different simulations have to be performed to take into account the uncertainties of model parameters but also different ignition points have to be considered. The number of simulations required in this case is very large and also the area to be considered. Therefore only very fast model prediction can be used for preventive risk analysis purposes.

In this framework the objective of this part of the thesis is to present the application of Proper Orthogonal Decomposition (POD) to wildfire physical modeling, with the aim of reducing the computational time but keeping the main features of the original model. First, a simple full physical model is tested with experimental data to check its ability to simulate wildfire behaviour and then it is reduced using the POD technique. It is shown that the reduced model is able to simulate fire propagation with small deviations with respect to the physical model with a drastic reduction of the computational cost. The results and the potential applicability of POD to more complex models are then deeply discussed. A fast 2D model is also implemented in order to perform quickly the wildfire landscape propagation. The topic is analyzed in depth in Chapter 6.

2

Compact model achievement: selected technique

2.1 Introduction

In the present Chapter the methods selected to obtain compact models for the analyzed systems are described. In paragraph 2.2 the Multi- Level approach is described. Multi-Level technique is applied to the modeling of the groundwater systems, for the evaluation of the thermal plume effects on the unperturbed condition (Chapter 3). In paragraph 2.3 the Proper Orthogonal Decomposition method is described; at first an introduction based on Principal Component Analysis is provided to explain the main idea the method is based on. The POD method demonstration has also been provided. Then the paragraph 2.4 includes a discussion on the POD-RBF technique. The POD-RBF model has been applied to the Turin DHN for the development of a fast tool for the optimization of the operating conditions. In particular it has been applied to a model for optimizing the pumping system strategy (Chapter 4) and to a fluid-dynamic model for the thermal peak shaving (Chapter 5). In the end, the application of POD to physical model reduction technique is explained. This approach has been implemented to show its capability to create fast physical models for wildfire propagation prediction.

2.2 Multi-Level Approach

Multi-level is a model reduction technique based on the idea of considering the different parts of a systems with different levels of detail. Often it is not worth to consider all parts of a system with the same level of detail. In these cases, the use of CFD models for simulating the behaviour in these areas produce an high increase of the computational cost without particular improvements in terms of accuracy of the results. In these cases it is useful to adopt different models in the different parts of the systems for having a good description of the zones where the most important phenomena occur. Usually, a full CFD model is used in the areas where quantity of interest show a full 3D behavior. On the other hand the reduced model is employed where less detailed analysis is required. This method is particularly efficient in reducing computational cost when the full 3D model is used only in a small portion of the entire computational domain. In particular the area where the most important phenomena occur, and the variable assume an high variability in more than one component, is called near field. The area where the variable gradient are small is called far field.

As already mentioned in the introduction chapter, many works in literature show the interest in such approach. A subject where multi-level approach has been widely used in simulation related to human body, like modeling of blood flow (Quarteroni *et al* 2001, Kerckhoffs *et al* 2007, Blanco *et al* 2009) and tissue perfusion (D'Angelo and Quarteroni, 2008). More generically a fluid flow in compliant vessel is analyzed in Formaggia *et al* 2001. Another important field where this kind of approach has been used is the tunnel ventilation analysis in case of fire (Colella *et al* 2011).

In a multi-level model, the full CFD and the reduced parts exchange each other information at the interfaces. There are two different coupling types: the 1-way coupling and the 2-way coupling (Colella 2010).

- In the ***1-way coupling*** the information are exchanged in only one direction; one of the two models passes its results to the other model but it does not receive any information from the other model. This coupling approach can be used when one of the two coupled parts of the system does not affect the other.
- In the ***2-way coupling*** information flows in both the direction. Therefore the most detailed model provides its results to the less detailed one; in the same way the less detailed model passes its results to the more detailed one. In this case both the parts of the system affect the others. When a 2-way coupling is used an iterative approach has usually to be applied in order to continuously pass information trough the interface.

In general the information that are passed through the interfaces represents the boundary conditions for the receiving part of model, for both coupling approaches. Coupling differs on the

basis of the type of boundary conditions that are passed. In case of 1-way coupling, the results of a model have to be manipulated in order to make them suitable to be applied as boundary conditions of one or more simplified models. In case of 2-way coupling a more detailed work is necessary because in both the interface side the boundary conditions have to be imposed. In this case there are three kinds of information passage at the interface (Quarteroni and Valli 1999):

· Dirichlet boundary condition applied at both the sides.

· Dirichlet boundary condition applied to one side and Neumann to the other side

· Neumann boundary condition applied at both sides.

During the information passage a proper manipulation has to be perform to make the results of a model suitable for the use in the receiving model. This can be obtained through interpolation.

2.3 Proper Orthogonal Decomposition

2.3.1 Introduction of POD

Proper Orthogonal Decomposition (POD) (Pearson 1901) is a reduction method based on the idea that the output of a systems at different times contains the essential behaviour of the system. This approach is frequently used to reduce many CFD problems. POD method allows one finding, as demonstrated in paragraph 2.3.3, among the problem decomposition, the best one, in terms of approximation error. The strong point of POD is that it can be applied to both linear and non-linear problems, described with a system of ordinary equations, and it gives an optimal projection of the problems, as detailed in the next paragraph. This method has received much attention for the reduction of complex physical systems and it was used in different fields of science and engineering, such as the analysis of turbulent fluid flows (Lumley at al. 1967; Holmes P. at al. 1993), multiphase flow (Brenner at al. 2012), unsteady thermal systems (Buljak *et al*. 2011), structural dynamics (Krysl *et al*. 2001), images processing (Rosenfeld and Kak 2014), systems involving chemical reactions (Shvartsman *et al*. 2000) and many other fields.

2.3.2 POD method basic idea

The mathematical procedure POD is based on has been developed in the last century and applied to different fields with different names (Buljak 2011). In 1933 POD theory was developed in the statistic field, with the name of Principal Component Analyses (PCA, Hotteling 1933). It is a method which aims at reducing the dimensionality of a data set including large numbers of correlated variables. Considering **n** variables for each p observations, they can be gathered in a matrix as follows:

$$\begin{bmatrix} x_{11} & x_{12} & \dots & x_{1n} \\ x_{21} & x_{22} & \dots & x_{2n} \\ \vdots & \vdots & \vdots & \vdots \\ x_{n1} & x_{n2} & \dots & x_{nn} \end{bmatrix} \tag{2.1}$$

where, x_{ik}, gives the value of the k^{th} variable during the j observation. In order to give an idea of PCA it is convenient to consider a case where n=2. Supposing to have **p** sets of data described with x_1 and x_2, the set of data can be easily plot as shown in Figure 2.1a. In order to reduce the number of variables to 1, losing the smallest amount of information, the best way is to consider, as new variable, the one which maximizes the data variance. The variable maximizing the data variance, y_1, is reported in Figure 2.1b. The same approach can be extended for large number of variables and, more generally, can be applied for model reduction.

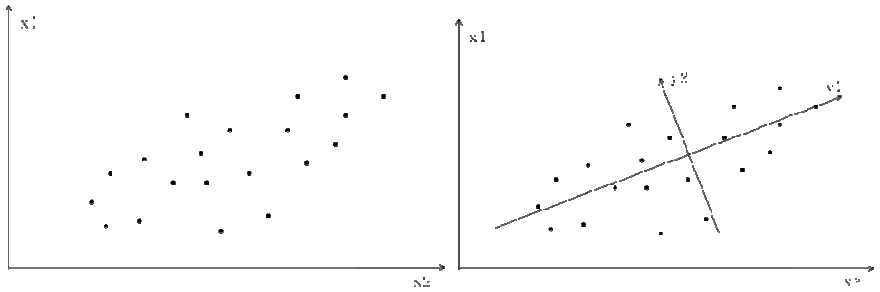

Figure 2.1. PCA applied to a bivariate case

The POD technique for dimensionality model reduction was presented to Sirovich in 1987. The approach is based on the main idea that a function, can be expressed as a linear combination of the mode eigenfunctions. In particular let U be a function depending on x and t, it is possible to write it as a linear combination of eigenfunction b_1, $b_{2,...,}$ b_k as reported in (2.2):

$$U(x,t) \cong \sum_{j=1}^{k} b_j(x)\alpha_j(t) \tag{2.2}$$

where $\alpha_i(t)$ are the amplitudes. The same concept can be written in the matrix form:

$$\boldsymbol{U \cong B\,A} \tag{2.3}$$

The problem is therefore projected in a subspace W defined through the basis B; A includes the coefficients of the subspace projection.

The representation in (2.2) is not unique. In fact, many sets of functions and coefficients satisfy the relation. The selection has to be done in accordance with some criteria.

At first the eigenfunctions have to be orthonormal, with the property in (2.4), in order to exploit some related advantages.

$$\int_{\Omega} b_{k1}(x)b_{k2}(x) = \begin{matrix} 1\ if\ k1 = k2 \\ 0\ otherwise \end{matrix} \tag{2.4}$$

Furthermore the basis has to allows to obtain, for any number K, the best approximation of T which minimizes the least square error. In other words, POD technique allows one to find the sequence of orthonormal functions so that the first two functions give the best possible two-term approximation, the first three functions give the best possible three-term approximation and so on (Buljak *et al*. 2011). This is the most interesting property of the POD. Among all possible decompositions, POD allows to obtain the most efficient in the sense that for a given number of modes, the projection on the subspace used for modeling the random field includes the most energy possible (Berkooz *et al* 1993). Equation (2.2) is called the Proper Orthogonal Decomposition.

2.3.3 Theoretical POD derivation from projection

Considering a function U expressed as a set of vectors (M N-dimensional vector), the goal is to find the best set of basis that allows one to approximate the function according the equation (2.2). In particular the error can be expressed as the projection error of the function on the new subspace. The projection $\tilde{v}$ of the vector v on B is, according to the definition:

$$\tilde{v} = \frac{(\mathrm{v,b})}{(\mathrm{b,b})}\mathrm{b} \tag{2.5}$$

where (,) is the inner product and b the eigenfunction describing the space B. The error can therefore be expressed as:

$$error = \boldsymbol{U} - \sum_{j=1}^{k} \frac{(\boldsymbol{U},b_j)}{(b_j,b_j)} b_j \tag{2.6}$$

and the function U can be expressed as the summation of the approximation and the error

$$\boldsymbol{U} = \sum_{j=1}^{k} \frac{(\boldsymbol{U},b_j)}{(b_j,b_j)} b_j + \left(\boldsymbol{U} - \sum_{j=1}^{k} \frac{(U,b_j)}{(b_j,b_j)} b_j\right) \tag{2.7}$$

The ortogonality among approximation and error can be written trough the L^2 norm $\|\cdot\|$ as:

$$\|U\|^2 = \left\|\sum_{j=1}^{k} \frac{(\boldsymbol{U},b_j)}{(b_j,b_j)} b_j\right\|^2 + \left\|\boldsymbol{U} - \sum_{j=1}^{k} \frac{(\boldsymbol{U},b_j)}{(b_j,b_j)} b_j\right\|^2 \tag{2.8}$$

The minimization of the error correspond thus to the maximization of the time average $\langle\cdot\rangle$ of the approximation:

$$\left\langle \sum_{j=1}^{k} \frac{(\boldsymbol{U},b_j)^2}{(b_j,b_j)} \right\rangle \tag{2.9}$$

For more details on the development reader can refer to (Freno *et al*. 2013 and Freno and Cizmas 2014). The maximization of the quantity in (2.9) corresponds to the eigenvalue problem:

$$\boldsymbol{A}b = \lambda b \tag{2.10}$$

where A is the autocorrelation matrix expressed trough:

$$\mathbf{A} = \mathbf{U}\mathbf{U}^{\mathbf{T}} \tag{2.11}$$

The equation (2.11) allows one to evaluate the best set of eigenfunction defining the subspace W, that minimizes the projection error.

The POD technique can be applied for both interpolation and projection approaches. This two methods perform differently under different situation, as discussed in Wang *et al* 2012. Wang *et al* prove that POD projection method is more robust and adaptive than the interpolation method, despite interpolation method allows to reach higher accuracy than to the projection approach in some cases. In the following paragraph both approaches have been introduced. The POD interpolation method has been applied to the RBF interpolation technique. In particular in Chapters 4 and 5 the POD interpolation method has been used for reducing the DHN model applied to the specific Turin test case. In Chapter 6 the POD projection method has been used to reduce a wildfire propagation model, used to solve a generic problems with a high input data variability.

2.4 Interpolation approach: POD for fast RBF interpolation models

2.4.1 Radial Basis function method

Radial Basis Function are a means to build an approximation of a multivariate functions. The necessity of approximating functions can occur for many purposes, among them (Buhmann 2000) :

- if a function cannot be implemented exactly, but only through an infinite expansion;
- when the function is not known and only a set of data is given;
- because in some case the use of interpolation approaches reduce the computational cost respect on using a known function.

In all these cases, the aim is to build an interpolation among the existing data. Common methods seek for a function through the interpolation of the data in a certain neighborhood. Radial Basis Function allows to find a function in all the domain depending on the entire set of data.

Considering a set of N multivariate data where S the is data dimension, if Y includes the N set of S values (S x N) that the function assumes in the x points, it is possible to build an interpolation as a linear combination of N RBFs:

$$\boldsymbol{Y} = \mathbf{A} \cdot \boldsymbol{G} \tag{2.12}$$

where A is a coefficient matrix S x N,

G is the radial basis function matrix N x N.

In particular the more commonly used types of radial basis functions include:

Gaussian $$g_j = \mathrm{e}^{-a\,\|x - x_j\|} \tag{2.13}$$

Linear $$g_j = \|x - x_j\| \tag{2.14}$$

Cubic $$g_j = \|x - x_j\|^3 \tag{2.15}$$

If the radial basis function used is a linear spline G assumes the form:

$$\mathrm{G} = \begin{bmatrix} \|x_1 - x_1\| & \|x_1 - x_2\| & \dots & \|x_1 - x_N\| \\ \|x_2 - x_1\| & \|x_2 - x_2\| & \dots & \|x_2 - x_N\| \\ \dots & \dots & \dots & \dots \\ \|x_N - x_1\| & \|x_N - x_2\| & \dots & \|x_N - x_N\| \end{bmatrix} \tag{2.16}$$

The RBF are able to provide an approximation for the entire domain where the data are located. This method is characterized by many strengths:

- it can be applied to almost any dimension;
- the data distribution has not to be regular (it is just required that they are at distinct points); RBF can be effective also with scattered data (Fornberg and Flyer 2005);
- good convergence properties.

For any other details refers to Buhmann 2000.

2.4.2 POD-RBF technique

The POD-RBF technique for model reduction is a fast method that aims at producing an approximate function able to reproduce the behavior of the system. Therefore the main goal is to evaluate a certain relation among the system input and the system output that can be used instead of the physical simulation. Given some sets of input, collected in the vector **p,** the POD-RBF method looks for a function able to provide the output **u**:

$$f(p) = u \tag{2.17}$$

In particular the function it is built starting from a set of data collected during simulations or experimental analysis. The set of data includes a certain set of output **U** and the input data collected in **p,** vector of N relevant physical quantities, used to obtained the collected output. The RBF properties allows to perform a continuous approximations in the entire inputs domain. Considering the generic RBF matrix equation (2.12), it can be reduced trough the POD approach in order to obtain a more compact approximation. In fact the Y matrix, that corresponds to the snapshots matrix, can be represented as:

$$u = \widetilde{\mathbf{B}} \cdot f_R(p) \tag{2.18}$$

where $f_R(p)$ represents the approximate function and B the reduced set of eigenfunction describing the subspace where the problem is projected on. The function $f_R(p)$ is therefore built in a reduced space with respect to the function f and it is obtained through a RBF approximation:

$$f_R(p) = \boldsymbol{D} \cdot \ g(p) \tag{2.19}$$

In particular eq. (2.12) becomes:

$$\widetilde{\boldsymbol{R}} = \boldsymbol{D} \ \cdot \boldsymbol{G} \tag{2.20}$$

Therefore combining (2.18) and (2.12) it is possible to obtain:

$$f(p) \cong \widetilde{\mathbf{B}} \cdot \mathbf{D} \cdot \mathrm{g(p)} \tag{2.21}$$

where $\widetilde{\mathbf{B}}$ is the truncated set of eigenfunctions, obtained by means of the set of snapshots **U**, $\widetilde{\mathbf{R}}$ is the corresponding amplitude matrix and G the radial basis function interpolation matrix. For more details related to POD-RBF technique see Buljak 2011.

2.5 POD Projection approach

POD projection method allows one converting a physical model applied to N nodes into a reduced model of order K<<N, which approximates the original one in an effective way, i.e. without losing important information. The best set of eigenfunctions is built using a collection of sampled values of the considered field, called the snapshots. The snapshots at M different time frames are collected in the so-called *snapshot matrix* **S**, which is a N x M matrix. Snapshots can be obtained using experiments or simulations. If $\mathbf{B} \in \mathbb{R}^{NxM}$ is a matrix that contains the basis vectors of the model, matrix S can be expressed in the basis as:

$$\mathbf{S} = \mathbf{B}\boldsymbol{\alpha} \tag{2.17}$$

where $\boldsymbol{\alpha} \in \mathbb{R}^{MxM}$ are the coefficients of the expansion.

The procedure consists in using only a limited set of eigenfunctions, choosing those which contain the largest amount of information of the system behaviour. Therefore, a truncated basis

matrix $\widetilde{\boldsymbol{B}} \in \mathbb{R}^{NxK}$ is considered in order to express the snapshots matrix using a coefficient matrix $\widetilde{\boldsymbol{\alpha}} \in \mathbb{R}^{KxM}$ characterized by smaller size than $\boldsymbol{\alpha}$.

$$S \cong \widetilde{\boldsymbol{B}}\widetilde{\boldsymbol{\alpha}} \tag{2.18}$$

$\widetilde{\boldsymbol{B}}$ contains relevant information since eigenfunctions are chosen in order to provide the best approximation of the physical field. The K best modes for system description are evaluated solving the eigenvalue problem;

$$\mathbf{R}\vec{\mathbf{v}} = \boldsymbol{\lambda}\vec{\mathbf{v}} \tag{2.19}$$

where $\mathbf{R}$ is the correlation matrix and $\vec{\mathbf{v}}$ the eigenvector;

$$\mathbf{R} = \mathbf{S}\mathbf{S}^{\mathrm{T}} \tag{2.20}$$

the basis must in fact describe each snapshot with the minimum error. The larger the eigenvalue, the wider the information of the system behaviour provided by the corresponding eigenfunction. The K largest eigenvalues and the corresponding eigenvectors (casted in the matrix $\widetilde{\boldsymbol{B}}$) are selected in order to satisfy the constraint on minimal energy collected, ε. This quantity represents the amount of information of the system behaviour that is provided by the selected eigenfunctions. In the considered model the (2.18) can be used with the aims of obtaining, through a substitution of the solved quantity, the reduced model.

In order to obtain an energy value of 1 the complete information must be considered i.e. the full model. For details the interested reader can refer to Bialecki *at al.*2005.

$$\frac{\sum_{i=1}^{K} \lambda_i}{\sum_{i=1}^{N} \lambda_i} > \varepsilon \tag{2.21}$$

Clearly the larger the number of eigenfunctions that are considered, the more detailed the result which is obtained, but also the larger the computational time which is necessary to obtain the result.

3

Multi-level approach for groundwater analysis

3.1 Introduction

Among the modern energy-saving technologies heat pumps are expected to reduce significantly the primary energy required for heating and cooling with respect to traditional systems. When possible, heat pumps are coupled with the groundwater. A main advantage in this coupling is related with the fact that water temperature is almost constant during the year. In addition, a larger heat transfer coefficient with respect to air is obtained. These two aspects can be exploited in order to achieve a higher evaporation temperature in winter and a lower condensing temperature in summer, which results in a higher coefficient of performance. The temperature difference between the extracted water and the re-injected water causes a perturbation of temperature field of the groundwater. This phenomenon may affect the performances of other heat pumps installed in the neighborhood especially in the case of densely populated areas.

This kind of systems are difficult to analyze experimentally, therefore numerical modeling is a suitable research approach to get information about energy, economic and environmental aspects. Nevertheless the domains involved in such problems are very wide and long times (of the order of

years) have to be computed to obtain results. These systems are often studied considered only small areas, coarse grid, or steady state conditions; this leads to the exclusion of important aspects.

In this work a multi-level approach is used for the first time to analyze a real scenario of a groundwater heat pump system, considering a large scale domain; it is obtained by coupling a full CFD model with a reduced model (Sciacovelli *et al*. 2014). In particular the full 3D CFD model is used to simulate the zone near the wells. This model is coupled with an equivalent network model to control the evolution of the thermal plume far from the wells.

In the followings paragraphs, after a literature overview related to the groundwater thermal plume modeling, the considered system and the multi-level physical model are described. In the last part, the results of the multi-level model are reported in terms of pressure, velocity and temperature fields.

3.2 Literature overview

As introduced in the previous paragraph the use of model simulations is particularly suitable for analyzing this kind of systems. Zhou. and Zhou 2009 use a convection-dispersion model to obtain the temperature field of the thermal affected zone. The results obtained show that the extension of the thermal plume is significantly influenced by the wells distance and by the load variations. It is also shown that heat transfer in such problem is dominated by convection. Diao *et al*. 2004 studied the conduction-advection problem considering a line heat source in 2D space medium by means of Green function. The authors obtained temperature field that illustrate the importance of the fluid flow in the phenomena. Molina-Giraldo *et al*. 2011 developed an analytical model to evaluate the effect of conduction on the temperature distribution in the groundwater. Results obtained from a complete 2D model and a 1D model without the conductive term illustrate that conduction is a relevant contribution. Than it is possible to conclude that a reliable model of heat transfer phenomena in subsurface must include both convective and conductive terms.

To simulate realistic operating conditions and systems, more refined tools have to be used at the expense of computational cost. Besides in-house codes several authors carried out numerical studies using the software FEFLOW (Diersch 2005) to simulate the temperature distribution of groundwater. Nam and Ooka 2010 use FEFLOW to study the temperature behavior on a small area near wells to evaluate the maximum performance coefficient for both heating and cooling conditions. Lo Russo *et al*. 2011 studied the temperature distribution in a quite large zone of subsurface using FEFLOW. Numerical models implemented in commercial codes such as FEFLOW demand high computational costs, since these kind of systems involve large domains and long operating time. For this reason such models only consider small zones near wells or coarse grid on a large scale geometry.

Another common approach adopted to reduce computational cost is to consider only steady state conditions. Ni *et al*. 2011 simulated a single-wells system for both pumping and re-injection of the water. They illustrate that the steady state is reached quickly and that the larger thermal plume correspond to the maximum load. McKeown *et al*. 1999 simulated the groundwater temperature using a 2D steady state coupled fluid and heat flow simulation code by means of the software OILGEN to study a potential site for the location of an underground repository for radioactive waste. Freedman *et al*. 2012 used a steady-state numerical model to investigate the behavior of a large-scale groundwater heat pump to understand the impact of the extracted water mass flow rates and temperature difference between extracted and re-injected water. The authors indicate that a higher mass flow rate with a smaller temperature difference produces less impact respect a smaller mass flow rate with an higher temperature difference. Steady state model allows to treat more realistic geometries but the physical conditions are not realistic since some operating conditions such as thermal load change during time.

3.3 System and computational domain description

Figure 3.1 depicts a portion of the urban area in Turin (Italy) and reports the main groundwater heat pump installations. Groundwater flows in the south-east direction toward the river Po, which is about 2 km far from the building considered in this paper. Three installations already operate in this area while a fourth one has just been installed. The latter is studied in this paper. The system considered is the heating (and cooling) system of a new skyscraper fed by three geothermal heat pumps with a cooling power of 1250 kW and an heating power of 1400 kW. The groundwater system is composed by four different wells for each heat pump, two for the extraction of the water used in the cycle and two for the re-injection. The distance between re-injection and extraction wells is 150 m while the distance between the wells of different heat pumps is 80 m.

The new heat pump is expected to induce a thermal plume in the groundwater temperature along the direction illustrated in Figure 3.1, due to the position of the skyscraper and the Po river.

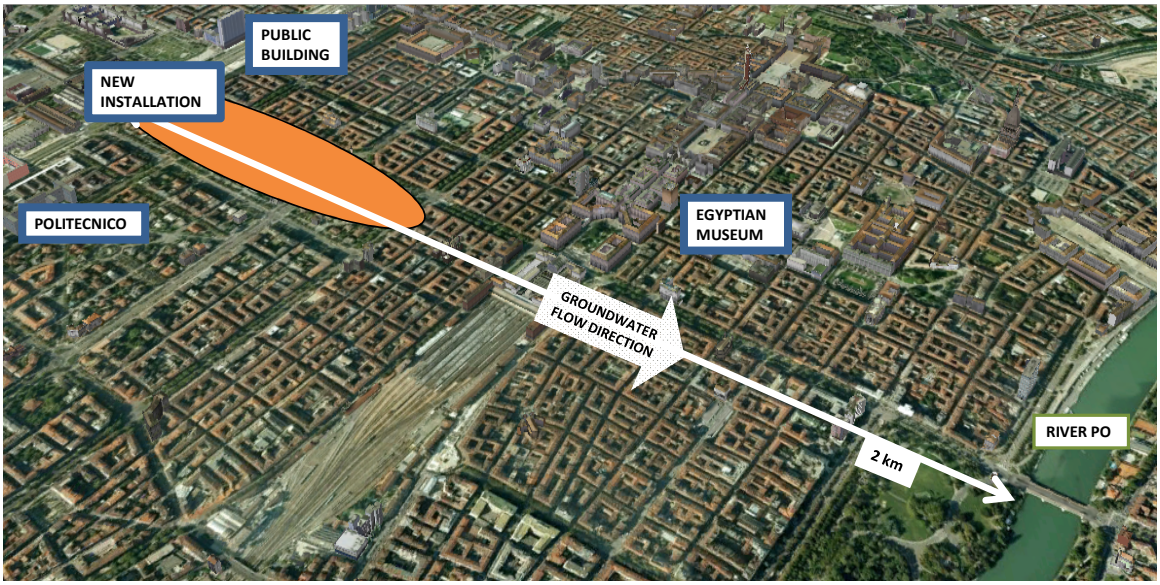

Figure 3.1: System description.

A model developed in Energy + (U.S. Department of Energy) has been used to estimate the thermal load of the building. The time evolution of thermal load over one year is depicted in Figure 3.2. The curve has been obtained as the interpolation of the results produced by the building model. It can be seen that cooling season lasts for about 6000 hours with a peak request of 7 MW. Heating period is of about 2800 hours with a peak heating load of 2.5 MW.

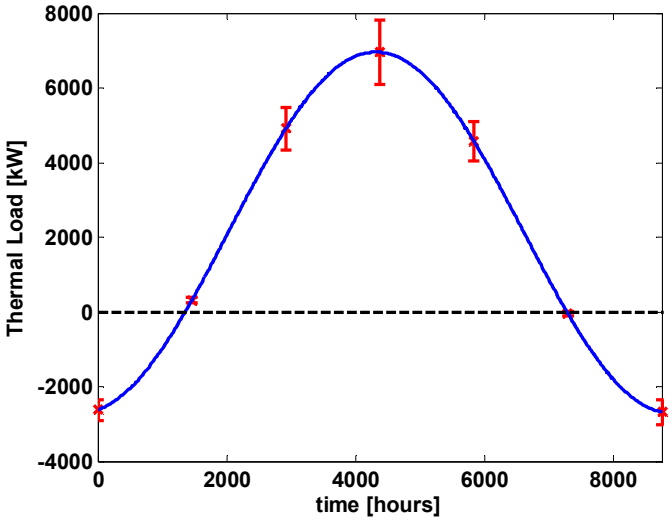

Figure 3.2: Thermal energy load.

At each instant of time water extraction temperature, water re-injection temperature and mass flow rate are related to the thermal load accordingly through Eq. (1) during heating season and through Eq. (2) during cooling season.

$$\Phi_{cond}\left(-\frac{1}{COP}+1\right)=\dot{m_{gr}}\,c_p(T_{inj}-T_{ext}) \tag{3.1}$$

$$\Phi_{evap}\left(\frac{1}{COP}+1\right)=\dot{m_{gr}}\,c_p(T_{inj}-T_{ext}) \tag{3.2}$$

where Φ_{cond} is the heat flux exchanged at the condenser,$\Phi_{evap}$the heat flux at the evaporator, COP the coefficient of performances, $\dot{m_{gr}}$ the mass flow rate extracted from the groundwater , c_p the specific heat, T_{inj} the temperature of the water re-injected in the ground, T_{ext}, the temperature of the extracted mass flow rate.

Two possible operating conditions are considered:

- the first scenario is characterized by a constant heat pump mass flow rate while water temperature difference between extraction and re-injection varies during time accordingly to Equations (1) and (2).
- the second scenario considers a variable mass flow rate while the temperature difference is considered constant and equal to 12°C.

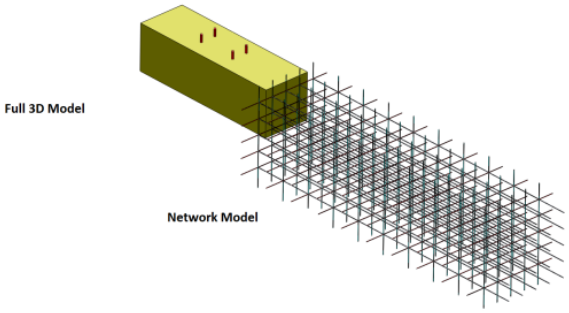

Figure 3.3: Model geometry

The model geometry is illustrated in Figure 3.3. The length of the full 3D model geometry is 600 m while the reduced model considers 2 km to investigate the distribution of the thermal plume until the injection of the groundwater in the river Po. The transversal section considered for full 3D model is 100 m high and 500 m wide in order to consider the diffusion of thermal plume also in the orthogonal directions.

3.4 Multi-level model

3.4.1 3D model

The zone near the wells has been modeled using the finite volume method by means of the software Fluent®. The fluid-dynamic behavior of the system considered has been modeled using the continuity equation and the classical Navier-Stokes equation:

$$\frac{\partial \rho}{\partial t} + \nabla \cdot (\rho \vec{v}) = 0 \tag{3.3}$$

$$\frac{\partial}{\partial t}(\rho \vec{v}) + \nabla \cdot (\rho \vec{v} \vec{v}) = -\nabla p + \nabla \cdot (\bar{\bar{\tau}}) + \vec{S} \tag{3.4}$$

where ρ is the fluid density, v the groundwater flow velocity and τ the stress tensor. Porous media are modeled by the addition of a momentum source term $\vec{S}$ to the standard momentum equation. This term is expressed as:

$$\vec{S} = -\frac{1}{K}\,\mu \vec{v} \tag{3.5}$$

where K is the permeability coefficient, 0.0015 m/sec.

The standard energy transport equation (3.6) is used to evaluate temperature distribution under the assumption of thermal equilibrium between fluid and solid phases. The thermophysical properties are modified to take into account the presence of the porous matrix. In particular, the thermal conductivity in the porous medium is computed as the weighted average of the fluid conductivity and the solid conductivity.

$$\rho\, c\, \frac{\partial T}{\partial t} + \nabla \cdot \left(\rho\, c_p\, v\, T\right) = \left[k_{eff} \nabla^2 T\right] \tag{3.6}$$

$$k_{eff} = \gamma\, k_f + (1 - \gamma) k_s \tag{3.7}$$

where T is the groundwater temperature, γ the ground porosity, k_f and k_s the thermal conductivities of the liquid and the solid phase. Table 3.1 reports the values of the parameters used for the analysis.

Permeability (K)	**6.6×10^{-9} m^2**
Unperturbed temperature	15°C
Unperturbed water velocity	1.58 m/day
Porosity (γ)	20%
Thermal conductivity of the liquid phase (k_f)	0.65 W/mK
Thermal conductivity of the solid phase (k_s)	3 W/mK

Table 3.1: Input Parameters

The adapted computational grid is a non-structured mesh near the wells while a structured mesh is adopted in the vicinity of inlet and outlet sections. Overall 2.5x106 cells are used with the element dimension varies between 0.5 and 5 m.

Adiabatic boundary conditions are applied to the four lateral faces. Unperturbed groundwater temperature and constant groundwater velocity are imposed at the inlet face.

The wells are modeled using a distributed inlet mass flow rate condition for the re-injection wells and an outlet mass flow rate condition for the extraction wells. In the case of constant mass flow rate strategy, the momentum equation is solved under steady state conditions as the velocity field does not vary with time. Then, the time-dependent energy equation is solved. On the contrary, in the case of variable mass flow rate strategy, energy and momentum unsteady state equations are solved simultaneously, since both velocity and temperature fields vary with time. A Second Order Implicit Euler method is used to solve the problem. The convergence is considered reached when the residuals are lower than 10^{-5} for mass and momentum equations and lower than 10^{-8} for the energy equation.

3.4.2 Network Model

A network model is used to investigate the zone of the subsurface far from the wells. The computational grid for the network model consists of about 27000 nodes. Energy balance equation (3.7) is written for each node of the network considering the control volume depicted in Figure 3.4:

$$\rho c_p \frac{\partial T}{\partial t} S\Delta x = +\sum_j k_{eff} S \nabla T \cdot n|_j + \sum_j \rho c_p S v \; T_j \qquad (3.8)$$

where Δx the discretization step and S is the surface.

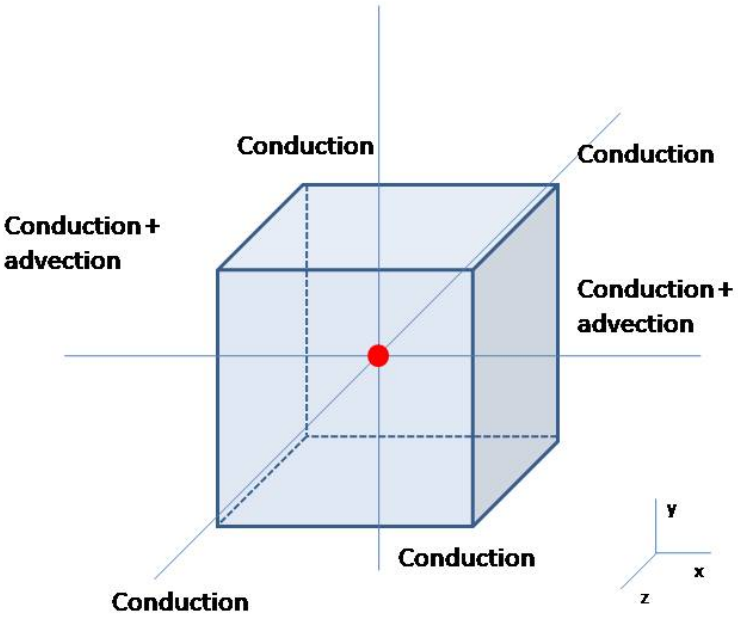

Figure 3.4: A detail of the network model

The conductive contribution is computed along all the directions. The advective contribution is evaluated at the cells boundary but only along y direction since the x and z component of the groundwater velocity are zero. Adiabatic boundary conditions are applied to the four lateral faces, while on the outlet section the following condition is imposed:

$$k\nabla T \cdot n = 0 \tag{3.9}$$

which means that no heat conduction occurs on the outlet surface.

Simulations are carried out considering the heat pump operating for three years to take into account the effect of the previous seasons on the thermal plume. The time step is about 10 hours for both models.

3.4.3 Coupling strategy between the CFD model and network model

The multi-level analysis requires to couple the CFD and network models. A 1-way coupling strategy is here adopted. In fact the information are exchanged in only one direction: the CFD model results are provided to the network model but at the same time the CFD model does not receive any information to the network model. The CFD model is indeed independent on the network model. In particular, as regards the information exchange, a Dirichlet boundary condition (temperature boundary condition) is prescribed at the interface between the two models. At each instant of time, the temperature field along the outlet section of the 3D domain is passed to the network model and it is prescribed at the inlet face of the network model. In order to implement

such condition an appropriate matching procedure has been used. This is necessary because the number of nodes on the outlet section of the 3D model is significantly larger than on the inlet section of the network model. For this reason a two-dimensional interpolation is performed in order to reconstruct the temperature distribution on the inlet section of the network model. Such a coupling strategy is performed at each time step of the numerical simulations.

As regards the fluid dynamic quantities, it is not necessary to perform any coupling because an unperturbed groundwater velocity field is prescribed. Such assumption is fully justified since the velocity perturbations induced by the heat pumps are confined to a small region near the wells. Thus, the groundwater velocity field is unperturbed in most of the domain of interest.

3.5. Results and Discussion

3.5.1 Constant mass flow rate case

In this section, the results obtained for the constant mass flow rate scenario are reported. Pressure and velocity fields along an xy-plane 20 m below the top surface are shown in Figures 3.5a and 3.5b.

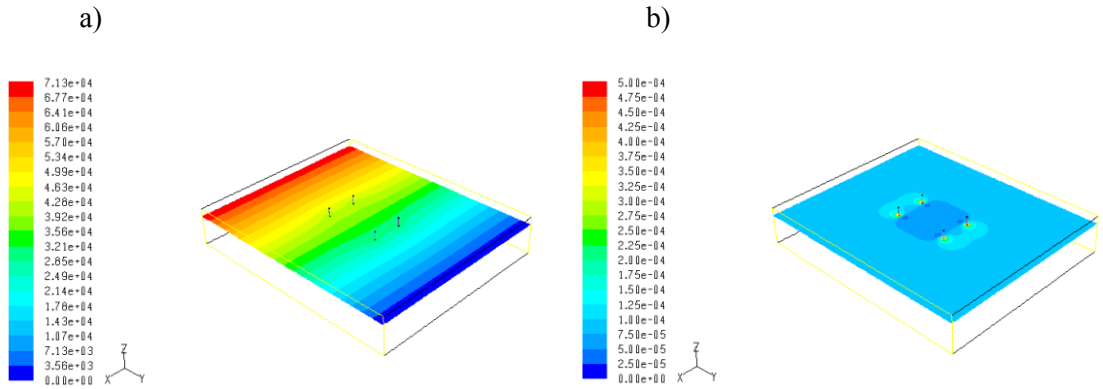

Figure 3.5: a) Groundwater pressure [Pa] field. b) Groundwater velocity [m/s] field.

It can be noticed that water extraction creates a pressure drop near the first couple of wells, while pressure increases near the second couple of wells because of the reinjection of water. Overall, pressure decreases along y direction because of groundwater average velocity field. It can be seen from Figure 3.5b that the velocity magnitude differs from the undisturbed value only near the wells. In fact, the velocity increases behind the extraction wells due to the pressure drop induced by the water extraction. The velocity between the wells is smaller than the groundwater undisturbed velocity since part of mass flow rate in this zone is by-passed. Finally, it can be seen that the reinjection creates a velocity increase downstream the second couple of wells.

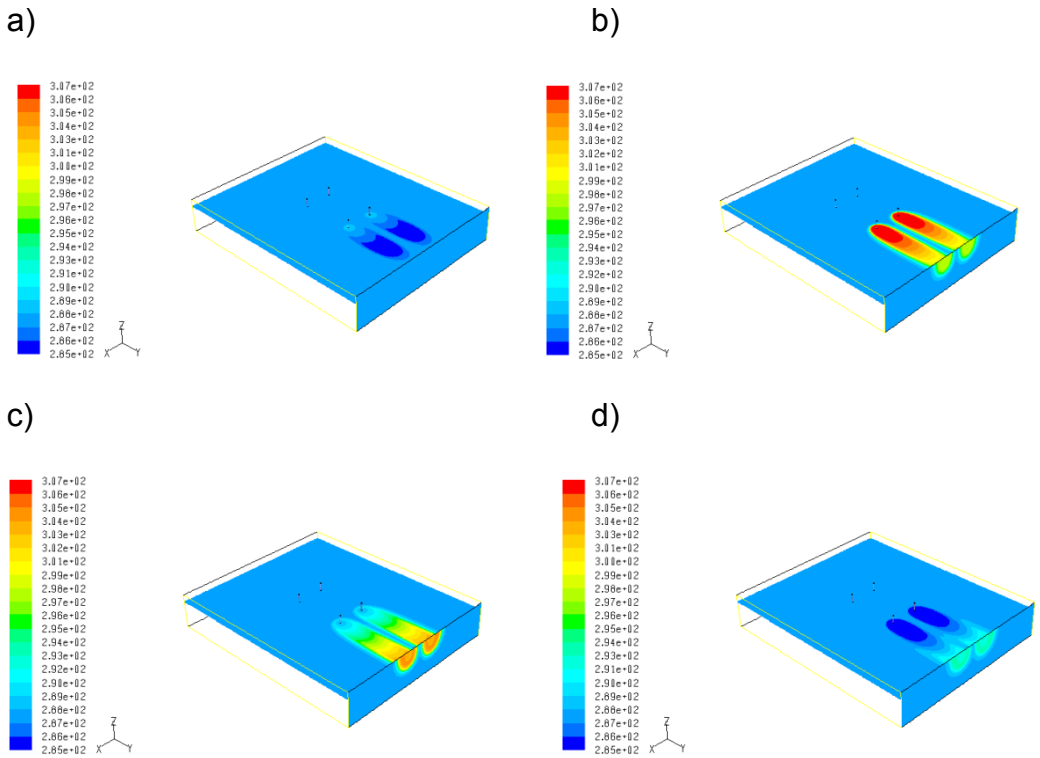

Figure 3.6: Groundwater temperature [K] field at different times:
a) 2 months, b) 6 months, c) 10 months d) 12 months; constant mass flow rate case.

Figure 3.6a shows the temperature field 2 months after the start-up of the heat pumps. This instant of time corresponds to the beginning of cooling season, as can be observed in Figure 3.2. A thermal plume around and below the re-injection wells can be seen in the groundwater temperature field. The temperature of the thermal plume is about 285 K, except for a small area near the re-injection wells where it is slightly higher due to the beginning of the cooling season. Figure 3.6b reports the temperature field at the peak of the cooling load. At this specific condition, groundwater reaches the maximum temperature of 307 K in the neighborhood of the re-injection wells, since the cooling load is maximum.

The thermal plume reaches a temperature of about 300 K along the outlet cross section of the domain, as depicted in Fig. 3.6b. Small temperature variations can be noted along transversal directions due to heat conduction. The temperature field after 10 months is depicted in Figure 3.6c. At such instant of time the thermal plume shows a higher temperature near the outlet section of the domain, while the temperature field near the re-injection wells is affected by the beginning of the heating season.

Figure 3.6d illustrates the temperature field after one year. The temperature of the thermal plume is around 293 K along the outlet section due to summer cooling. Near the wells, a minimum temperature of 285 K is observed because of the heating season.

The time evolution of the thermal plume in the following months in the 3D domain is similar to the results already illustrated because the thermal load evolves according to Figure 3.2 also for the second and third year of operation.

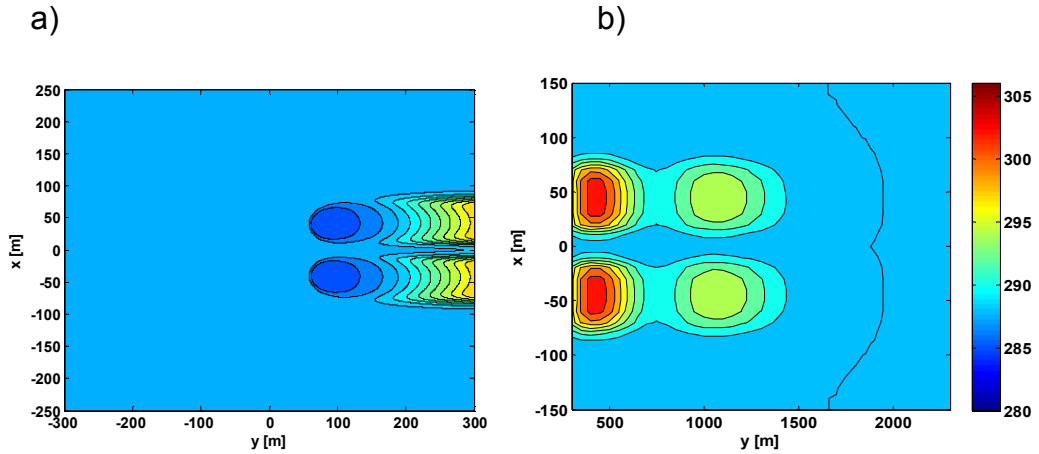

Figure 3.7: Groundwater temperature [K] field after 2 years for constant mass flow rate case; a) full 3D model domain; b) network model domain.

Figure 3.7 shows the temperature field after 2 years in a longitudinal cross section of the entire multi-scale model domain. Figure 3.7a reports the result of the full 3D model while Figure 3.7b shows the result of the network model at the same instant of time. Different scales are adopted for the two plots in order to make the results more readable. The temperature shows two local maxima, the first one is about 304 K, while and the second presents a temperature of about 296 K. Thus, the maximum temperature in the thermal plume decreases of 3 K along the first 400 m and of 11 K in 1200 m. The temperature difference between the thermal plume and the unperturbed groundwater is 8 K at 1.2 km downstream the re-injection wells. Moreover, it can be observed from Figure 7 that the water temperature is around 305 K at about 500 m from the re-injection wells, i.e. 17 K higher than the unperturbed one.

The temperature field after 3 years over the computational domain analyzed by the network model is depicted in Figure 3.8a. It is possible to observe that the thermal plume extends up to about 2 km along the groundwater flow direction and that temperature perturbation is about 4 K at y = 1.8 km. This indicates that the thermally affected area is rather wide after three years and almost reaches the river Po.

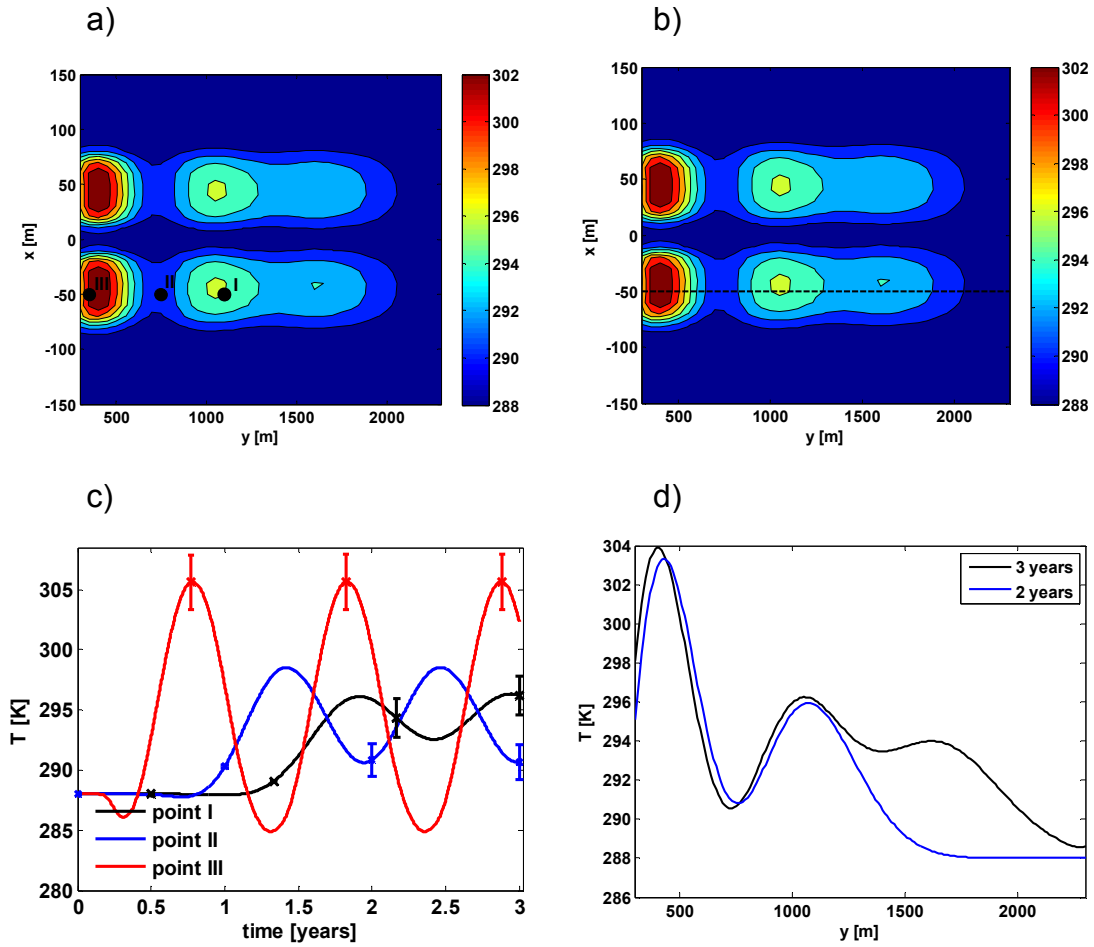

Figure 3.8: Temperature time evolution and temperature distribution for constant mass flow rate case. a) monitoring point position; b) temperature time evolution; c) longitudinal direction x = -50 m; d) temperature distribution along x = -50 m.

Figure 3.8c shows the time evolution of the groundwater temperature at the three points indicated in Fig. 3.8a. The time variation of temperature strongly depends on the considered position and the amplitude of the thermal perturbation diminishes far from the heat pump wells. The maximum temperature perturbation is about 18 °C at point III, while it decreases to 11°C at point II and to about 8°C at point I. It can be observed from Fig. 3.8c that the time evolutions of temperature at points I and III are in phase, i.e. the maximum temperature occurs at similar time for points I and III. On the contrary, temperature at point II shows a local minimum when temperature is maximum at the points I and III. The temperature of the thermal plume is always higher than the unperturbed groundwater temperature at points I and II. On the contrary, near the skyscraper (point III), the heat pump induces a local temperature which is lower than the unperturbed one during the heating season. After 2.5 years the temperature perturbation at the peak of the cooling load is about -1°C at point III, while it increases to 10°C at point II and to about 5°C at point I. These features of the time evolution of temperature are an important aspect that has to be analyzed when possible new heat pump installations are considered. In fact, the thermal

perturbation due to the already existing heat pumps may significantly affect the performance of other heat pumps, depending on the position of the latter. Figure 3.8c also reports the expected temperature deviations due to the variation of thermal load indicated in Fig. 3.2 by the error bars. It can be noticed that uncertainties in the thermal load may lead to a maximum temperature deviation of about 2.5°C near the heat pump installation (point III). The temperature deviation downstream the heat pump (points I and II) is about 1.5 °C.

The numerical predictions of temperature perturbation obtained by the multi-level model allows one to estimate COP variation due to the presence of the thermal plume. According to the studies carried out by Marcotte et. al 2010 and Fatouh and Elgendy 2011 the COP of a heat pump installed at point II (Fig. 8c) would be lower of about 15-20% at the peak of the third cooling season. The COP reduction for an heat pump installed at point I would be of only 8-10%, since the perturbation of groundwater temperature is less marked at such position.

Figure 3.8d depicts the temperature profile along the line x = -50 m after two and three years. The plot confirms that the advection effect of groundwater flow dominates the heat transfer phenomenon. The temperature profile for y smaller than 1100 m does not change significantly from two to three years. This means that heat conduction is not particularly relevant in such portion of the domain. On the contrary, the extent of the thermally affected area clearly augments in the time span of one year. In fact, the thermal plume reaches the position y = 1300 m after about two years, while it is found at y = 2200 m after three years because of the groundwater flow.

The computational time needed to solve the full 3D model on a single 3.3 GHz CPU is about 2 days for the constant mass flow rate case. On the other hand, the network model requires about 2 hours to complete the simulation in a domain 2 km long. This result clearly demonstrates that the multi-level method allows one to significantly reduce the computational cost and to obtain results in an acceptable time.

3.5.2 Variable mass flow rate case

In this section, the results corresponding to the variable water mass flow rate case are illustrated. Figure 3.9a reports the pressure distribution when the water mass flow rate of the heat pump is maximum. Such a condition occurs when the thermal load is maximum, as can be noticed from Figure 3.2 and Eqs. (3.1) and (3.2). The pressure distribution is very similar to the one obtained for the constant mass flow rate case. However, the pressure perturbation near the wells is more marked, since the maximum mass flow rate is higher in the case of variable water mass flow rate. Figure 3.9b reports the velocity field corresponding to the maximum value of the mass flow rate.

The velocity field is similar to the one presented for the constant mass flow rate case, but the local values are slightly higher because of the larger mass flow rate.

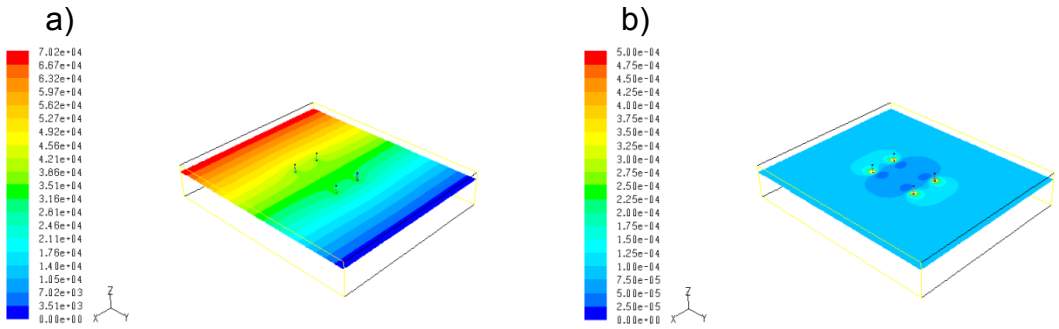

Figure 3.9: a) Groundwater pressure [Pa] field after 6 months.
b) Groundwater Velocity [m/s] field after 5 months.

The temperature field is significantly affected by the heat pump operating mode as can be appreciated by comparing Figure 3.6 with Figure 3.10b. The thermal plume after two months is less extended than in the case of variable mass flow rate. This is due to the fact that at the beginning of the heating season the mass flow rate is smaller in the case of variable water withdrawal. Moreover, the thermal plume shows a lower temperature in the case of variable mass flow rate. Thus, the groundwater temperature is less perturbed.

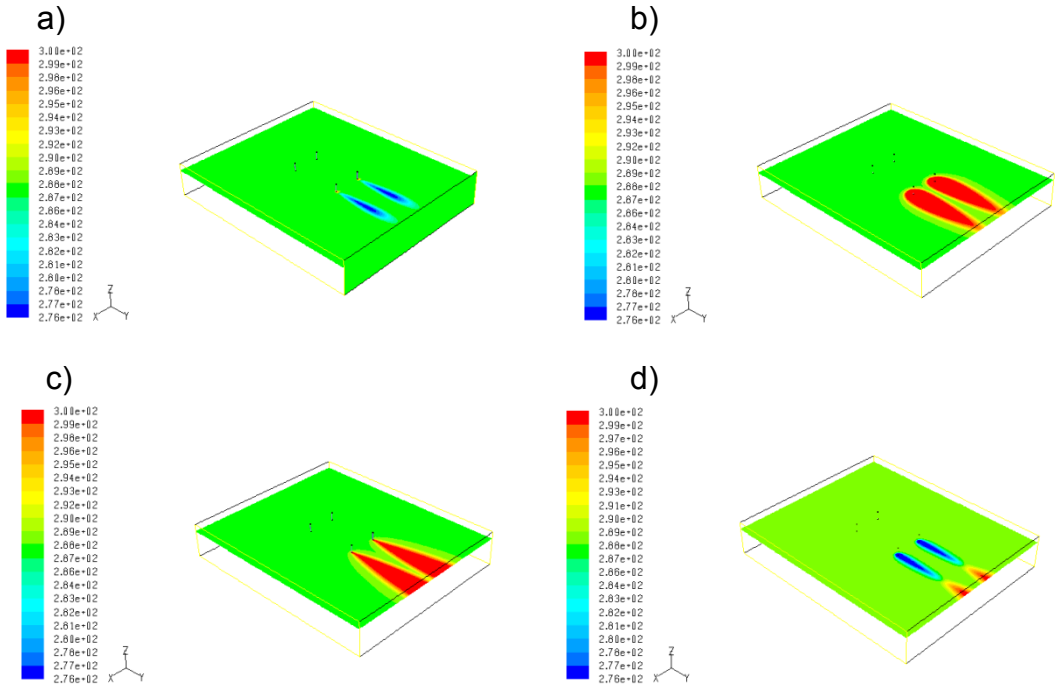

Figure 3.10: Groundwater temperature [K] field at different times a) 2 months; b) 6 months c) 10 months d) 12 months; variable mass flow rate case.

After about 6 months, the thermal load reaches its maximum and so the mass flow rate. Consequently, the thermal plume is wider, as illustrated in Figure 3.10b. The temperature of thermal plume is nearly constant and equal to 308 K. On the contrary, in the case of constant mass flow rate (Figure 3.6b) the temperature of thermal plume diminishes along the downstream direction. After 10 months (Figure 3.10c) the thermal plume is particularly wide at the outlet section of 3D domain, while it shows a small extension near the re-injections wells. At the beginning of the heating season the thermal load is negligible, therefore also the water mass flow rate extracted by the heat pump is small.

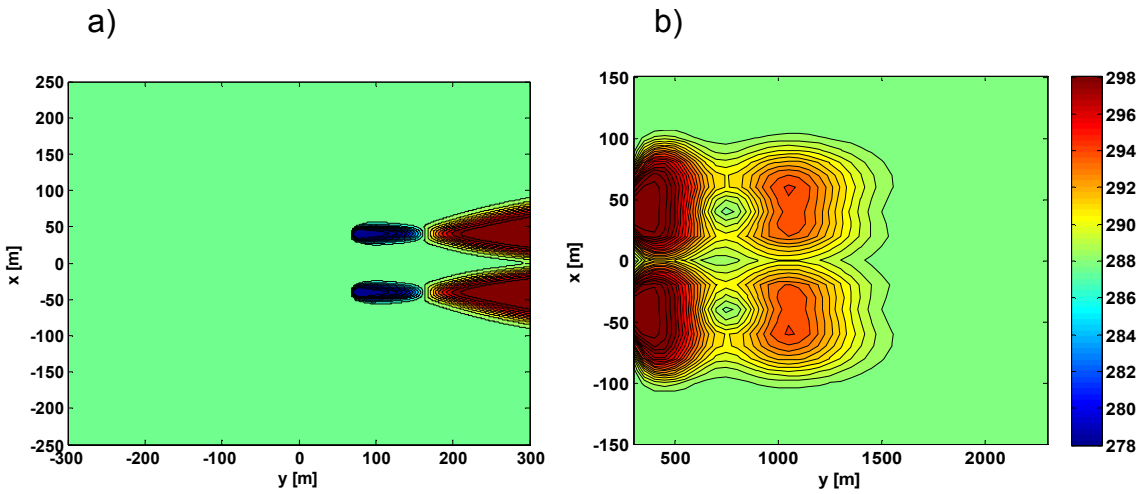

Figure 3.11: Variable mass flow rate case; groundwater temperature [K] field a) after 2 years full 3D model domain b) after 2 years network model domain.

Figure 3.11a shows the results of the full 3D model after two operating years. Figure 3.11b illustrates the results of the network model at the same time. Different scales are adopted for the two plots in order to make the results more readable. The temperature field presents two local maxima due to the time evolution of the thermal load. The first maximum has a temperature of 300 K while the second one presents a temperature of 294 K. The maximum temperature of the thermal plume decreases of 7 K along the first 400 m and of 13 K in 1200 m. Thus the difference between maximum temperature and unperturbed groundwater temperature 1.2 km downstream the wells is of 6 K. From a comparison of Figure 3.6 and Figure 3.10 it is possible to claim that groundwater temperature is less perturbed when the heat pump operates with a variable mass flow rate. However, the extent of the thermal plume is larger when the heat pump operates with variable mass flow rate.

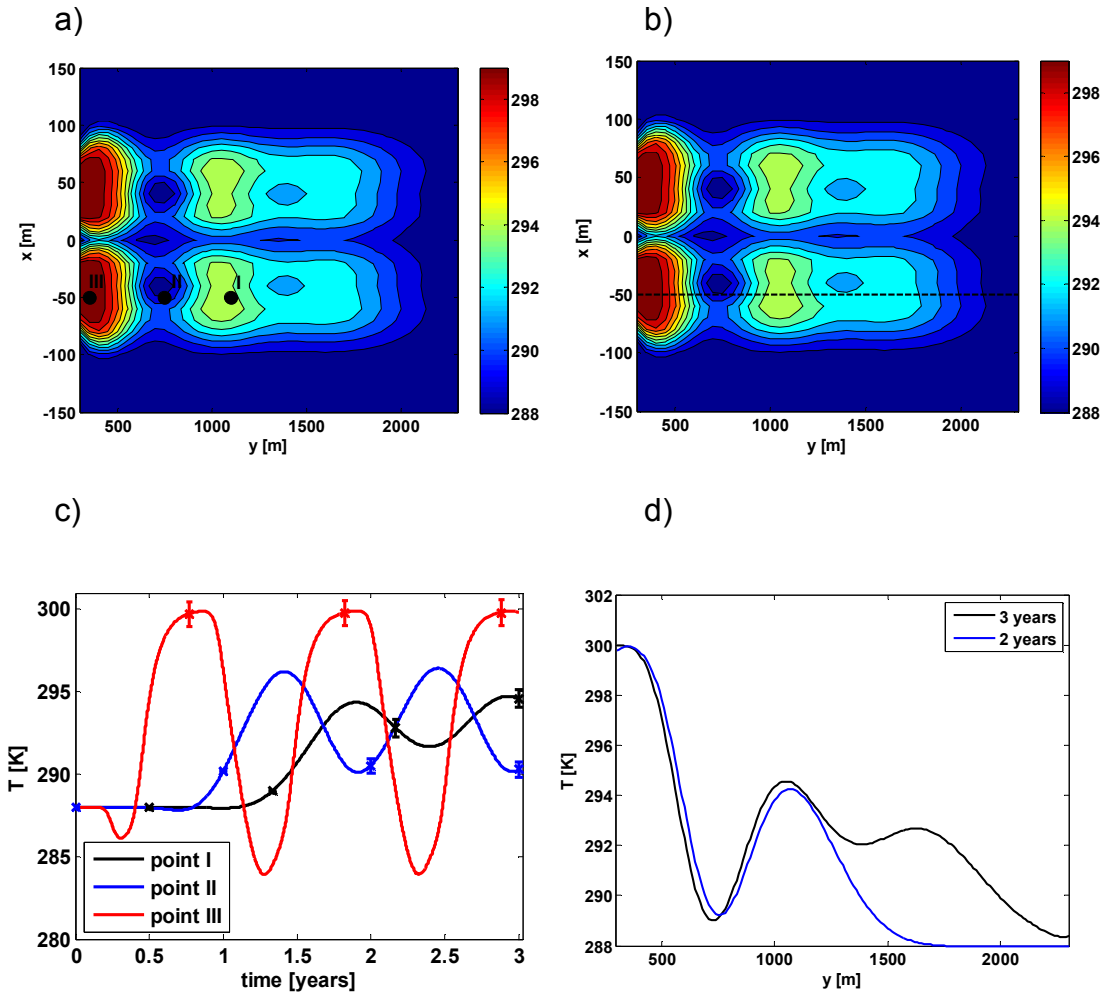

Figure 3.12: Temperature time evolution and temperature distribution for variable mass flow rate case.
a) monitoring point position; b) temperature time evolution;
c) longitudinal direction x = -50 m; d) temperature distribution along x = -50 m.

This is particularly evident from Figure 3.12a where it can be seen that the width of the thermal plume is about 200 m, while it is about 150 m for the constant mass flow rate case (Fig. 3.8a). The longitudinal extent of thermal plume after 3 years is about 2 km and at y = 1.8 km the temperature perturbation is about 3 K.

The time evolution of the temperature at three different positions is illustrated in Figure 3.12c. It can be noticed that the maximum temperature perturbation is about 12°C at point III, 8°C at point II and to about 6°C at point I. This confirms that maximum perturbation of groundwater temperature is lower if heat pump operates with a variable mass flow rate. Figure 3.12c also illustrates the temperature deviations due to the thermal load uncertainties for the variable mass flow rate case. Finally, Figure 3.12d shows that advection is dominant also for the variable mass flow rate case and that heat conduction is not particularly relevant in the zone already affected by the thermal plume.

The computational time necessary to solve on a single 3.3 GHz CPU the full 3D model for the variable mass flow rate scenario is about 6 days. The computational time is higher in this case compared to the constant mass flow rate case since it is necessary to solve the unsteady state momentum equation.

The time necessary for the network model to complete the simulations is about 2 hours.

3.6. Concluding Remarks

In this chapter, a thermal fluid-dynamic study of the groundwater temperature evolution due to the installation of a geothermal heat pump has been performed. A multi-level model is used to examine a large computational domain in a reduced computational time. The multi-level model adopted in this paper couples a full 3D finite volume model used to investigate the more complex zone of the system (near field), and a network model employed to capture the evolution of the thermal plume in the far field area. The model has been used to compute the time variation of groundwater temperature for 3 years. Two possible scenarios have been considered: a constant heat pump mass flow rate case and a variable heat pump mass flow rate case.

The analysis shows that the multi-level method allows one to reduce the computational time required by the simulations. In fact, a computational time of a about 2 days is needed to solve the full 3D model in a domain 600 m long. On the other hand, the computational time required to solve the network model in a domain 2 km long is about 2 hours.

The analysis indicates that the presence of heat pumps significantly perturbs the groundwater temperature field. However, the shape and the extent of the thermal plume are strongly affected by the heat pump operating mode. The thermal plume temperature is about 308 K in the zone near the re-injection wells when the heat pump mass flow rate is variable. The thermal plume width changes in time according to time-wise thermal load variation. In particular, the thermal plume is more marked in the vicinity of the wells when the cooling load is maximum. According to the results obtained through the network model, the temperature is considerably perturbed also at large distances. At 1.8 km downstream the wells the difference between the unperturbed temperature and thermal plume temperature is about 3 K when the heat pump operates with a variable mass flow rate.

When the heat pump operates with a constant mass flow rate, the thermal plume width is constant near the wells and its overall extent is smaller compared to the variable mass flow rate case. However, the perturbation of the groundwater temperature is more relevant. In fact, at 1.8 km downstream the thermal plume temperature is 5 K higher than the unperturbed one.

The results also illustrates that a key aspect is the temperature time evolution due to unsteadiness of thermal load. At a fixed position in space, the thermal perturbation shows strong variations in time, although the amplitude of such a perturbation depends on the considered position. The maximum perturbation is of about 18°C for the constant mass flow rate case, while it is about 12°C when heat pump operates with variable mass flow rate. Furthermore, the time wise variation of the groundwater temperature may lead to about 10-20% performance reduction of new heat pump installations in the area affected by the thermal plume.

This part of the thesis shows that the performances of a heat pump can be significantly affected by upstream installation, with an effect strongly dependent on the distance between the two heat pumps. Heat pump performances can be subjected to an improvement or a reduction. As an example, a possible installation located 400 m downstream the skyscraper would show an increase in its performances during winter operations of about 45% with respect to the case of unperturbed groundwater. This evaluation has been performed considering a condensing temperature of 60 °C and evaluating the COP using equation 3.10:

$$COP_{HP\_th} = \frac{T_{cond}}{T_{cond} - T_{ev}} \tag{3.10}$$

Similarly, an installation located 700 m from the skyscraper would register a reduction of its theoretical performance during summer operation of about 50%. This evaluation has been performed by evaluating the COP through equation 3.11

$$COP_{F\_th} = \frac{T_{ev}}{T_{cond} - T_{ev}} \tag{3.11}$$

It possible to conclude that the methodology illustrated in the chapter is very promising and can be extended to investigate large heat pump installations in urban areas. Furthermore multi-level modeling can help to investigate heat pump performance and evaluate how perturbed groundwater temperature affects the energy efficiency, which is an important aspect in the case of global energy planning.

4

District Heating Network modeling for pumping cost reduction

4.1 Introduction

Optimization of the operating conditions of a District Heating Network (DHN) is a very important aspect for primary energy savings in DH systems. Often the analysis is limited to the reduction or minimization of the primary energy consumption related with heat generation. Nonetheless, an additional aspect which should be considered is the role played by the pumping system. In fact, the thermal request of the various buildings connected with the network varies during the day, week and season depending on the external conditions as well as on the user behavior. Pumping systems are used in DHNs to supply the users with their thermal request through proper adjustment of the circulating mass flow rate. In the case of small networks, pumps are usually located at the thermal plant(s). In the case of large networks, instead, various different booster pumps may be installed along the network. Configurations with multiple pumps make it possible to obtain a correct water distribution with a variety of control strategies. Figure 4.1 shows two possible alternative strategies that can be applied to supply the same thermal load to the users in the case of one pumping group at the plant and one booster pumping group. Each of these strategy

typically involves a different pumping power, due to the different mass flow rate that should be pumped in each pumping group, therefore an optimization can be performed with the goal of minimizing the requested electric power. Such problem becomes quite complex to solve in the case of looped networks.

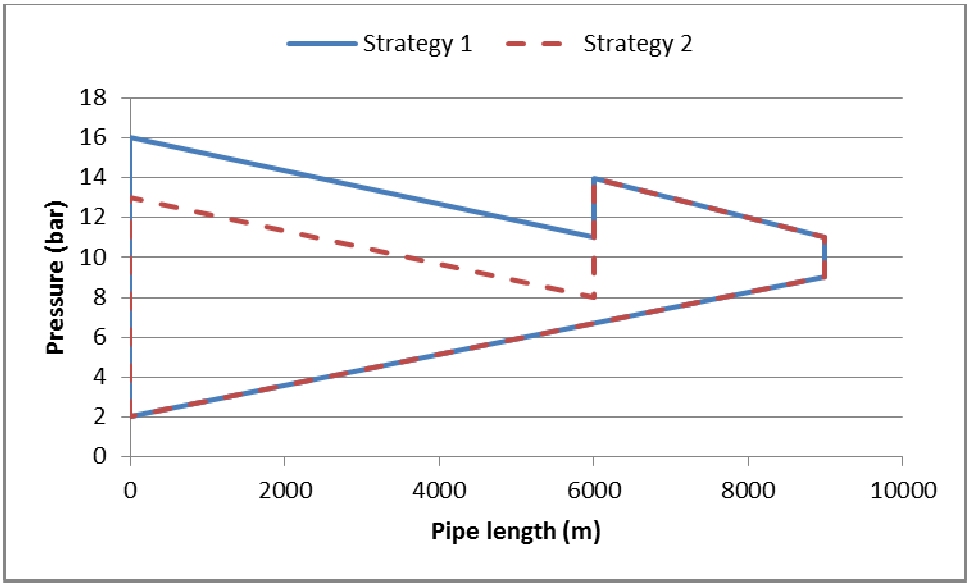

Figure 4.1: Example of alternative pumping strategies in a district heating network

The energy consumed for pumping operations is not negligible, in particular in large DHNs, when distances involved are long. This aspect is further stressed in the case of low temperature district heating systems, typically operating with small temperature differences between the supply and return networks and large mass flow rates (Tol and Svendsen 2012). Moreover, pumps work continuously during the heating season, even when heat demand is low. For instance, the DH system of the city of Turin, which is considered in this dissertation as a case study, requires up to about 6 MW of power transferred to the fluid, depending on the thermal load, i.e. about 17 MW of primary energy (assuming 0.6 global efficiency of the pumps and 0.58 electric efficiency of the combined cycles located in the thermal plants). The primary energy consumption at the peak request is about 790 MW (about 215 MW in the cogeneration plants and 578 MW in the boilers). This means that pumping represents about 2% of the primary energy consumption at peak request and increases to about 6-8% at night. In this part of the work a physical model has been developed for minimizing the electricity consumption for pumping operations. After a literature overview and a description of the DHN used as test case, the model is described and tested using experimental data. The model has been reduced through a POD-RBF technique and the results of the model reduction are discussed (Guelpa *et al* 2016). The obtained tool has been used for optimizing operations in case of different power plant configurations and in case of malfunctions.

4.2Literature overview

The importance of energy consumption due to pumping in DHSs is also highlighted in various papers in the literature. Most of these works propose implementations of fluid dynamic models of the network for design purpose or for the analysis of the effects in off-design conditions of possible control strategies.

In the literature, different approaches for district heating networks modeling have been proposed. These can be classified in two main groups: black box approaches and physical approaches. In black box approaches, the physical composition of the network is disregarded and modeling is in form of standard transfer function models or neural networks. Physical approaches, instead, involve the use of mathematical methods for computing flow and temperature distributions in the network (Palsson 2000). As far as this second approach is concerned, different types of models have been developed, starting from the pioneering Hardy Cross method (H. Cross 1936). More recently, various models have been proposed in order to overcome the problems related to convergence, computational cost and limitations that affect Hardy Cross method (Lindell 2006). All these methods are based on the graph representation of the network, which allows one to obtain a compact definition of the topology which can be directly used in matrix calculations (Harary 1995). Further details are available in section 4.4. One of the most used approach to solve district heating hydraulics is the loop equation method (Stevanovic *et al* 2007). Aggregated models which use a lower number of equivalent branches in order to simplify the network have been also developed (Larsen *et al*. 2002). Furthermore, a node-based model has been proposed, which keeps track of how long water mass has been on its way from the previous node (Benonysson *et al*. 1995). Both aggregated and node-based models do not solve fluid-dynamic and thermal transient conservation equations within all the nodes of the network (Stevanovic *et al*. 2009). Stevanovic *et al*. 2009 solve the thermo fluid-dynamic problem of an existing network, neglecting heat losses; no information about computational costs are provided. A nodal method for the fluid dynamic and thermal analyses of large fluid networks has been proposed in Calì and Borchiellini 2002. This method has similarities to the approach adopted in the present work, but it does not allow one handling systems where pumps are installed along the network, as the effect of pumps is considered through boundary conditions. In this approach, the momentum equation in the various branches is written in a way that mass flow rates are expressed as the function of the total pressure differences at the branches; this equation is then substituted into the mass balance equation in order to obtain an equation set with as many unknowns as the number of nodes, which is solved to obtain the total pressures and then the mass flow rates. An advantage of this method is that it is particularly suitable for exergy and thermoeconomic analysis, which can be applied to the analysis of optimal planning of networks, as shown in Verda and Ciano 2005.

Concerning specific applications where the pumping system is involved, a method for district heating network design, based on the probabilistic determination of the flow rate for hot water heating, is carried out in Koiv *et al*. 2014; network costs, pumping energy consumption, and power of boilers are considered. In Wang *et al* 2015 a multi-objective optimization is performed for the best network design. Both initial investment for pipes and pumping cost for water distribution are considered in order to obtain the best pipe diameters that reduce the total cost. A technical-economical optimization with the aim of minimizing both the pumping energy consumption and the thermal energy losses while maximizing the yearly annual revenue is performed in Ancona *et al*. 2014. In Fang et Lahdelma 2015, a method for optimized the production and distribution cost of a DHS is carried out with a particular attention on the pumping cost.

Most works available in literature are focused on small DHNs. When a large DHN is considered, the computational cost to solve a physical based model becomes very high; this excludes the use of full physical models for fast multi-scenario and fast optimization applications. In the present dissertation a large network is considered. This is presented in section 4.3.

4.3. System description

The Turin district heating network is the largest network in Italy. It currently connects about 55000 buildings with an annual thermal request of about 2000 GWh. The maximum thermal power is about 1.3 GW. An expansion of the system, to reach about 72 million cubic meters of buildings is already planned (Tripodi 2012). The water supply temperature is constant and its value is almost 120°C while the return temperature varies with mass flow rate circulating in the network and thus with the thermal load.

The complete network can be considered as composed of two main parts hydraulically connected: a transport network and the distribution networks. The transport network, consists in large diameter pipes, usually larger than 200 mm, and connects the thermal plants to the thermal barycentres. Each barycentre is the point that links the main network to a distribution network which supplies water to the thermal substations in the connected building. In the Turin network there are 182 barycentres. The transport network is a loop network, while the sub-networks are mainly tree-shaped networks. Figure 4.2 depicts the transport pipeline network and, in detail, 3 barycentres with their corresponding tree-shaped networks. The model developed in this work only considers the main transport network. The total length is about 515 km. The distribution networks are instead modeled considering equivalent hydraulic resistances.

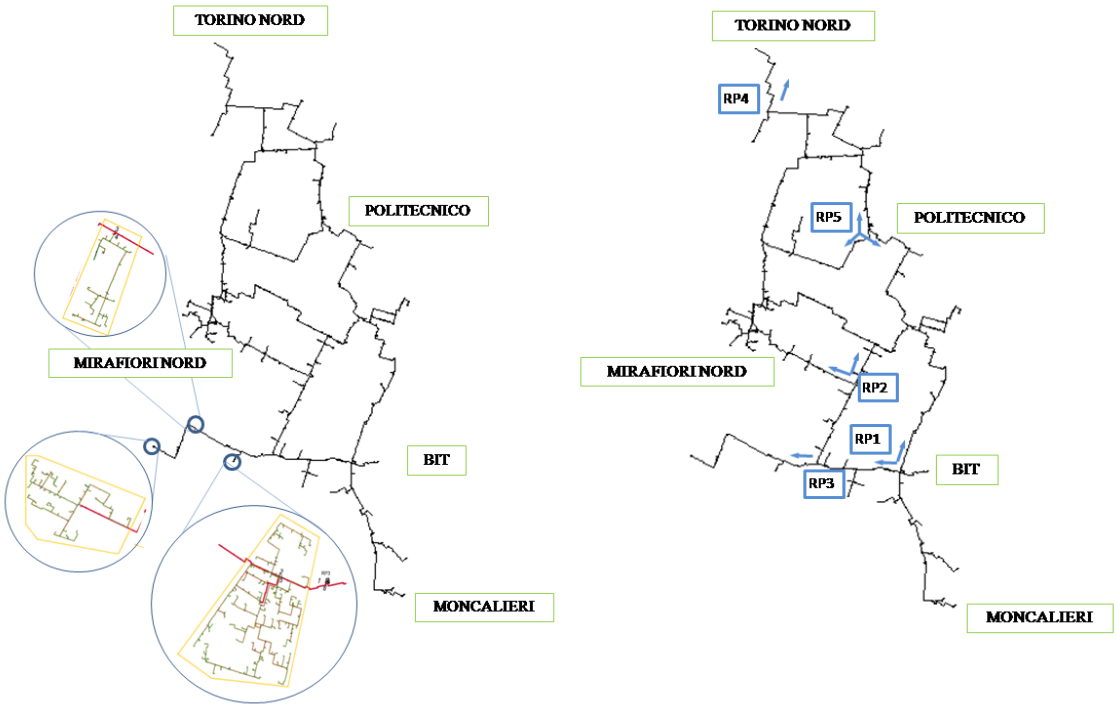

(a) (b)

Figure 4.2: Schematic of Turin District Heating Network (a) In detail 3 barycentres (b) Pumping system

Five thermal plants, which are highlighted in green in Figure 4.2, provide heat to the network. The main characteristics of the plants are reported in Table 4.1. The most usual start-up strategy of the thermal plants is the following: the two cogeneration plants in Moncalieri starts first (when the thermal request is below 260 MW one plant is operating, while the second one is operating when the request is below 520 MW), then the cogeneration plant in Torino Nord is started up and then the storage units in Politecnico and in Torino Nord. Larger thermal requests are covered using the boilers in Politecnico, Torino Nord, Mirafiori Nord, BIT, Moncalieri. In the case some of the plants are not available or when specific constraints due to electricity production must be fulfilled, a different order can be selected.

Plant	Acronym	Power [MW]	Type
Moncalieri	Monc.	520	Cogeneration (two
		141	Boilers
BIT	BIT	255	Boilers
Mirafiori Nord	M.N.	35	Boilers
Martinetto	Storage	60	Storage
Politecnico	Poli.	255	Boilers
		60	Storage
Torino Nord	T.N.	220	Cogeneration
		340	Boilers
		150	Storage

Table 4.1. Characteristics of the thermal plants

Regarding pumping systems, the main pumping stations are located at the thermal plants and 9 booster pump groups are located along the network. The main pumping stations allow the desired hot mass flow rate to be pumped into the network, from the operating thermal plants to the users. Booster pumping stations are used in order to distribute the correct mass flow rate to each user, contrasting friction losses and hydraulic head. Booster pumping stations and direction of the pumped flow are indicated in Figure 4.2b. RP1 and RP2 include two groups of pumps, each pumping in a specific direction; RP5 includes three groups of pumps; RP3 and RP4 include only one group of pumps. The latter is not considered in the simulations because it is used in a network configuration different to that examined in this work. The use of RP4 will be necessary when the network developments, which are already planned, are completed. A further utilization of this pump is possible in the case of malfunctions.

4.4. Description of the Model

In order to minimize the pumping energy consumption, to provide the users with their thermal request, an optimization is performed. In the optimization, each scenario is defined by setting the total thermal load and the contribution of each plant to the thermal load, i.e. the heat production of each plant does not vary in the optimization procedure. Mass flow rates at the various plants are obtained dividing the heat production by the specific heat and the temperature difference between supply and return network.

As already mentioned in the introduction to this chapter there are various different settings of the pumping groups which allow combining the production of plants and the request of the users, each corresponding with a different total power consumption. The independent variables are the pressure differences in the pumping stations; therefore there are 8 independent variables, one for each pump located along the network. Only the booster pumping stations are considered in the

optimization while the settings for the pumps in the plants are dependent variables. A maximum pressure of 17 bar has been set as a technical constraint.

The objective function is the energy consumption, also called the energy cost. It has been calculated as:

$$C = \sum_p \frac{G_p \Delta p_p}{\rho} + \sum_r \frac{G_r \Delta p_r}{\rho} \quad (4.1)$$

where subscript p indicates pumping systems located in the thermal plant, which are the dependent variables in the optimization problem, and subscript r indicates the booster pumping systems, which are the independent variables. The water density in the plants was evaluated as the average value between the supply and the return temperatures. This procedure should be repeated for different thermal loads in order to build an optimal control strategy.

Two approaches have been used to perform the optimization: a fluid dynamic approach and a POD approach.

As regards the fluid dynamic approach, a genetic algorithm (Golberg 1989) is applied to the model described in the next section. The algorithm starts the search for the optimal values from multiple initial points. Consequently various cases (also called "individuals" in the literature) must be created to run the optimization. This set of cases is usually named the "population". The number of individuals in the population is kept constant during the optimization process, but the values of the independent variables associated with each individual are modified at each iteration. Iterations are usually called "generations" in GA nomenclature. To create the initial population to be used in the optimization, the non-dimensional variables are randomly selected. A population of 100 elements and a maximum number of 100 iterations have been selected here. The 100 sets of pressure differences randomly selected constitute the first population. The genetic algorithm runs until the convergence is reached, when further changes in population members do not affect the minimal cost obtained. The convergence has been reached after about 50-60 generations depending on the thermal load selected. The procedure is shown in Figure 4.3a. The pressure differences can vary between the values selected in order to obtain, for the most cases simulated, a maximum pressure value lower than the upper pressure limit.

The second optimization is performed using a POD-RBF approach. The POD-RBF model is built using the simulation results conducted in various scenarios using the fluid dynamic full model. Each set of full model results is called snapshot. In this work each snapshot consists in a set of mass flow rates in the branches where the pumping stations are located and the corresponding pumping cost. Once the model is built, it can be used to simulate cases different than the ones

used to build the model or used as an optimization tool. The procedure is represented in Figure 4.3b.

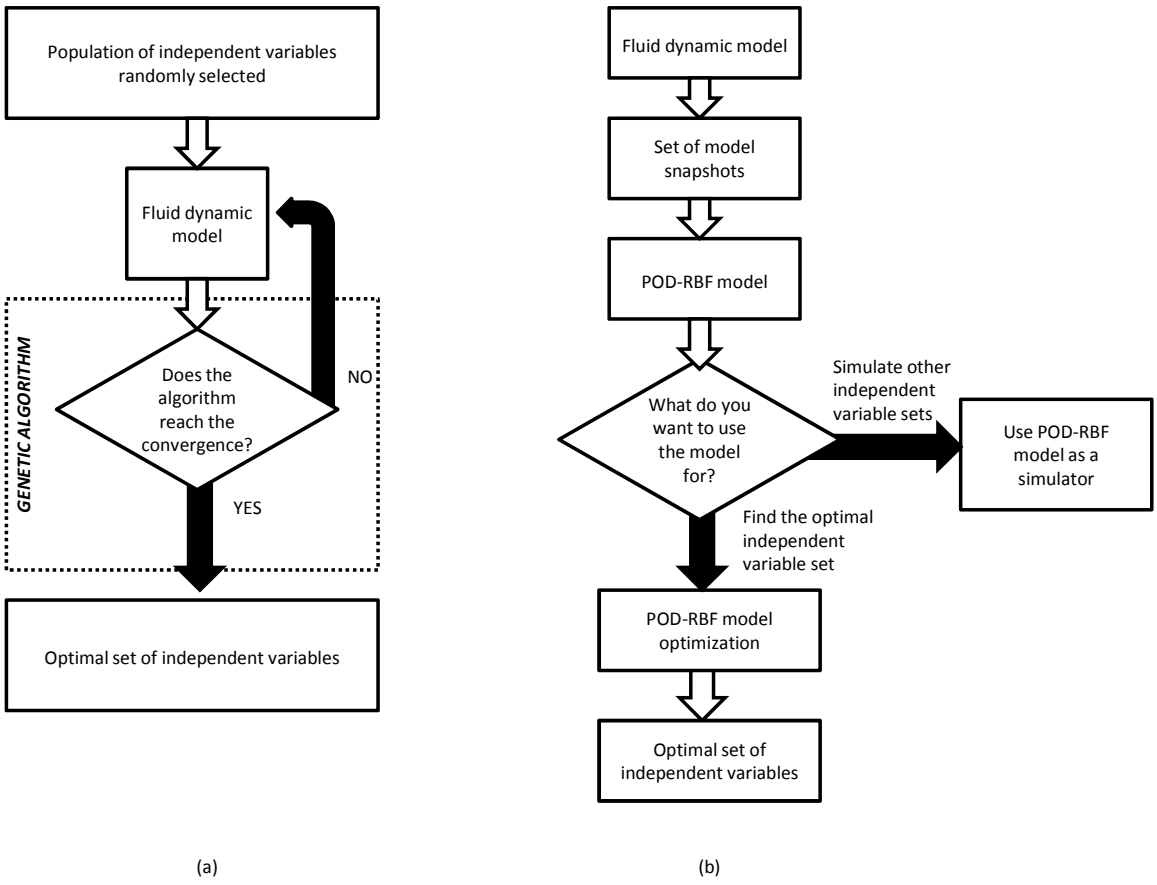

Figure 4.3: Schematic of the two optimization approaches (a) Fluid dynamic model (b) POD-RBF model

An optimization conducted using the fluid dynamic model is highly time consuming because the model considers a detailed analysis of the system behavior in all the network zones, even if information in some sections is required (in this case in the booster pumping power branches). The POD-RBF model instead provides an approximate value of the objective function, but the search for the optimum is much faster. These two methods are discussed in detail and compared in the next sections.

4.5 Fluid-dynamic model

A one dimensional model has been developed to detail the thermo-fluid dynamic behavior of the main pipeline of the network (i.e. the transport network). The topology of the network has been described using a graph approach (Harary 1995). Each pipe is considered as a branch delimited by two nodes, which are identified as the inlet node and outlet node on the basis of a reference

direction (velocity is positive when the fluid is flowing in the same direction as the reference direction and negative when flowing in the opposite direction). The supply transport network considered in the present dissertation consists of 685 branches and 677 nodes, with 9 loops. The incidence matrix A, is used in order to describe the network topology by expressing the connections between nodes and branches. Matrix A has as many rows as the number of nodes and as many columns as the number of branches. Its general element Aij is equal to 1 or -1 if the branch j enters or exits the node i and 0 otherwise.

The fluid-dynamic model considers the mass conservation equation applied to all the nodes and the momentum conservation equation to all the branches. In the fluid-dynamic model a series of simplifications in the mass and the momentum conservation equations have been considered:

- The unsteady term has not been considered since fluid-dynamic perturbations travel the entire network in a period of time of about 5 s, smaller than the time step adopted for calculations (60 s).
- The density has been considered as constant which also means that the velocity changes between the inlet and the outlet of a branch have been considered negligible.

Under these hypotheses, the mass balance of a node can be written as:

$$\sum G_{in} - \sum G_{out} = G_{ext} \tag{4.2}$$

where Gin are the mass flow rates entering the nodes from upstream branches, Gout the mass flow rates exiting the node and entering downstream branches and Gext a mass flow rate exiting outwards.

Using this matrix the mass balance equation written using matrix form is:

$$\mathbf{A} \cdot \mathbf{G} + \mathbf{G}_{\mathrm{ext}} = 0 \tag{4.3}$$

where G is the vector containing the mass flow rates in the branches and G_{ext} the vector that contains the mass flow rates exiting the nodes outwards. The terms in G_{ext} are different than zero in the case of open networks, i.e. when only a portion of the entire closed circuit is considered (e.g. only the supply or the return network as often considered in the analysis (Fang and Lahdelma 2014).

The steady-state momentum conservation equation in a branch for an incompressible fluid is written in (4.4) including the gravitational term in the static pressure:

$$(\mathrm{p_{in}} - \mathrm{p_{out}}) = \frac{1}{2}\frac{\mathrm{f}}{\mathrm{D}}\mathrm{L}\frac{\mathrm{G}^2}{\rho \mathrm{S}^2} + \frac{1}{2}\sum_{\mathrm{k}}\beta_{\mathrm{k}}\frac{\mathrm{G}^2}{\rho \mathrm{S}^2} - \mathrm{t} \tag{4.4}$$

where the first and the second terms on the right-hand side terms are the distributed and the localized pressure losses, while the last term is the pressure rise due to the pumps that may be located in the branch. Equation (4.4) can be rewritten as:

$$G = Y(p_{in} - p_{out}) + Yt \tag{4.5}$$

where the term Y is the fluid dynamic conductance of the branch, expressed as:

$$Y = R^{-1} = \left[\frac{1}{2}\frac{G}{\rho S^2}\left(\frac{f}{D}L + \sum_k \beta_k\right)\right]^{-1} \tag{4.6}$$

The friction factor f has been evaluated using an explicit Haaland correlation (Haaland 1983) in order to avoid iterative calculations and thus reduce the computational cost of the simulations.

Momentum equation can rewritten in matrix form. This formulation is obtained using the incidence matrix in order to relate the quantities that are defined at the branches (mass flow rates and pressure variations due to friction and pumping) with pressures at the inlet and outlet nodes:

$$\mathbf{G} = \mathbf{Y} \cdot \mathbf{A}^T \cdot \mathbf{P} + \mathbf{Y} \cdot \mathbf{t} \tag{4.7}$$

The diagonal matrix **Y** represents the fluid dynamic conductance of branches. Because of the dependence of **Y** on mass flow rate, the obtained system of equation is non-linear. Equation (4.7) is finally modified by setting proper boundary conditions. At least one pressure should be set in a node. In the case of analyses applied to an entire network pressure is set on the node representing the pressurization system. In the case of supply network analysis pressure is set at the master plant. Considering boundary conditions involving mass flow rates at the nodes (G_{ext}) these are usually adopted when a portion of the network is analyzed. These are imposed at the barycentre or the user nodes and at the nodes associated with the slave plants.

Because of the non linearity of Eq. 4.7 and the coupling between mass and momentum equations, the problem is solved using a SIMPLE (semi implicit method for pressure linked equation) algorithm (Patankar 1980). This is a guess and correction method: a pressure vector $\mathbf{P'}$ is first guessed and during the iterations it is corrected together with the mass flow rate vector obtained using (4.7). Through the initialization P=$\mathbf{P'}$ it is possible to evaluate $\mathbf{G'}$ as

$$\mathbf{G'} = \mathbf{Y'} \cdot \mathbf{A}^T \cdot \mathbf{P'} + \mathbf{Y'} \cdot \mathbf{t} \tag{4.8}$$

where **Y'** is built considering an initial guess of mass flow rate $\mathbf{G}_0$'. Eq. (4.8) is nonlinear, therefore a proper algorithm has to be used for its solution. A fixed point algorithm (Lefschetz 1937) has been implemented for this purpose in this work. The correction of the mass flow G_{corr} rate and the pressure P_{corr} are defined as:

$$\boldsymbol{P} = \mathbf{P'} + \boldsymbol{P_{corr}} \tag{4.9}$$

$$\boldsymbol{G} = \mathbf{G}' + \boldsymbol{G_{corr}} \tag{4.10}$$

Combining together equations (4.6) and (4.8) it is possible to obtain:

$$\mathbf{G} - \mathbf{G}' = \mathbf{Y} \cdot \mathbf{A}^{\mathrm{T}} \cdot \mathbf{P} - \mathbf{Y}' \cdot \mathbf{A}^{\mathrm{T}} \cdot \mathbf{P}' + (\mathbf{Y} - \mathbf{Y}') \cdot \mathbf{t} \tag{4.11}$$

which becomes:

$$\boldsymbol{G_{corr}} = \mathbf{Y} \cdot \mathbf{A}^{\mathrm{T}} \cdot \boldsymbol{P_{corr}} \tag{4.12}$$

under the assumption of ($\mathrm{Y} = \widetilde{\mathrm{Y}}$). Substituting Eq. (4.10) in Eq. (4.3) it is possible to obtain Eq. (4.13).

$$\mathbf{A} \cdot \boldsymbol{G_{corr}} = -\mathbf{A} \cdot \mathbf{G}' - \mathbf{G}_{\mathrm{ext}} \tag{4.13}$$

The substitution of (4.12) in (4.13), allows one to write Eq. (4.13) as follows:

$$\mathbf{A} \cdot \mathbf{Y}' \cdot \mathbf{A}^{\mathrm{T}} \cdot \boldsymbol{P_{corr}} = -\mathbf{A} \cdot \mathbf{G}' - \mathbf{G}_{\mathrm{ext}} \tag{4.14}$$

which can be rewritten in a simpler form:

$$\boldsymbol{H} \cdot \boldsymbol{P_{corr}} = \boldsymbol{d} \tag{4.15}$$

considering:

$$\mathbf{H} = \mathbf{A} \cdot \mathbf{Y}' \cdot \mathbf{A}^{\mathrm{T}} \tag{4.16}$$

$$\mathbf{d} = -\mathbf{A} \cdot \mathbf{G}' - \mathbf{G}_{\mathrm{ext}} \tag{4.17}$$

Eq. 4.15 can be used to evaluate the pressure correction $\mathbf{P_{corr}}$, while it is possible to evaluate **P** through Eq. 4.9. Furthermore **G** can be obtained by using Eq. 4.12 and Eq. 4.10. **P** and **G** can thus be used as new guess values for the following iteration. The procedure is carried out until the convergence is reached. In order to evaluate the convergence level, residuals can be calculated through Eq. 4.18 and 4.19; the convergence is reached when the values R1 and R2 are both lower than the tolerance value. In this case a tolerance value of 0.001 is selected.

$$\mathbf{G}' - \mathbf{Y}' \cdot \mathbf{A}^{\mathrm{T}} \cdot \mathbf{P}' - \mathbf{Y}' \cdot \mathbf{t} = \boldsymbol{R_1} \tag{4.18}$$

$$\mathbf{A} \cdot \mathbf{G} - \mathbf{G}_{\mathrm{ext}} = \boldsymbol{R_1} \tag{4.19}$$

To improve the process of convergence, an under relaxation factor (α) can be used while updating pressures and mass flow rates, therefore Eq. (4.9) and Eq. (4.10) become:

$$\boldsymbol{P} = \mathbf{P}' + \alpha\, \boldsymbol{P_{corr}} \tag{4.20}$$

$$\boldsymbol{G} = \mathbf{G}' + \alpha\, \boldsymbol{G_{corr}} \tag{4.21}$$

As regards boundary conditions, the mass flow rates entering and exiting the system are included in the vector $\mathbf{G}_{\mathrm{ext}}$. Moreover a pressure value should be set at least on one boundary node. To express such boundary condition, the pressure value is imposed in the initial guess vector **P'**;

furthermore, as the value of the pressure in such node is known, no correction is applied on it. This means that matrix **H**, in the column related to the node where pressure is imposed, has all zeros except for the value in the diagonal term which is 1, while in the vector **d** is zero in the corresponding row.

A schematic of the SIMPLE procedure is depicted in Figure 4.4. Further details can be found in Sciacovelli *et al.* 2013.

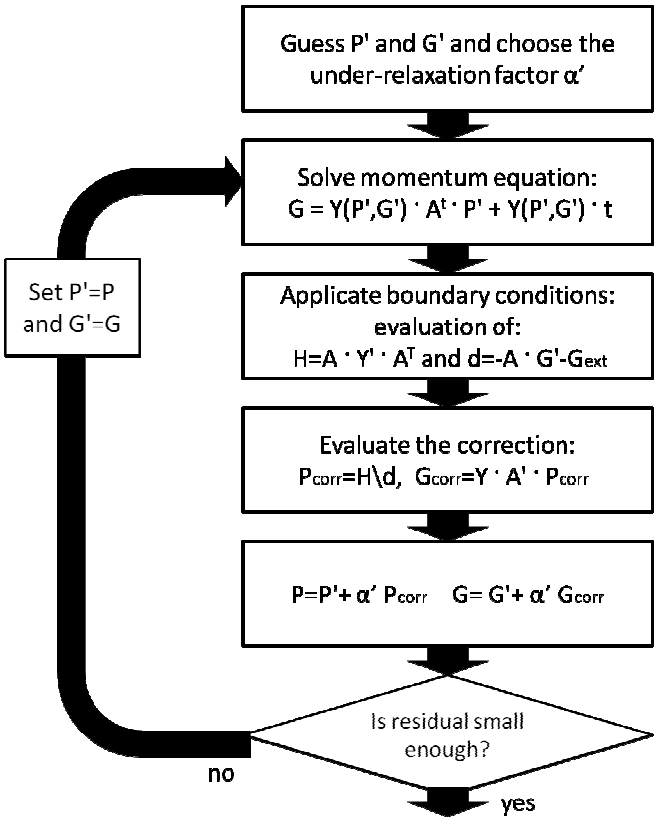

Figure 4.4. Schematic of the SIMPLE procedure

The model includes both the supply and the return pipelines (in total 1373 nodes and 1571 branches), which are connected in the barycentres. The network is open at the various plants. This means that each plant is considered through a node on the supply line and a node on the return line. From fluid dynamic viewpoint, barycentres are considered as pipes with their distributed and local (e.g. T-junctions, curves, etc.) resistances. In a general case, the mass flow rates supplied to the barycentres, Gut, differ from their requests, therefore an adjustment is necessary to model the valve controlling the barycentre mass flow rates. Therefore a variable resistance term is added to the fixed term. Resistances are expressed as equivalent lengths, which affect the term Y appearing in equation (4.5).

The variable resistance term is iteratively modified until an acceptable flow distribution is obtained, with all users supplied with the requested mass flow rate. To obtain the mass flow rate required from every user the value of L_{eq} in the nth-iteration is calculated as follows:

$$L_{eq}{}^{n} = L_{eq\_f} + L_{eq\_v}{}^{n-1}\left(\frac{G_{ut}{}^{n-1}}{G_{ut}}\right)^{2} \quad (4.22)$$

where L_{eq_f} is the fixed resistance and L_{eq_v} is the variable resistance. Subscripts n and n-1 refer to the current and previous iterations, respectively. The iterative procedure stops when the relative error between G_{n-1} and G_{ut} is smaller than a threshold value.

Concerning boundary conditions, the mass flow rate supplied by each plant is fixed on the corresponding node of the supply network. Similarly, the mass flow rate returning at each plant is fixed on the corresponding node on the return network, except for the node corresponding with Moncalieri plant, where the pressure is fixed. The latter boundary condition is required for proper solution of the fluid dynamic problem, as a further condition on the mass flow rate would result in a linearly dependent equation. Pressure is imposed on the Moncalieri plant, since the master pressurizing group is located there.

4.6 Full physical model validation

In order to validate the fluid dynamic model in the various operating conditions, a comparison with some measured data of the Turin district heating network has been carried out. The pressure differences between two nodes located at the outlet of a pump and at the inlet of the next pump located downstream have been evaluated in three different portions of the network where measurements were available for an entire heating season. In Figure 4.5, the pressure differences are reported as a function of the mass flow rate circulating in the network. The measured data reported in figure refer to the operating conditions in March, where a large variation takes place. In the figure, the results of the fluid dynamic model are also represented. In the case of the first portion, the model is able to capture the fluid dynamic behavior of the network with high accuracy. In the other sections the dispersion of data is much larger and of almost the same order as the pressure differences, mainly because these portions are closer to the centre of town, where a large number of sub-networks and buildings are located, therefore multiple variable extractions take place along these portions of network. In the model, the thermal request profile of the various barycentres was considered similar, i.e. with the same shape parameterized on the basis of the design request. In reality this does not occur as requests have different variability as the function of time, but these pieces of information is nowadays not fully available. In addition, the model was run considering strict compliance with the control strategy, while in real operation a deviation within an acceptable range is allowed. These are the causes of the large dispersion of data. Anyhow, the average deviation is lower than 0.3 bar, therefore it is possible to state that the fluid dynamic model is able to capture the hydraulic behavior of the network.

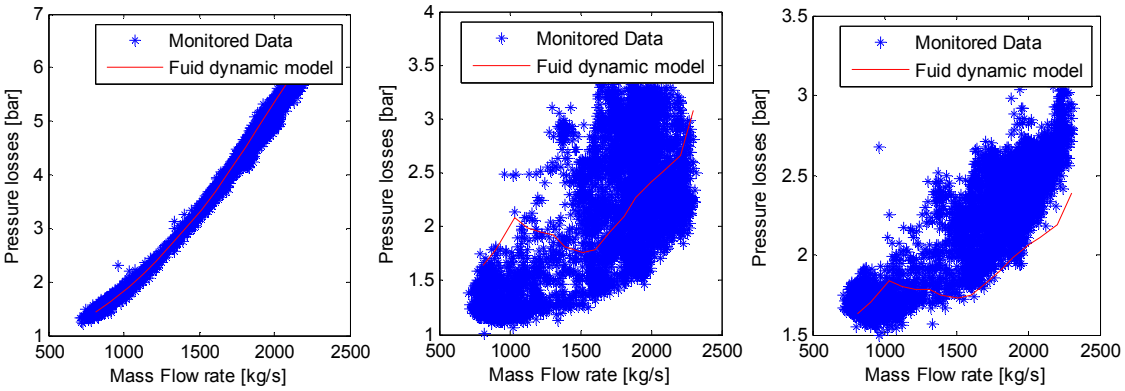

Figure 4.5: Test for Fluid dynamic model simulation capability: comparison with measured data

4.7 Fluid-dynamic model reduction

A POD-RBF model can be used constructed following the method of snapshots, as proposed by Sirovich 1987. A snapshot vector **u** of N relevant physical quantities obtained through the full physical model simulations is collected. The S input parameters of the simulation used to obtain the snapshots are collected in a vector **d**. In this work, pressure rise at the eight booster pumps, the percent thermal load (with respect to the maximum thermal load) and the contribution of each plant to the thermal load are chosen as the process parameters. For a given thermal load and contribution of the various plants, the eight values of pressure rise at booster pumps are the free variables that can be modified in the optimization process. It is worth remarking the fact that pressure rises in the pumps located at the thermal plants are not free variables. These should be adjusted in order to allow circulation of the selected mass flow rates exiting the various plants (this is necessary since the thermal load of each thermal plant is imposed).

Table 4.2 reports the maximum pressure selected for the various booster pumps, obtained after a pre-processing stage, which has been performed in order to limit the number of random combinations of the input that are rejected because of a maximum pressure exceeding the technical limit of 17 bar.

	P_{max}[bar]
RP1a	7
RP1b	7.5
RP2a	6.5
RP2b	7
RP3	6
RP5a	5
RP5b	5
RP5c	5

Table 4.2. Maximum pressure values for the each booster pumping stations

The response **u** of the system to a given set of the free variables is expressed by the mass flow rates at the booster pumps and by the total pumping power.

Different snapshots are obtained by varying the optimization independent variables within a predefined range. In order to avoid obtaining an ill-conditioned model, some precautionary measures have been adopted. First, the input data of the model have been normalized. Furthermore the snapshots have been randomly selected considering a uniform coverage of the input ranges. The complete collection of M snapshots constituted the snapshot matrix **U**. POD aims at approximating an arbitrary snapshot as follows:

$$\mathbf{u}^{a} = \bar{\Phi} \cdot \bar{\boldsymbol{\alpha}}^{\mathbf{a}} \tag{4.23}$$

where $\bar{\boldsymbol{\alpha}}^{\mathbf{a}} \in \mathbb{R}^{K\times 1}$ is a reduced state variable and $\bar{\Phi}$ is an orthogonal matrix. The latter is obtained by solving the following eigenvalue problem (Ostrowsky *et al*. 2005):

$$\left(\mathbf{U}\mathbf{U}^{T}\right) \cdot \boldsymbol{\varphi}_{i} = \lambda_{i}\boldsymbol{\varphi}_{i} \tag{4.24}$$

Matrix $\bar{\Phi}$ is then built using the eigenvectors $\boldsymbol{\varphi}_i$corresponding to the largest eigenvalues λ_i, which are ranked in decreasing order. Namely, $\bar{\Phi} = [\boldsymbol{\varphi}_1, \boldsymbol{\varphi}_2, \dots, \boldsymbol{\varphi}_K]$.

In the present analysis, the POD method has been coupled with radial basis functions (RBF). RBF are typically applied to approximate functions which are known only in a finite number of points. This interpolation technique involve all known values of functions and it is particularly effective when the distribution of nodes is scattered. Specifically, the reduced state variable $\bar{\boldsymbol{\alpha}}^{a}$ in Eq. (4.23) has been expressed as a linear combination of radial basis functions of the process parameters p:

$$\bar{\boldsymbol{\alpha}} = \mathbf{B} \cdot \mathbf{g}(\mathrm{d}) \tag{4.25}$$

where **g** contains the radial basis functions and matrix B the coefficients. Here, Euclidean norm was used as RBF:

$$g_i(p) = \|p - p_i\| \quad i = 1, \dots, K \tag{4.26}$$

Matrix B is found by enforcing that Eq. (4.25) is exact for each of the snapshots contained in the matrix U [31].

The evaluation of a snapshot corresponding to an arbitrary set of parameter p can be performed using Eq. (4.27). This is obtained by substituting Eq. (4.25) in Eq. (4.23):

$$\mathbf{u} = \bar{\Phi} \cdot \mathbf{B} \cdot \mathbf{g}(p) \tag{4.27}$$

The entire procedure has been built in Matlab® environment. To initialize the POD optimization procedure, a set of random combinations of the free variables has been collected into the initial snapshot matrix **U** and fed as input to the full physical model. The corresponding values of mass flow rates in each of the eight pumps and the total pumping costs have been obtained. Snapshots and results are used to create the POD-RBF model, which is the implicit function relating the free variables to the output.

4.8 POD model validation and performances

Starting from the full physical model, 15000 simulations have been performed, varying the free variables randomly within the predefined ranges. These have been used to create the POD-RBF model.

A test of the POD model has been first performed considering new random sets of the free variables, which were not included in the original set. The fluid-dynamics model is used in order to compute the pumping cost, selecting the independent variable randomly, i.e. the pumping pressure differences and the thermal load. The same data are used in order to calculate the output through the POD model. In Figure 4.6a the pumping costs resulting from the POD and Fluid dynamic model are compared. Results evidently show that the POD based tool in almost all cases is able to capture the system behavior.

Mass flow rates obtained from a random set of data using the two models are also computed. For each simulation, the branch containing the booster pumps where the largest mass flow rate is located is analyzed in Figure 4.6b. The figure shows that the reduced model is able to predict the mass flow rate for all cases with small deviations.

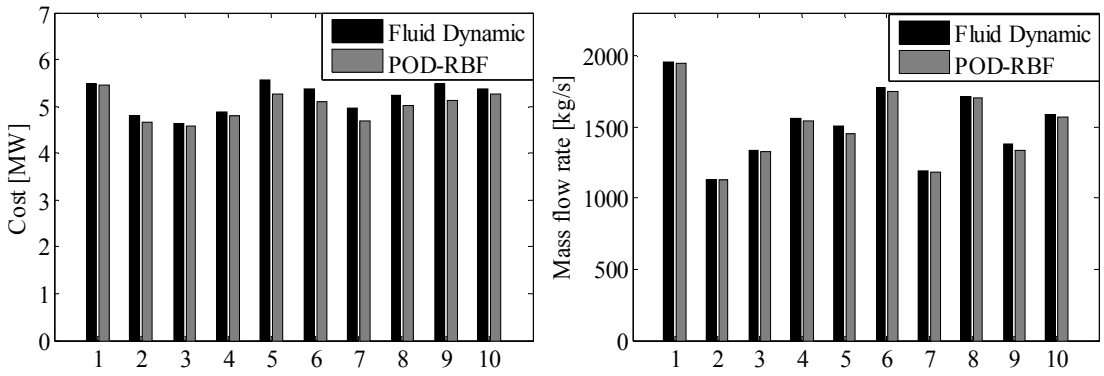

Figure 4.6. Test for POD simulation capability with 10 random cases a) pumping costs b) mass flows rate

The optimization has been performed for different heat loads. A comparison between the fluid dynamic model and the POD-RBF model is reported in Figure 4.7. Scenarios have been obtained considering the most typical start-up sequence of the thermal plants. As regards the fluid dynamic model optimization, Figure 4.7 shows that the larger the thermal load, the larger the optimal pumping cost, except for the scenario corresponding with 40% of the nominal load. The minimum cost for 40% of the nominal load is slightly larger than the minimum cost for 50% of the nominal load. This is due to the fact that when the thermal load is below 40% of the nominal load, only the Moncalieri thermal plant is operating (unless a different order is set, which can occur, for instance, in the case of network maintenance or depending on the production plans, especially related with the electricity production). When the request exceeds 40% of the nominal load, both the Moncalieri and Torino Nord thermal plants are operating. As these plants are located on opposite sides of the network, users in the North areas of the town (closer to Torino Nord plant) are reached by the water flow exiting Torino Nord plant. This allows a reduction in the pressure drops, therefore reducing the pumping cost despite an increase in the total mass flow rate flowing. When the mass flow rate further increases, the pumping cost tends to increase again.

The optimum pumping pressure sets obtained using the POD-RBF model were used as an input in the fluid dynamic model in order to compare the optima. Results show that the POD-RBF model is able to predict the optimal costs as a function of thermal load with average relative errors of about 5%.

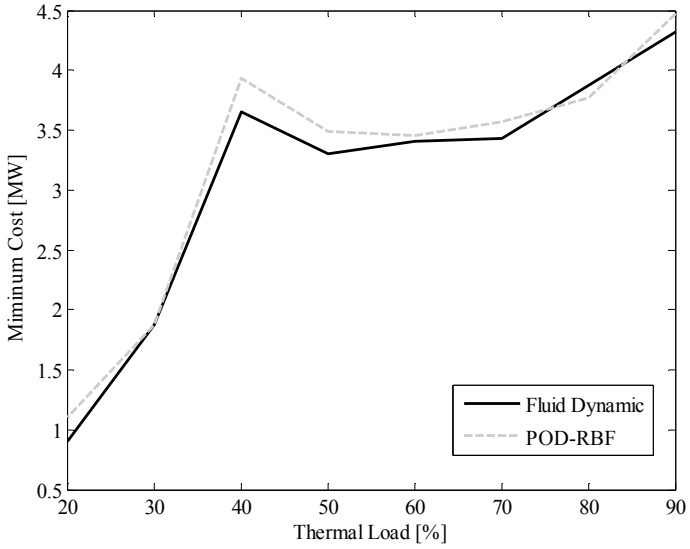

Figure 4.7: Best cost comparison

A comparison of the computational cost requested to obtain the optimum values with the fluid-dynamic model and the POD-RBF model is reported in Figure 4.8. Computational costs are evaluated as the summation of the time requested to obtain the minimum cost in all the thermal load conditions that have been analyzed on a single 3.3 GHz CPU. Using the POD-RBF, the total time required for the calculation is reduced by about 95% with respect to that required by the fluid dynamic model, which makes the reduced model more suitable for real time applications.

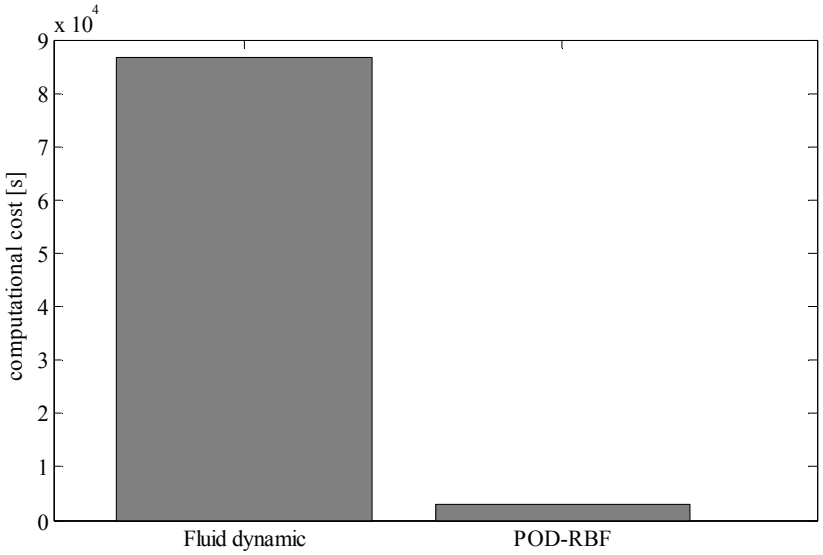

Figure 4.8. Computational costs comparison

4.9 POD model for energy cost reduction

4.9.1 Usual start-up sequence of thermal plants

In order to present the potential advantages that can be achieved using an optimized pumping strategy, a comparison between the pumping cost corresponding to the application of a pumping strategy similar to that currently adopted and the optimal strategy is reported in Figure 4.9. In this analysis, the usual start-up sequence of the thermal plants is considered. It is possible to notice that the use of the optimized control strategy instead of the current one allows the achievement of a significant reduction in the energy consumption for all thermal loads, particularly in the portion between 40% and 90% of the nominal thermal load. The differences between results obtained with the two optimization strategies (the POD-RBF and the fluid-dynamic model) are quite negligible in comparison with the difference between optimal and current strategy, therefore only the POD-RBF results have been shown, since it is the approach that can be reasonably used in real applications.

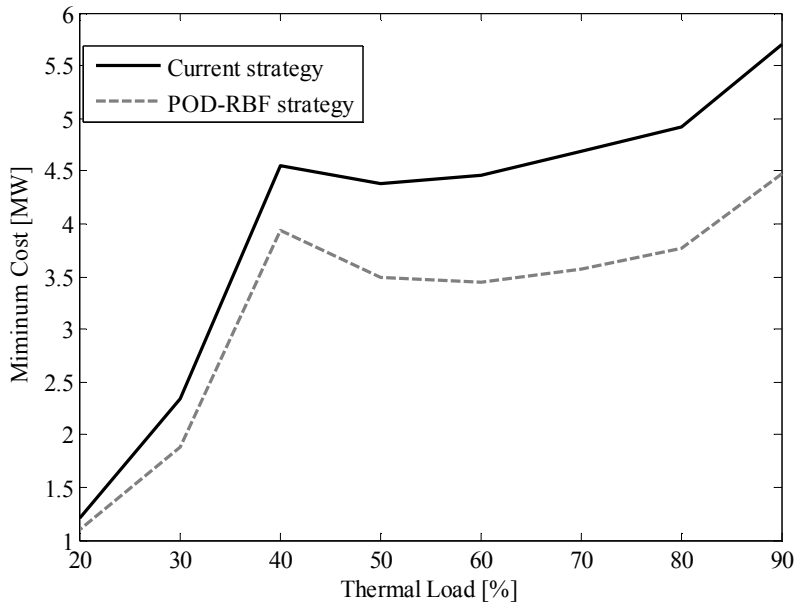

Figure 4.9: Energy consumption with current and optimized pumping strategy

To better visualize the energy cost reduction with respect to the current pumping strategy, the energy cost reductions in each thermal load is shown in Figure 4.10. Energy saving is between 8% and 24% and it is particularly large at high thermal load. The use of an optimized pumping strategy allows an annual reduction in primary energy consumption due to pumping of about 4.4 GWh/year (from 25.8 GWh/year in the case of the current strategy to 21.4 GWh/year in the case of the optimized strategy). This represents more than 0.5% reduction in the total primary energy consumption, which is about 842.5 GWh/year (about 768.0 GWh/year associated with heat

supplied to the users, about 48.5 GWh/year due to heat losses, and 25.8 GWh/year due to pumping).

These results suggest that application of the POD-RBF optimization approach allows significant improvements in the overall energy performances of large district heating networks. Further advantages related with the use of optimized strategies are discussed in the next sections.

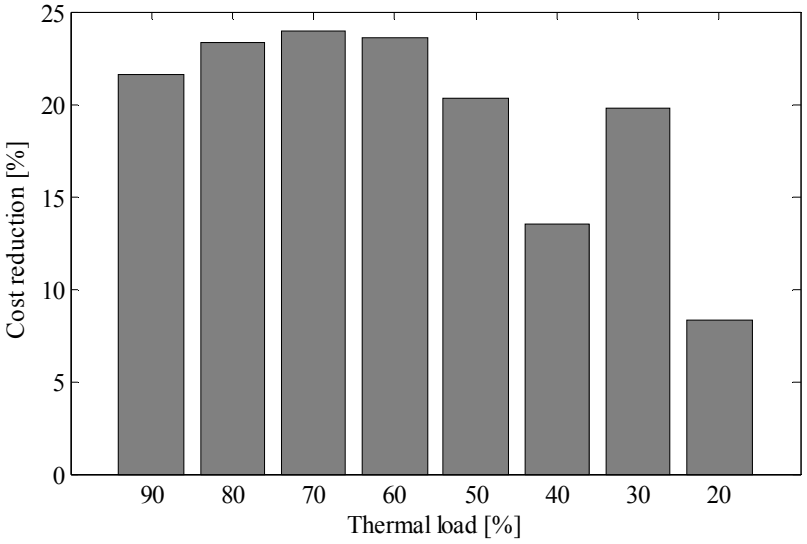

Figure 4.10: Energy cost reduction due to use of POD-RBF method instead of current pumps control strategy

4.9.2 Different start-up sequence of the thermal plants

The same POD-RBF model can be used in order to optimize the pumping strategy when different combinations of the plants is adopted in thermal production. These scenarios can be necessary in the case one of the plants is not available or if there are specific constraints on the electricity production by the cogeneration plants. When the configuration in heat production changes, also the mass flow rate distribution at the thermal plants changes, therefore a different setting of the pumps is necessary, even if the thermal request of the users remains unmodified. The optimization tool should be sufficiently flexible to allow fast optimizations in variable conditions. The POD-RBF model can been used by fixing the total load, by modifying the sequence of thermal plants that are used to cover it and by limiting the maximum DH mass flow rate that is elaborated by each plant (and thus the maximum thermal load supplied by each plant).

Table 4.3 shows four different scenarios, corresponding with different plant configurations at 60% of the maximum thermal request of the users. In Figure 4.11, the corresponding optimal settings of the pumping group obtained using the POD-RBF model are shown.

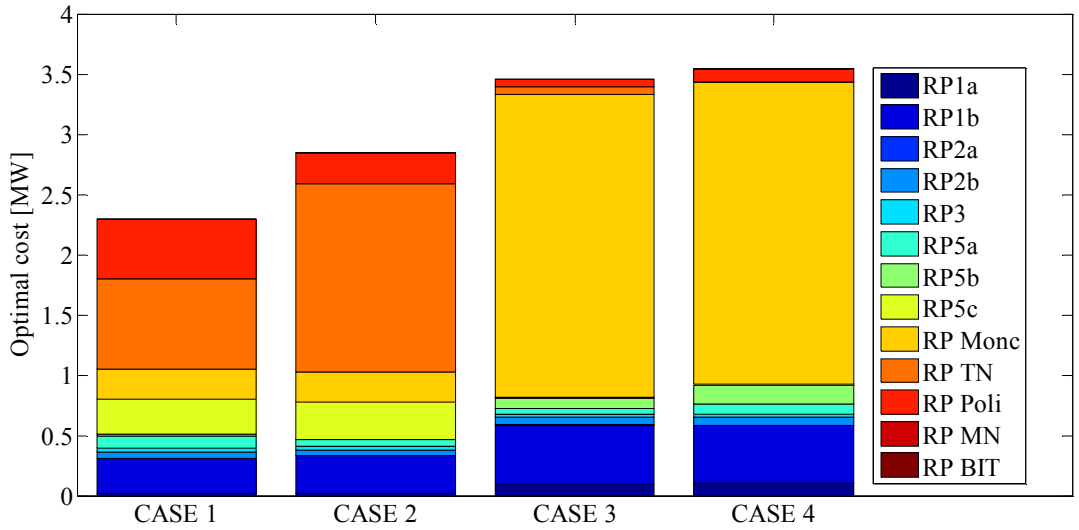

Figure 4.11: Optimal pumping costs with different plants start up strategy at constant load

CASE 1	CASE 2	CASE 3	CASE 4
Monc. Cog. Group 1	Monc. Cog. Group 1	Monc. Cog. Group 1 and 2	Monc. Cog. Group 1 and 2
T.N. Cog.	T.N. Cog.	T.N. Boiler	Politecnico
Politecnico	T.N. Boiler	Politecnico	
	Politecnico		

Table 4.3. Power plants start up strategies considered

Results show that the pumping cost is smaller when the two Moncalieri cogeneration plants are not used at 100% of their load. In fact in cases1 and 2, where just the Moncalieri cogeneration group 1 is switched on, the optimal cost is lower than in the cases3 and 4, where both the cogeneration groups in Moncalieri are used. This is due to the fact that the Moncalieri power plant is located at the south end of the network, therefore when large mass flow rate are supplied by these plants, a large pumping power is necessary. When one of the Moncalieri cogeneration plants is switch off, the power spent to pump the water from the south area to the city centre (R Monc, RP1a, RP1b) is smaller, while the power to pump water from the north to the south is larger (R T.N., R Poli and RP5c). The configuration which minimizes the pumping power corresponds to a more distributed production. In case 1, in fact heat is produced in three plants, one located in the south end (Moncalieri), one in the central area (Politecnico) and one in the north end (Torino Nord).

4.9.3 Operation in the case of malfunctioning pumping groups

The POD-RBF model is also been used in order to find the optimal set of pumping pressure when a failure in a pumping station occurs and therefore that piece of equipment cannot be used. In malfunctioning scenarios, minimization of primary energy consumption may become a secondary objective. Nevertheless, the fact that a constrained optimization is performed allows one to obtain the best pumping settings corresponding with fulfillment of the thermal request of the users, which is instead the main objective in malfunctioning scenarios.

The analysis has been performed for each pumping station. Results are reported in Table 4.4, considering 60% of the thermal request and the usual configuration for thermal production.

	Optimal Cost [W]
No malfunctions	3,57
Malfunction in pump 1a	3,63
Malfunction in pump 1b	4,06
Malfunction in pump 2a	3,58
Malfunction in pump 2b	3,57
Malfunction in pump 3	3,59
Malfunction in pump 5a	3,58
Malfunction in pump 5b	3,60
Malfunction in pump 5c	3,58

Table 4.4. Minimum costs in case of malfunctions

The minimum cost is obtained when no malfunctions occur. Nevertheless in most malfunctioning cases, the optimal costs do not differ significantly with respect to the case without malfunctions, except when a failure occurs in the pump 1b. This is due to the fact that this pump is located in a crucial position for water circulation and its unavailability causes longer paths to reach the users and thus larger friction losses.

Possible iterative interactions between pumping system settings and plant operation can be theoretically examined using the modeling approach proposed in this work. Such cases are meaningful in the case of possible malfunctions that may affect the hydraulic behavior of the network. In the case there are no pumping strategies that allow proper fulfillment of the thermal request, it is possible to examine scenarios where the production share among the plant is modified in order to help reducing the hydraulic issues.

These results show that POD-RBF model allows one to create a flexible operation tool, which allows optimal management of both normal and abnormal (malfunctioning) scenarios.

4.10 Concluding remarks

The present chapter reports the application of reduced modeling to the optimization analysis for the minimization of the pumping cost in a large district heating network. The optimization is carried out using two different approaches. The first approach, more conventional, is based on the application of a genetic algorithm to the full physical fluid dynamic model of the network. The second approach utilizes a reduced model, obtained through radial basis function (RBF) and proper orthogonal decomposition (POD) in order to capture the main features of the physical system. This last approach provides more approximate results due to model reduction but requires much smaller computational time. The errors of the POD model in the evaluation of the objective function are quite small.

Fluid dynamic model and the POD-RBF model are used to find the optimal values of pumping cost. Results show that a deviation of about 2% is obtained for both optima. Therefore POD provides a good approximation of the physical behavior of the system. In contrast the difference in computational time is very large. This is a crucial feature to allow optimal operation in real networks, as the operating conditions vary significantly depending on the thermal request and the availability of both the thermal plants and the pumping groups. In the case study considered in this work the optimization of the POD model requires about 4% of the time requested for the optimization using GA. This difference increases with the number of nodes that are used to represent the network topology, which means that the advantages of using such a technique increases in the case of large networks. In order to show the potential for energy saving in district heating network pumping systems, a comparison between the electricity consumption using the current control strategy and the optimized strategy was carried out. This comparison shows encouraging results which suggest the applicability of fast simulation to the optimal management of the pumping system in district heating networks. The simulation tool shows to be sufficiently flexible to allow one handling both normal operating conditions, corresponding with variation of the thermal request of the users and in the use of the thermal plants, and malfunctioning conditions of pumping groups. The same approach could be extended to the optimization when malfunctions occur in the pipes (at least the main portion of the network). In order to consider the possible advantages related with this approach an example is considered below.

One of the branches located downstream RP1 along the portion of network which proceeds straight ahead with respect to the portion linking Moncalieri to RP1 is considered as malfunctioning. This means that the entire mass flow rate reaching RP1 must proceed in the

direction towards RP3. Two strategies are compared at peak request: the current operation strategy and a strategy obtained through optimization. Results are shown in figure 4.12 in terms of pressures at the various nodes of the network. It is possible to notice that in the case of the current strategy, more than 80 nodes have a pressure larger than 16 bar, which is not acceptable. The only way for the network to operate in this scenario consists in limiting the mass flow rate supplied to the users, so that the corresponding pressure levels in the network can be reduced. Using an optimized strategy the number of nodes with a pressure larger than 16 bar is reduced to13. This means that still is not possible to fulfill the thermal request of the users, but the reduction in the mass flow rate to be applied is limited.

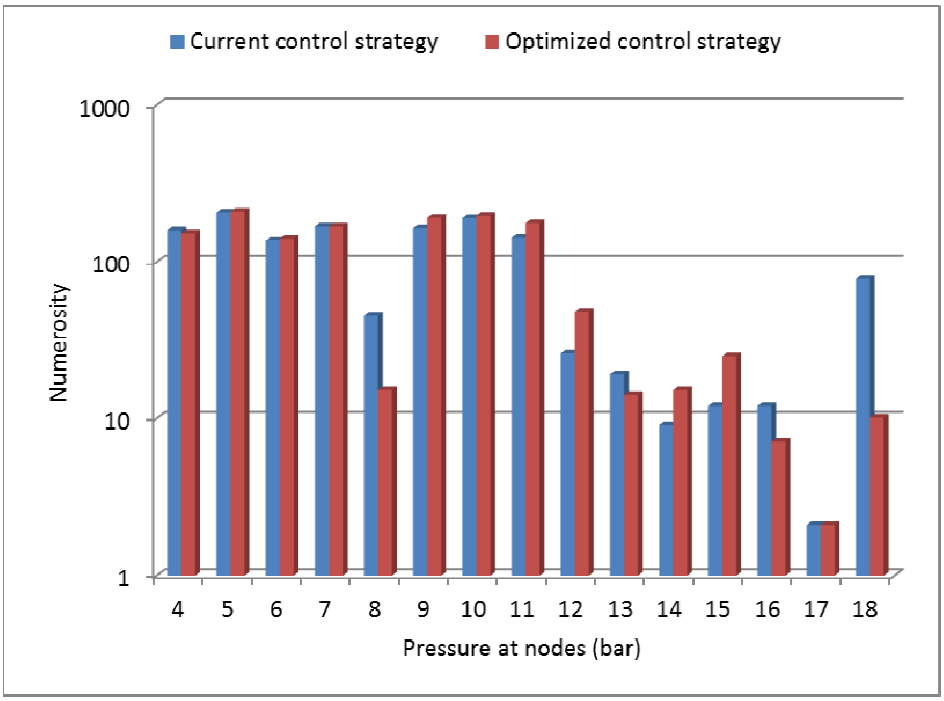

Figure 4.12: Comparison between current strategy and optimized strategy in case of a pipe malfunction

As a conclusion of this application it is possible to state that an optimized strategy would allow better network management also in the case of malfunctioning conditions. A reduced model is a prerequisite to apply such operational approach to large network. The feasibility analysis for a POD-RBF model has been performed here just analyzing a single case, while the full development and application of this tool is left as a future work.

5

District heating network modeling for thermal peak shaving

5.1 Introduction

A typical problem related to DHS in Mediterranean area is the peak of the total thermal request which occurs in the morning when most of the building heating systems are switched on. Cogeneration groups are usually not sufficient to provide heat to the users during the peak, therefore boilers have to be used, with a consequent reduction of the overall performances in terms of primary energy consumption. The thermal fluid-dynamic simulation modeling can significantly help in the analysis of the effects of possible changes in operation and system design. Model can thus be used to study how modifications, like users request variations, installation of local storage systems, and other management changes, affect the peak load.

In Figure 5.1, the global thermal request of the Turin DHS, is reported for a typical winter day. The plot shows that the global thermal load during the morning peak, at around 6 am, is almost double than the mean request during the day. When the thermal request is smaller than 740 MW, the heat is completely provided through cogeneration plants. When the request exceeds this value,

the storage systems are discharged providing a thermal power of 270 MW for a certain time period. When the request exceeds the 1000 MW,as it occurs during the peaks, boilers have to be used to provide the requested amount of heat to the users. Possible opportunities for thermal peak shaving may be particularly effective since they can reduce the amount of heat generated with boilers, i.e. the portion involving large primary energy consumption.

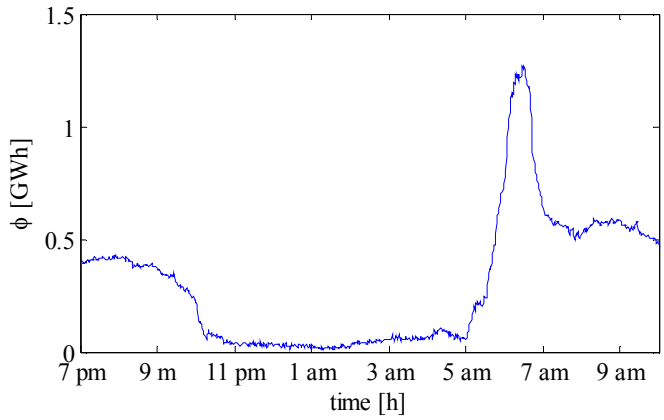

Figure 5.1. Global thermal request in a typical winter day in the Turin DHS

In this part of the work, a physical tool for the thermal analysis of large district heating network is described and tested; it has been used to predict the total thermal request at the thermal plants and for analyzing the possibility to modify the thermal request profile of some buildings as well as the installation of thermal storages. The goal is to obtain information on how the mentioned modifications may affect the peak, in order to increase the cogeneration exploitation. The physical model has been tested using experimental data; the temperature and thermal request evolution in different points of the DHN have been compared. In order to reduce the computational cost, a faster model, obtained through a POD-RBF reduction technique has been carried out. The reduced model capability to predict the total thermal request has been compared with the physical model results. At first, the model is used for studying the installation of storages, in a certain point of the network and quantifying the primary energy consumption reduction. Secondly an optimization tool has been carried out with the aim of finding the optimal set of anticipations in the time for switching on the heating systems in some of the buildings in order to minimize the primary energy consumption. This part of work has been developed under the Dimmer project, which has the aim of developing a web-service oriented, open platform with capabilities of real-time district level data processing and visualization. Through the web-service interface, some applications can be developed to monitor and control energy consumption in district heating systems.

5.2 Literature overview

The interest in investigating opportunities for thermal peak shaving, like users request variations, installation of local storage systems, and other management changes, is increasing, as documented in the recent literature. In Verda and Colella (2011) the use of storages systems which can be charged during the night and used during the start up transient are examined in order to reduce the morning peak. This is shown to be a very effective measure for reducing the boiler utilization and enhance cogeneration use. In (Jokinen *et al*. 2014) and (Verda and Baccino 2014) network models are used in order to study the opportunities to modify the thermal request profile of some users for maximizing the heat production from cogeneration or renewable plants. In Dotzauer 2002 a simple model has been implemented for DHSs heat-load forecasting based on the idea that the heat demand can be described relatively well as a function of the outdoor temperature and behavioral aspects. The possibility of using a dynamic simulation tool with the aim of studying interactions of CHP/DHN, with a particular emphasis on the network to heat storage capacity, is examined in Prato *et al* 2012. In Barelli *et al* 2006 a model is proposed for thermal load evolution as a function of the user thermal power installed, the seasonal hours of the burner operation, the timetable of the heating systems, the external daily temperature. Operation optimization is an interesting point that can be obtained using fluid dynamic models. In Lindenberger *et al*. 2000 a model for optimizing integration of boilers, heat pumps and cogeneration is performed. Fang and Lahdelma 2014 propose a steady state model a for computing mass flow rates, thermal losses and temperatures and in DHN using measurements at the users. The latter is one of the few works where the available measurements are exploited to provide information about the network state. The present dissertation aims at further contribution to this topic. In addition most of the works available in the literature are focused on small networks or a simplified representation is adopted. This thesis instead is focused on the transient analysis of large networks.

5.3 The thermo fluid-dynamic model

The model used for solving the fluid-dynamic problem is the same described in paragraph 4.4. The thermal model is based on the energy conservation equation applied to all the nodes. The energy conservation equation is expressed in transient form for two main reasons:

1. Thermal perturbations travel the network at the water velocity, which is the order of few meters per second; it depends on the request and the portion of network, in fact velocity is typically small at night and in the distribution networks. Therefore temperature variations take a lot of time to reach the thermal plants.
2. The network is characterized by a very large heat capacity.

The energy conservation equation for the i[th] node is written neglecting conduction in the fluid along the network, as:

$$\frac{\partial(\rho c \Delta T)_i}{\partial t}\Delta V_i + \sum_j c G_j T_j = U_{TOT}(T_i - T_{env}) \quad (5.1)$$

where the first term is the unsteady term, the second term represents the contribution due to mass flow rates in all the j[th] branches linked to the i[th] node and the right-hand side term contains the contribution of thermal losses. In order to relate branches and nodes an Upwind scheme (Ferziger and Peric 2002), that assigns to the j[th] branch the temperature of the previous node considering the actual fluid flow direction, is used. Equation (5.1) can be written in matrix form for all nodes:

$$\mathbf{M} \cdot \dot{\mathbf{T}} + \mathbf{K} \cdot \mathbf{T} = \mathbf{g}\,, \quad (5.2)$$

Dirichlet boundary conditions (i.e. node at imposed temperature) and an inlet mass flow rate are imposed in all the inlet sections connected to just one pipe. In the case inlet section is connected to more than one pipe so that the mass flow rates mix together, the node temperature cannot be imposed, therefore an inlet mass flow rate characterized by an imposed temperature is used. In each outlet sections an outlet mass flow rate was imposed.

5.4 Modeling Strategy

The described model can be used in order to simulate the behaviour of the supply and the return sides of the network considering them as a whole network. The correct mass flow rate required by each substation available from measurements is imposed as a constraint. This approach has been used in Sciacovelli *et al*. 2013, in Cosentino *et al*. 2014 and Cosentino *et al* 2014 (2) in order to simulate the main pipeline of the Turin DHN (500 km with 1389 branches and 1373 nodes). In this work the full network is considered. It includes about 800 km with about 20000 nodes. In Figure 5.3 the time required to solve a single iteration of the thermo fluid-dynamic model is reported as a function of number of nodes; if number of nodes become large, the computational cost dramatically increases. Therefore it is not possible with the normal physical approach analyze the whole network especially in the case multiple simulations are required. The analysis has been performed considering separately the transport pipeline and the distribution networks to allows the computational cost to be acceptable,. The entire network is modeled using a two-step approach: first the distribution network is simulated and then the obtained results are used as boundary conditions to the transport pipelines. As a results the total computational time is much lower than the one considering the whole network together.

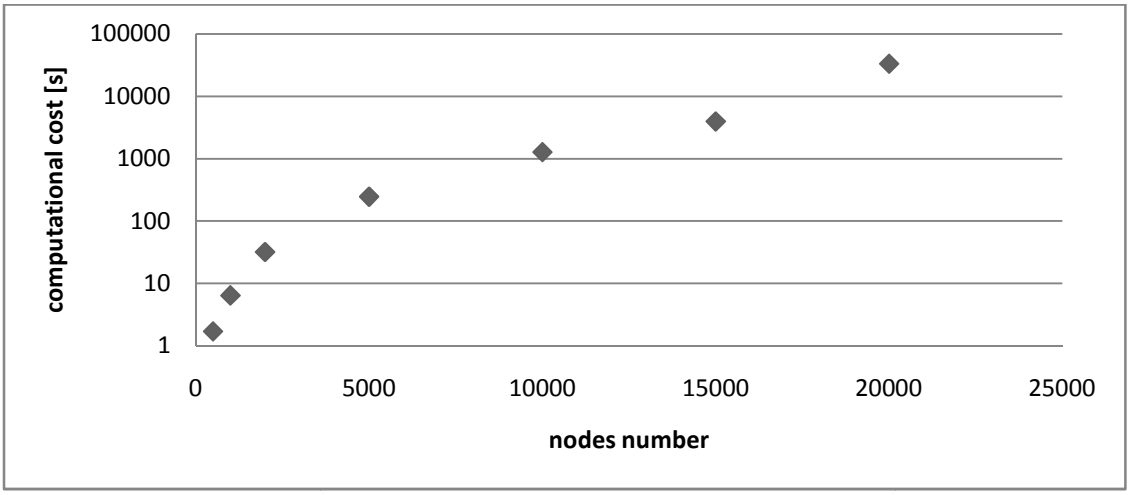

Figure 5.3. Computational time to solve the thermo fluid-dynamic model as function of the nodes number

The goal of this work is to use the fluid-dynamic model to predict the thermal request of the plant. Figure 5.4 reports a schematic of a generic district heating network that connect power plants and users with the involved thermo fluid-dynamic variables.

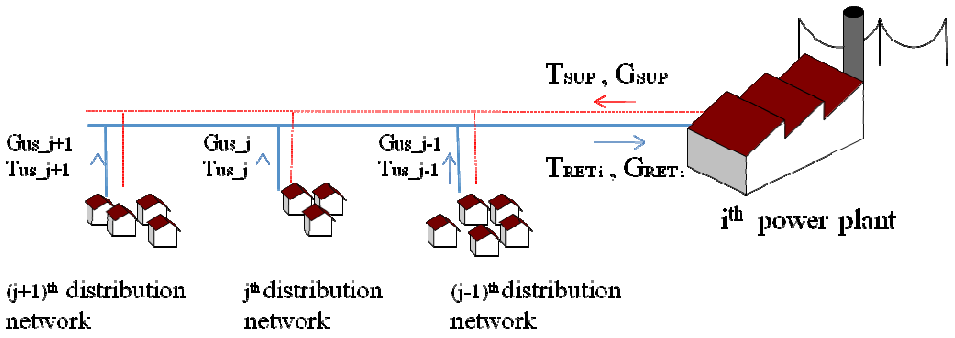

Figure 5.4. Schematic of inputs for the main pipeline model

The total heat power required to the network has been computed using the energy equation at the thermal plants, which can be expressed as:

$$\Phi = \sum_i G_{RET_i}\, c\, (T_{SUP} - T_{RET_i}) \qquad (5.3)$$

where, G_{RET_i} is the mass flow rate that enters (and exits) the i^{th} plant ,T_{SUP} is the water temperature at the outlet of the power plants (supply pipeline), T_{RET_i} is the water temperature at the inlet of the i^{th} plant (return pipeline) and c the specific heat. Mass flow rate entering the various power plants, G_{RET_i}, is a consequence of the request of the users and the start-up thermal plants strategy. The supply temperature is considered as constant at about 120°C. Water exiting the heat exchangers in the buildings flows on the return network and mixes with the various

streams coming from the various distribution networks. These streams are at different temperatures, due to the different distance of the distribution networks from the plants, which involves the fact that flows corresponding with the same portion of the request profiles reach the junction point at different times. In the end, temperature evolution at the plant is significantly different than that at the users. The present model is used for determining the temperature evolution at the plants, T_{RET_i}, starting from information at the buildings, which is crucial to investigate possible effects of actions operated at the buildings such as night attenuation or the installation of local thermal storage systems. Temperatures of water exiting the heat exchangers of the buildings in the primary side are available. These can be directly used as boundary conditions in order to simulate the return network in current operating conditions.

5.5 Thermal Model Validation

The pipeline model provides values of pressure and temperature in each node and mass flow rate in each branch. The validation of the model has been carried out comparing the temperature in some nodes of the distribution network and the corresponding experimental data. In particular, the temperatures at the inlet section of the some heat exchangers, at the primary side, have been selected. The temperature evolutions in two days, obtained with both the model and the experimental data, are compared in Figure 5.5. For each temperature evolution the corresponding mass flow rate entering the heat exchanger is also appended in order to clarify the system behaviour. During the transient, the temperature at the inlet section of user mass flow rate is not constant. During the night the temperature reaches low values in all the considered heat exchangers. This decrease is due to the very low mass flow rate in the pipeline, as shown on the right sides of the Figure 5.5, and the almost constant heat losses towards the environment. This also means that the ratio between heat transport and heat losses decreases. During the day the analyzed temperature evolutions present different peculiarities, depending on the heating strategy adopted by the user. In the case of the two buildings shown in Figures 5.5a and 5.5b the temperature is almost constant during all the day. This is due to the non-stop heating strategy of the system. In these figures it is possible to notice that a peak request occurs when the system is switched on. This is related with the decrease in the temperature of the local heating circuit (secondary side) taking place at night. When the system is switched on, the heat flux exchanged by the heat exchanger is much larger than the design value because if the very large temperature difference between primary and secondary sides. The large mass flow rate is necessary to supply such heat flux. Systems depicted in Figure 5.5c and 5.5d, contrarily, are switched off at different times during the day. The fact that the heating system is switched off can be clearly noticed from the mass flow rate evolution. Each time the system is switched on, the mass flow rate presents a peak even if this is much smaller than that occurring after night. This is because the temperature

decrease of the secondary side during the pauses is limited. The comparison between model results and experimental data demonstrates that the model is able to reproduce the daily temperature evolution in the points of the considered network with sufficient accuracy. The mean relative error is lower than 10%. In particular the model perfectly detects the temperature when the heating system is operating. During the network cooling transient, also, the model simulates properly the temperature reduction, even if the reduction takes place slower. During the daily switching off the model detects the temperature reduction but here also the trend obtain using the simulator shows a slower decrease with respect to the experimental data. The difference among model results and experimental data could be due to an imperfect isolation of the pipes where the thermocouples are located.

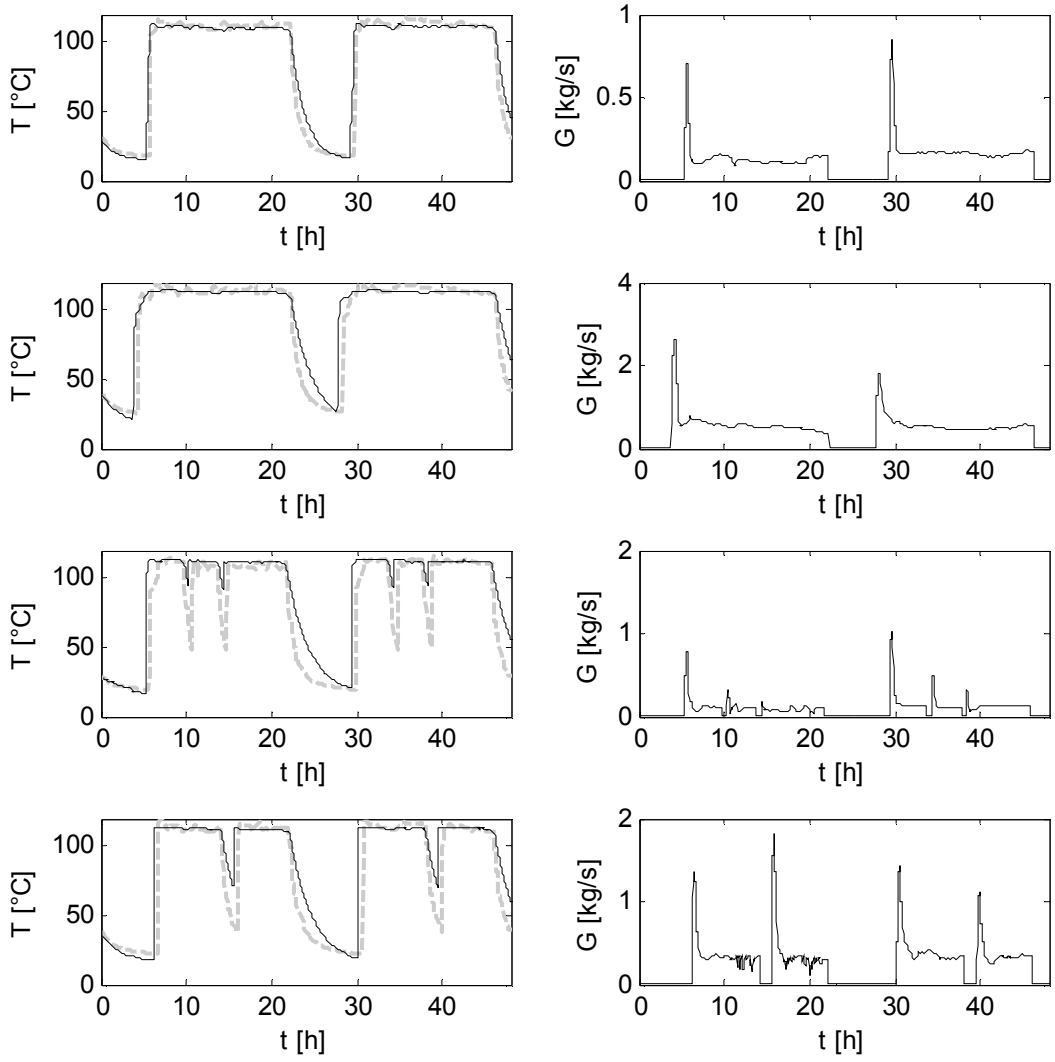

Figure 5.5. Temperature and mass flow rate at the inlet section of some users heat exchangers temperature: dashed line= experimental data, solid line=model results

The return distribution networks and the return main pipeline have been analyzed for the evaluation of the thermal energy power evolution while the supply temperature is known. The temperature in some barycentres are reported in Figure 5.6a; the corresponding mass flow rates are also shown in Figure 5.6b. The analyzed distribution networks are characterized by different values of volume of buildings connected. In particular a large, a medium and a small distribution networks, in terms of total amount of connected building volume, have been considered. Therefore, mass flow rates in the distribution networks are very different.

In general mass flow rate is constant during the last hours of the evening, then it dramatically decreases at 11 p.m. and it remains about constant during the night. Early in the morning the mass flow rate gradually increases between 5 a.m. and 6.30 a.m. in order to satisfy the start-up requirements. Then it decreases and after 8 a.m. it remains constant. Temperatures are between 40°C and 50°C. These values remains quite high also during the night because some of the connected users require thermal power also during the night.

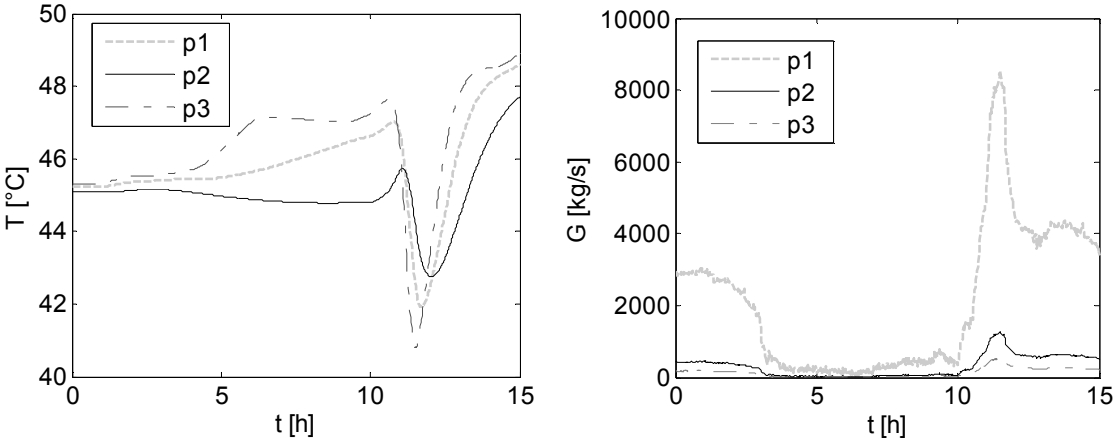

Figure 5.6. Temperature in some points linking a distribution networks with the return main pipeline

The heat power required to the thermal plants are collected in order to evaluate the total load. The results obtained are reported in Figure 5.7. In the examined scenario, which corresponds to a cold day of April, the base thermal power is mainly provided to the Torino Nord power plant, which is a cogeneration power plant. The other cogeneration plant, i.e. Moncalieri power plant, is used only during the start-up transient, in the morning. The energy storage units provide heat in the evening and during the morning peak, while during night they are charged, as shown to the negative values in Figure 5.7. The Bit power plant is not used. The comparison with measured data shows that the model is able to predict with a good level of accuracy the thermal load required to each thermal plant.

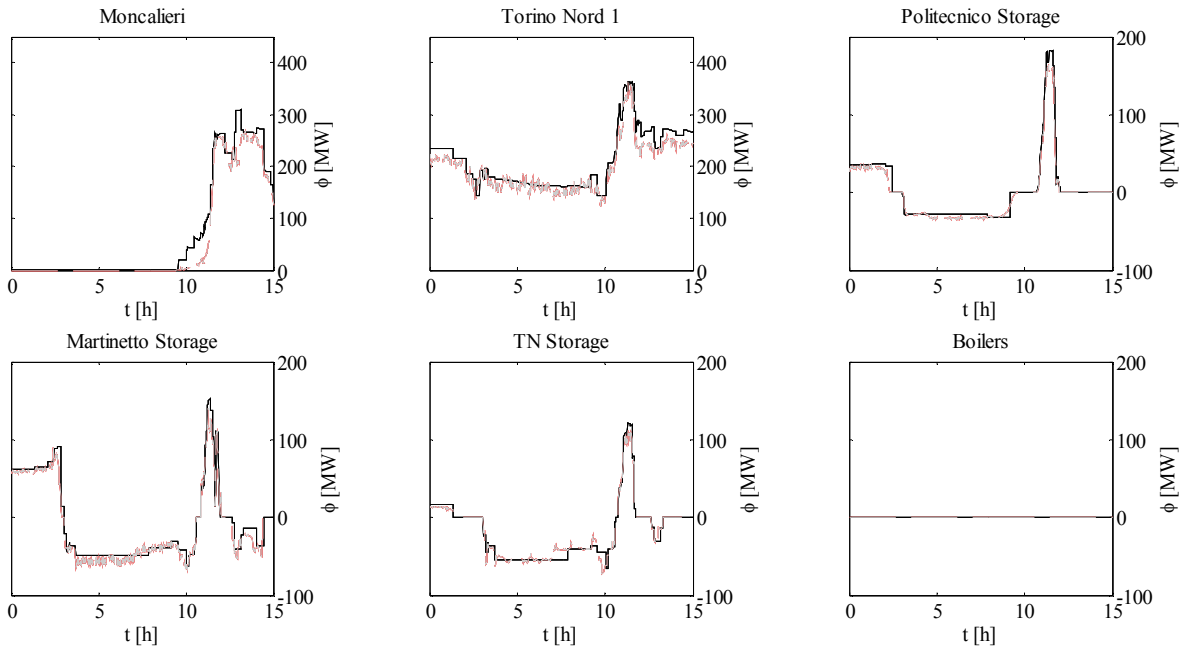

Figure 7. Heat Flux evolution at the thermal plants

The evolution of total thermal power during the transient between 7.00 p.m. and 10.00 a.m. is reported in Figure 5.8. During the evening the heat power is almost constant and it is about 330 MW. In this part of the analyzed period the model slightly overestimates the required power. During the night, the load reduces to about 70 MW and remains almost constant until early morning. In this portion of curve the model is able to simulate real data with good accuracy. The energy demand reaches the maximum value of about 800 MW during start-up, at 6.45 a.m. After that the heat required slightly decreases until a value of about 450 MW.

The thermo fluid-dynamic model is able to detect the heat power evolution during the considered period; it is able to predict the peak load position and with a certain level of approximation also the quantity of power required. However the small differences occurring between real and simulated power evolution are probably mainly due the uncertainties related to the available data as well as on the fact that the data registered by the monitoring system refer to about 50% of the connected users, therefore the lacking data have been obtained through extrapolation.

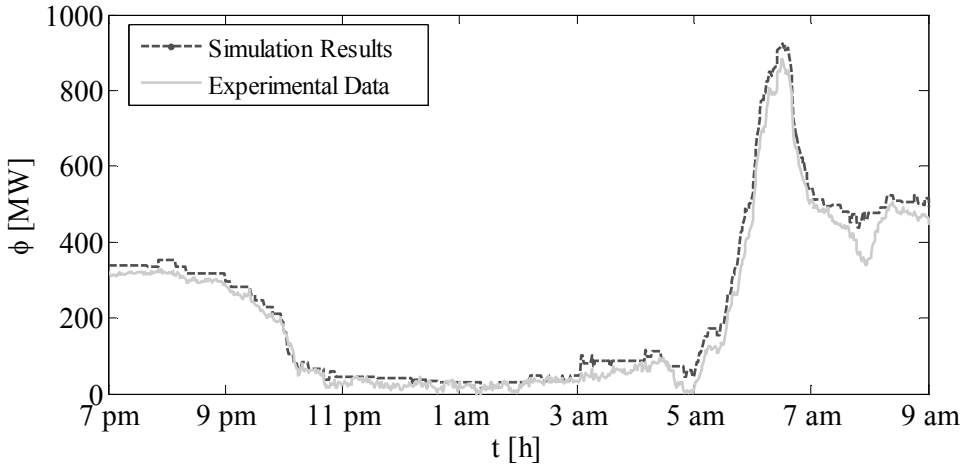

Figure 5.8. Total heat power evolution during the night transient. Comparison between real data and simulation results.

The results provided to the model could be used to predict the thermal power demand and peak load position with different load conditions in order to implements primary energy saving plans strategies.

The computational time needed to solve the thermo fluid-dynamic model for the entire transient on a single 3.3 GHz CPU is about 800 s. Therefore it seems that this model can be used in order to simulate behavior of large district heating network with an appreciably low computational cost.

5.6 Model Reduction

5.6.1 Model Reduction Approach

As detailed in paragraph 4.5 the fluid-dynamic problem, that is nonlinear, has been solved using a SIMPLE algorithm (Patankar 1980), that is a prediction and correction method. The SIMPLE make the computational cost quite high. Each time step fluid-dynamic simulation in the Turin main supply network needs about 2 s, as detailed in Figure 5.3. When the period that has to been simulated is long or when multiple simulation are necessary, a too high computational cost can reduce the practical usage of the tool. In order to make the model faster, a POD-RBF model has been applied to the main network model. In fact, the main issue of the fluid-dynamic model is the evaluation of the mass flow rate flowing in the different loops; once those values are calculated the mass flow rates in all the other nodes are directly obtained through the mass balance reported in Eq. (4.3). The POD-RBF model has been used to obtain the mass flow rates in the different loops. In this case, the input vector **d** includes the mass flow rate produced from each power plant. The POD-RBF model outputs, collected in the snapshots matrix **u**, are the mass flow rates in each loops. The POD-RBF procedure described in paragraph 2.4 has been used.

5.6.2 Reduced Model test results

The reduced model has been tested in order to evaluate its effectiveness for calculating the total thermal load required to the network. At first, the model capability of evaluating the direction and the quantity of water flowing inside each loop is tested. Results are depicted in Figure 5.9. The direction of the flow inside the loop is always captured by the POD-RBF model. The quantity of water is always well detected. A maximum error of 10% has been encountered.

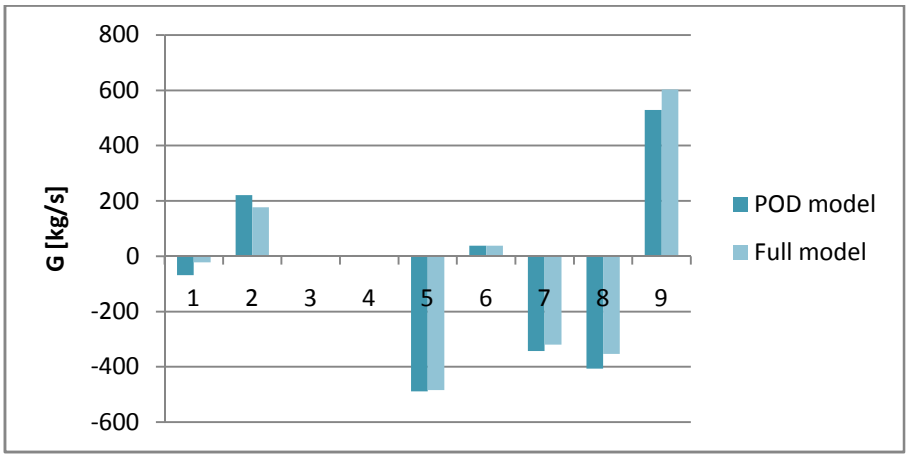

Figure 5.9. Comparison between Full and Reduced models: mass flow rates in each network loops

The error becomes negligible when the total heat power required by the users are compared. This is the most important result in order to evaluate the POD-RBF applicability to this kind of system. Results reported in Figure 5.10 suggest that the use of the POD-RBF model does not reduce the simulation accuracy significantly. The two evolutions in the graph are not discernable, therefore it is reasonable to assume that the reduced model can be used instead of the full model without any significant loss of detail in the results.

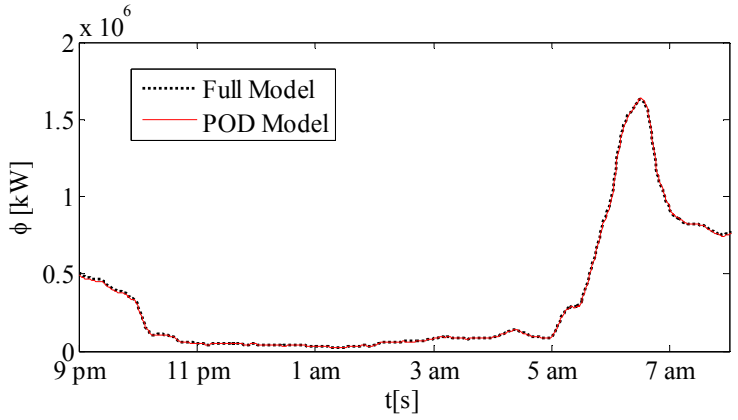

Figure 5.10. Comparison between Full and Reduced models: total power required to the power plants

In Figure 5.10 the computational cost to run the Full and Reduced models in 15 hour operation simulation are reported. Simulations have been performed on a single 3.3 GHz CPU. The use of the POD model allows a computational cost reduction of 90 % respect to the use of the full model. This characteristics makes the reduced model suitable for real time operation analysis and district heating management improvement and optimization.

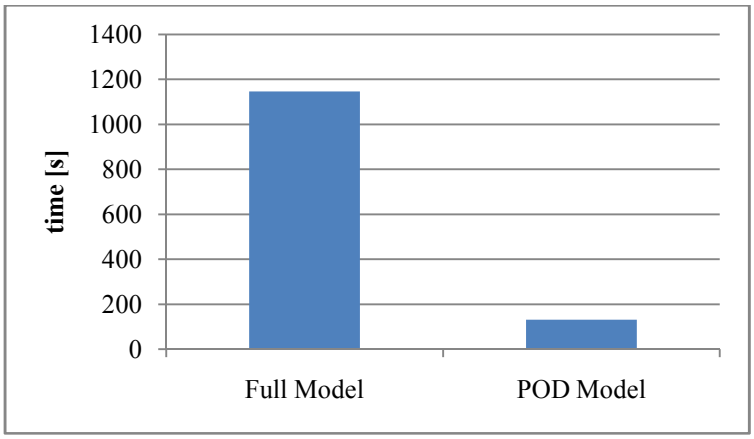

Figure 5.11. Comparison between Full and Reduced models: computational cost

5.7 Thermal Model application for storage installation

The physical simulation tool can be applied to large district heating networks for the analysis of peak load shaving. Here the model has been used to analyze possible future network improvements. In fact the connection of an additional part of network has been already planned. In particular the opportunity of using some storage systems to feed the new part of network is currently being examined. Therefore the proposed simulation tool is used to study the network including the new part. The goal is to quantify how the additional part of the new network may affect the peak thermal load, considering two different cases, with and without the installation of storage units. The storage units are supposed to be fed one hour before the heating systems starting. In Figure 5.12 the comparison is shown; Figure 5.12a shows the full transient operation, while in 5.12b the peak detail is reported. The presence of the storage induces an increase in thermal request between 4.30 a.m. and 5.30 a.m. and a remarkable reduction of the peak thermal load. This allows the use of the cogeneration plants for a larger fraction of the thermal request. In fact the peak shaving allows a lower use of boiler with a consequent primary energy saving. In particular, the maximum peak is here reduced of about 60 MW. The total energy amount removed to the peak thanks to the storage installation, in the day considered, is about 25 MWh.

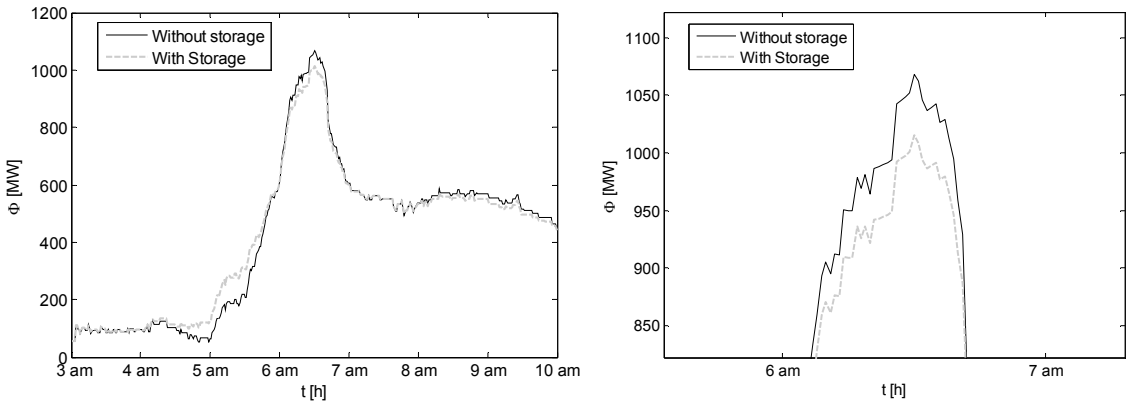

Figure 5.12. Thermal load after the inclusion of the new area.
a) Full transient operations b) Peak comparison

5.8 Thermal Model for Optimizing switching on time of the heating systems

The physical model is used for studying the possibilities for peak shaving trough optimal changes in user thermal requests. In particular, changes in the start-up time of heating systems of some users located in a distribution network have been studied. The optimization tool allows to evaluate the best set of anticipations of the heating system start-up time in order to minimize the energy fraction produced trough boilers. The effects of the heating system start-up time on the total request evolution of the district heating network have been simulated using a physical model. This is necessary because of the long distances involved in the network, which cause a temperature evolution at the barycentre significantly different than that at the users. The optimizer has been applied to one of the distribution networks of the Turin DHN (see section 4.3). Details about the distribution network are available in the next paragraph.

5.8.1 Distribution network description

The selected distribution network is the one shown whit the yellow circle in Figure 5.13. This is indicated in the full network topology as BCT_414. It is 4.7 km long and links the transport network to 103 buildings. It is included in the so-called Polito District, which is the district selected for the DIMMER project. This is a university district not far from the city center and it includes public and private buildings with different intended uses.

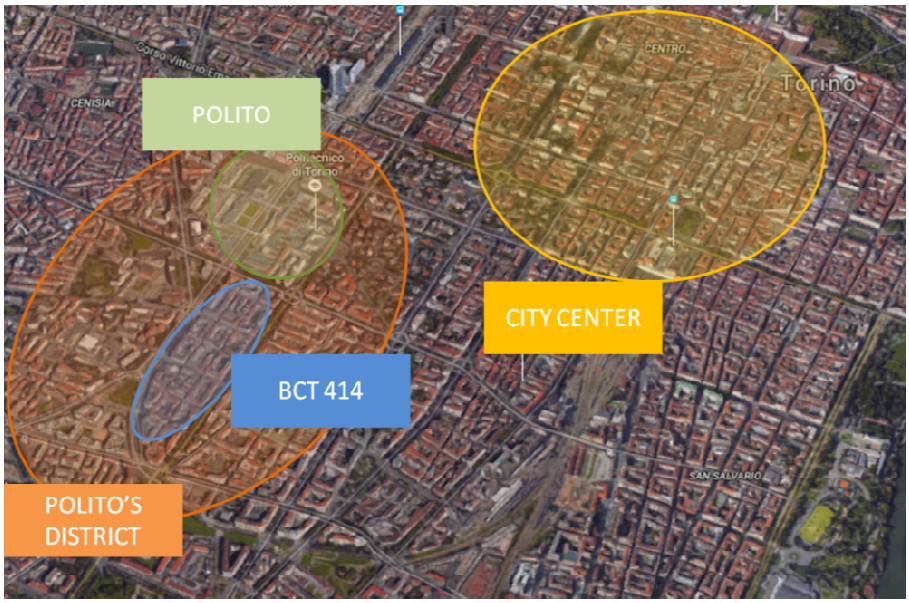

Figure 5.13. Description of the selected area

The Polito District is a good test case in order to analyze energy saving opportunities and the possibility to extend methodologies and results to other districts of the city. To show that Polito District can be considered as representative of the Turin DHS an analysis of the building typologies has been conducted. Various pieces of information at a global level have been collected: annual heating consumption, volume, surface, year of construction. In Figure 5.14 some of the characteristics analyzed are reported: users typology (Figure 5.14a), buildings energy performances (Figure 5.14b) and construction period (Figure 5.14c).

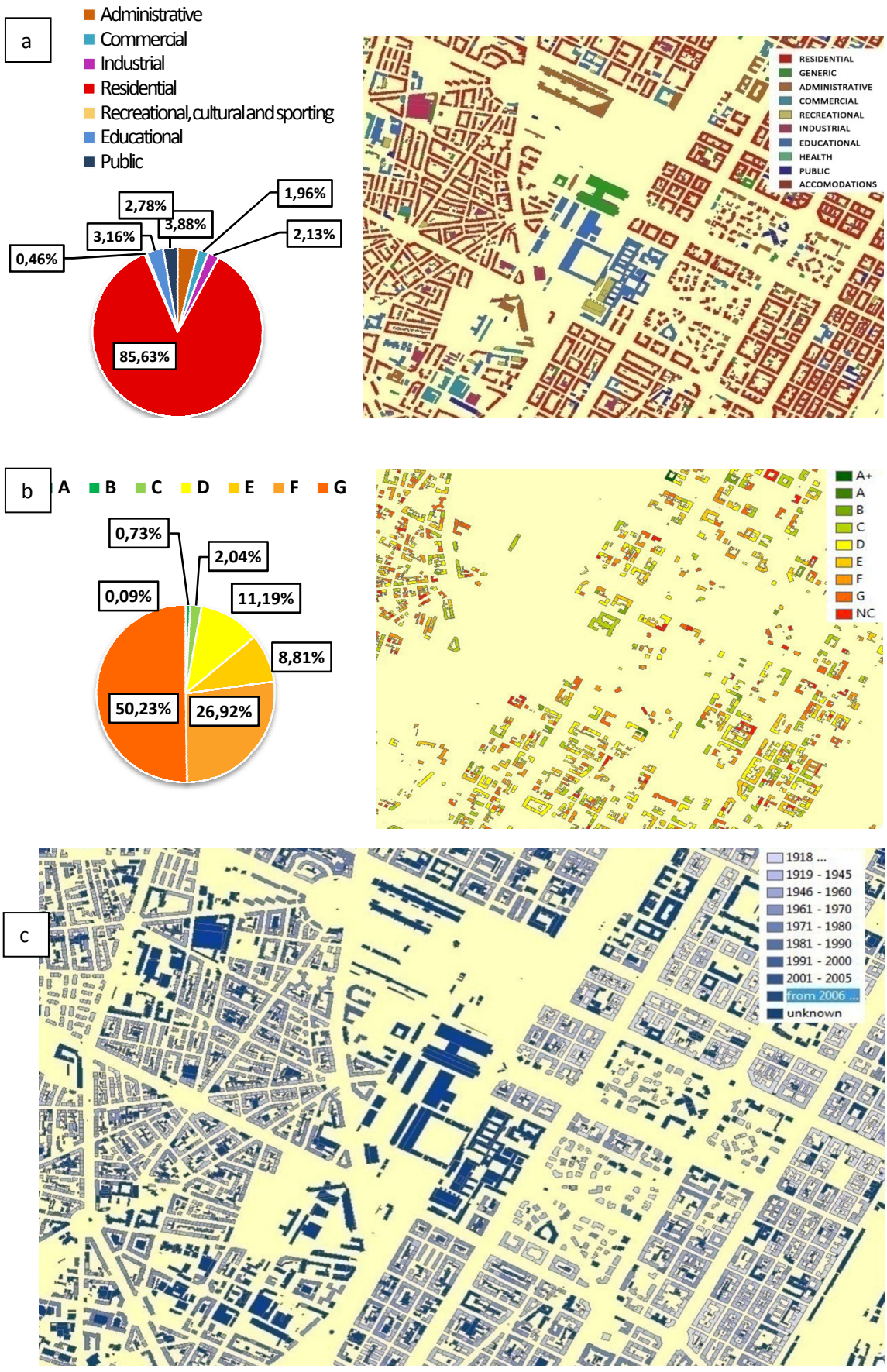

Figure5.14. Analysis of the Polito District: a) Buildings use b) Buildings Energy performances 3) Buildings construction period

The analysis of the Polito District with respect to the entire town is based on data collected for about 5% of the buildings connected to the district heating network. The buildings are distributed along the network in several areas; this guarantees the representativeness of the buildings selected.

Concerning the year of construction, the thermal request as a function of the construction period are reported in Figure 5.15. The five epochs of construction are selected as follows:

- epoch 1: before 1918 ; 44% of the buildings;
- epoch 2: between 1918 and 1945 ; 14%
- epoch 3: between 1946 and 1960 ; 21%
- epoch 4: between 1961 and 1970 ; 17%
- epoch 5: after 1971 ; 4%

The average value is the same for the various buildings (between 31 kWh/m3 and 36 kWh/m3). The standard deviation obtained for the examined buildings is also shown in the figure.

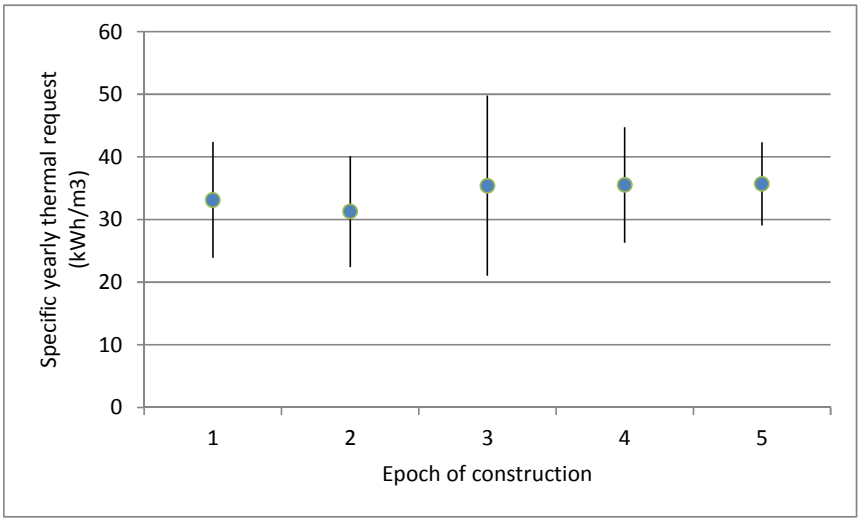

Figure 5.15– Specific yearly thermal request of the buildings depending on the epoch of construction

The annual thermal request as a function of volume and shape factor (that is ratio between surface and volume) is performed. The results, depicted in Figure 5.16 show the correlation among the buildings volume and the thermal request. The same figure shows that the shape factor does not significantly affect the thermal demand.

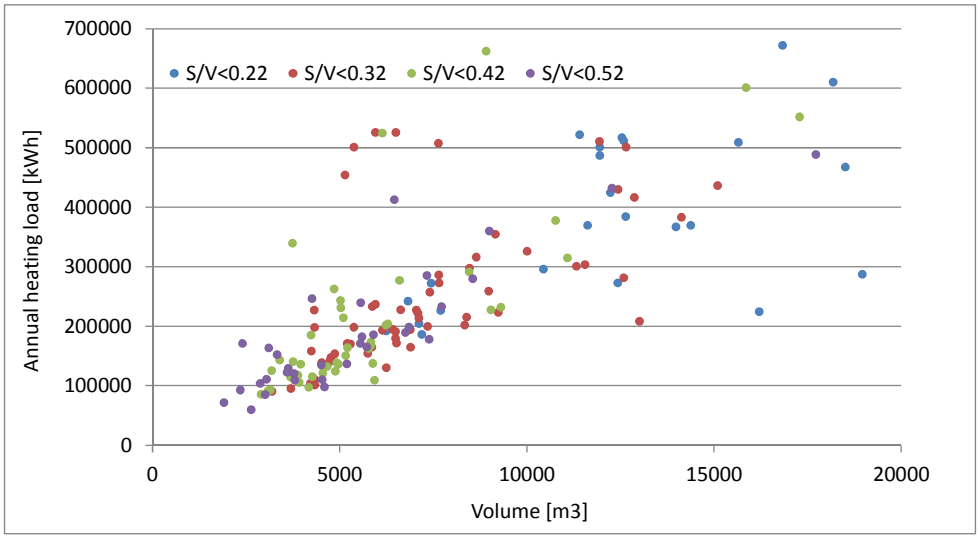

Figure 5.16– Annual thermal request of the buildings as the function of volume, for four groups of shape factors.

This analysis shows that the district is sufficiently representative of the entire network, since the distribution of volumes is similar to the one of the buildings selected in different areas of the network. Distributions for Turin (5% of the buildings) and the Polito District are shown in Figure 5.17.

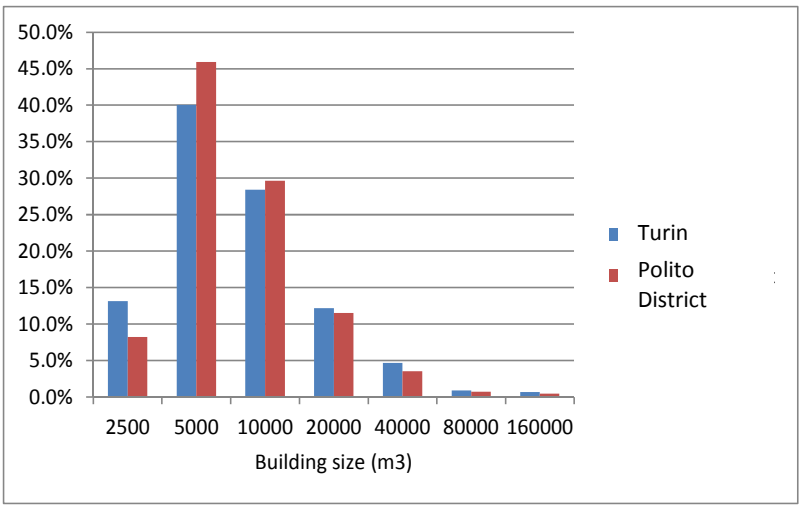

Figure 5.17 – Volume distribution of the buildings in the district and in town.

The BCT 414 (reported in Figure 5.18) is used as a case study because of the large number of buildings connected to this network that are monitored using the data gathering system. Moreover about 30% of the buildings have a switching on schedule which can be varied.

Figure 5.18. Schematic of the selected distribution network

5.8.2 Data gathering

In order to performed the optimization of the switching on times of the heating systems, it is necessary to know the expected thermal profile of each building. With this aims, the data gathering system has been used. In particular when a particular future day (DATE1) is chosen for carrying out the optimization, the expected external temperature for that day is selected through weather forecast. Also the day type of DATE1 is selected, as the user behavior affect the energy consumption evolution Fang and Lahdelma 2014. If the day selected is Saturday, offices are closed therefore the heat demand is lower than in working days, while if it is Sunday most offices are closed and the request is even smaller than in the other days. If it is Monday the heat request is larger because of the need of increasing the temperature in the buildings that switch off the heating system during the weekend. The other days are considered to have a similar temperature request at a given external temperature.

Secondly a past day (DATE2) with an external temperature similar to the one of DATE1 and the same day of the week (Saturday, Sunday, Monday or other days), is selected. The data collected through the gathering system for the DATE2 are used as the expected thermal request for the day DATE1.

In the considered distribution network a system for the data gathering is installed in almost all the heat exchangers of buildings connected to the distribution network. The data collection system

has been created out with the aim of gathering quantities that allow one to characterize the energy consumption and the comfort conditions.

Most of the heat exchangers in the BCT_414 have been equipped with a flow meter on the primary sides. Three of the four temperatures at the inlet and outlet sections of the heat exchangers are also monitored: the inlet (T1) and outlet (T2) temperatures on the primary side (the distribution network side) and the temperature of water supplied to the building heating systems (T3). Some of the heat exchangers have been recently equipped with a fourth temperature sensor on the inlet section of the secondary side. In Figure 5.19 the data collected in a winter day have been reported.

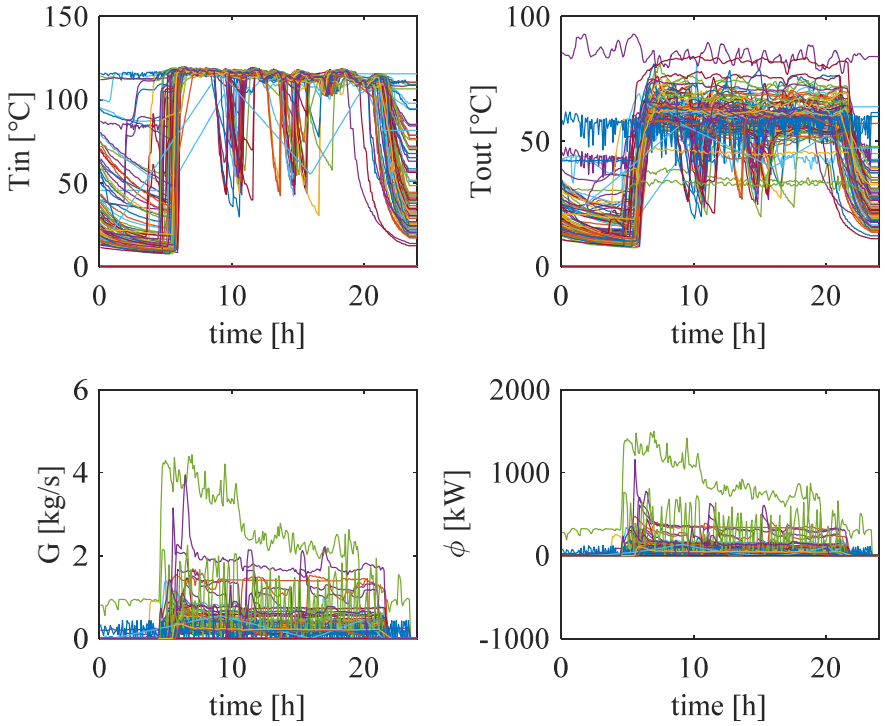

Figure 5.19. Data collected at the heat exchangers of users in the BCT_414

Figure 5.19 reports the evolution of the temperature at the inlet section, the outlet section, the mass flow rate at the primary side and, as an elaboration of these 3 sets of data, the heat flux requested evolution. Through the analysis of the inlet temperature evolution, it is clear that most of the heating systems are switched off during the night and are switched on between 5 a.m. and 6 a.m. During the day, the inlet temperatures are all between 115°C and 118 °C. Some of the users are never switched off and their inlet temperatures are about constant. The difference of these values is due to the different distances from the transport network and the user nodes. In fact a user located near the transportation pipeline receives water at a higher temperature than a user

located far from the transportation pipeline, because of the different thermal losses. The larger the distance between the user and the thermal barycentre, the larger the thermal losses and the lower the inlet temperature at the heat exchanger. The temperature in the outlet section of the heat exchanger depends on the inlet temperature, on the mass flow rate and the temperature level at the secondary side. Most of the values are between 55 °C and 75 °C. As regards mass flow rate and heat power evolutions, they often present various peaks during the daily transient. These peaks occur when the heating system is switched on; the highest peak is the early morning peak (that is the one that has to be reduced). This point is confirmed also from Figure 5.20, which depicts the sum of the power request of all the users (in the left part) and a detail of the peak time (on the right part). In particular, the time period considered for the peak analysis and minimization, as reported in Figure 4b, is between 5.00 a.m. - 8.00 a.m.

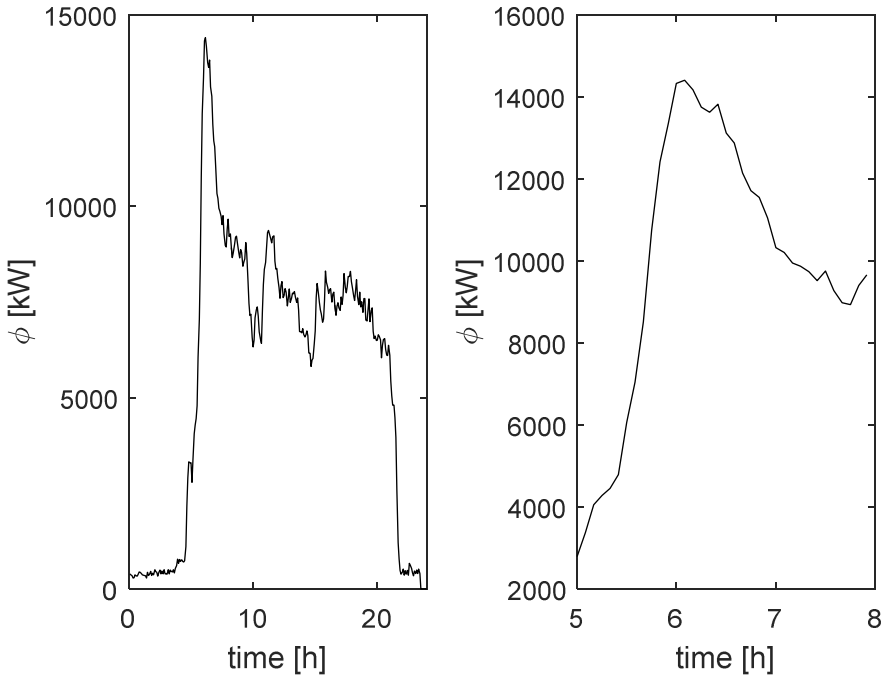

Figure 5.20. Total heat request at the BCT_414

Unfortunately for technical reasons not all the considered distribution networks can be included in the anticipation evaluation. Some users can be included only in some periods and other users can never be included. The distinction from the user that can, always or sometimes, be varied and the users that can never be varied is detailed in Figure 5.21. It is clear from the figure that most of the thermal power request can be modified trough a switching time rescheduling.

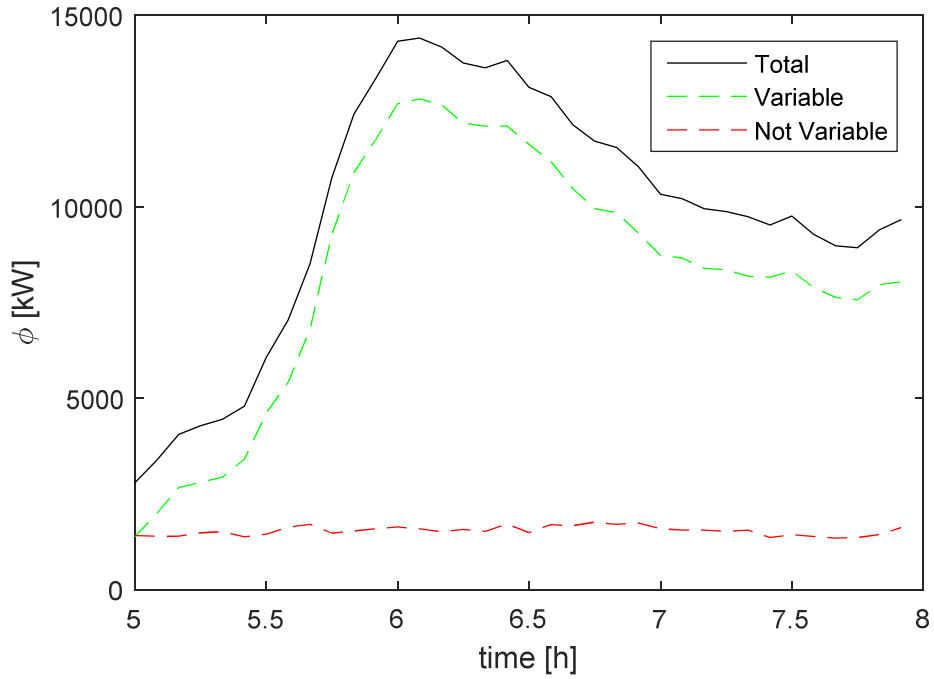

Figure 5.21. Variable and not variable amount of heat requests at the BCT_414

5.8.3 Optimization tool description

The optimization model aims at finding the best set of start-up time anticipations for the heating systems x that allows to minimize the chosen objective function. As not all the 103 thermal profiles can be changed, only a fraction of the buildings is considered in the optimization, while the other requests are considered as not adjustable. Therefore the total number of independent variable, with the control system used nowadays, is 96; as a consequence x is a vector 96x1.

Before discussing the optimization approach two aspects should be considered. Variations in the request profile involve possible changes in the indoor temperature. These should be checked using a proper model of buildings. In the case the indoor temperature should not decrease below the values prior to the anticipation, a larger thermal request for the buildings is registered. Thanks the larger exploitation of cogeneration, primary energy consumption is expected to decrease despite the additional heat request.

The variable x can assume only discrete values since the time demand modification is performed considering slots of 10 minute multiples. This assumption is related with the structure of the ICT system which commands the rescheduling. As the optimization tool still does not integrate the indoor temperature simulator (see paragraph 5.9) , the change in temperature profiles are limited to 20 minutes. This allow one not to increase too much the heat request. Therefore each profile

start-up time modification can be chosen among the following values: 0 minutes, 10 minutes, 20 minutes. In order to further limit the heat request, when a 20 minutes modification is selected, a partial heat recovery is considered through 10 minute anticipation of the time the system is switched off. This means that currently the user thermal request can increase with respect to the current operation of an energy consumption equal to an extra 10 minute operation.

A genetic algorithm, specifically set for integer-values, has been used to perform the minimization. The selected population members is 30 and the selected generation number is 20.

The network model is used to take into account the effects of the long distances on the water temperature. The streams coming from the different users are at different temperatures, due to the different distance of the users respect to the barycentres. Water exiting the heat exchangers flows on the return distribution network and mixes with the various streams coming from the users located in the other areas, thus changing its temperature. This is the reason why the temperature evolution at the barycentre is significantly different than that at the users and a thermal fluid dynamic mode is required. Temperature of water returning to the plants is further different and affects the thermal power exchanged at plants. This point is discussed with an example in section 5.8.4.

Different objective functions can be considered in order to select the desired optimization criteria.

1. In the first case the set of optimal values x allows one to minimizing heat produced through boilers in order to increase the cogeneration exploitation. The objective function that has to be minimized is the time integral of the thermal power when the thermal power exceeds the cogeneration maximum heat flux.

$$Q_{Non\_cog\_hp} = \int_{t_a}^{t_b} \Phi_{th_{tot}}(t)dt - \Phi_{maxCog}(t_b - t_a) \tag{5.4}$$

In the case of the application to a distribution networks the maximum heat flux produced in cogeneration mode is calculated as proportion of the nominal request the barycentre 414 with respect to the total request of the network. Te current request of the barycentre is:

$$\Phi_{BCT_{414}}(t) = G_{TOT\_BCT_{414}}(t)\, c_p\, (T_{supply} - T_{ret\_nodeBCT_{414}}(t)) \tag{5.5}$$

where t_a is time when the heat request exceed the maximum cogeneration power, tb is time when the system starts requiring only cogeneration power, $T_{ret\_nodeBCT_{414}}$ is the temperature of water exiting the distribution network and $G_{TOT\_BCT_{414}}(t)$ is the circulating mass flow rate. The various quantities are reported in Figure 5.22.

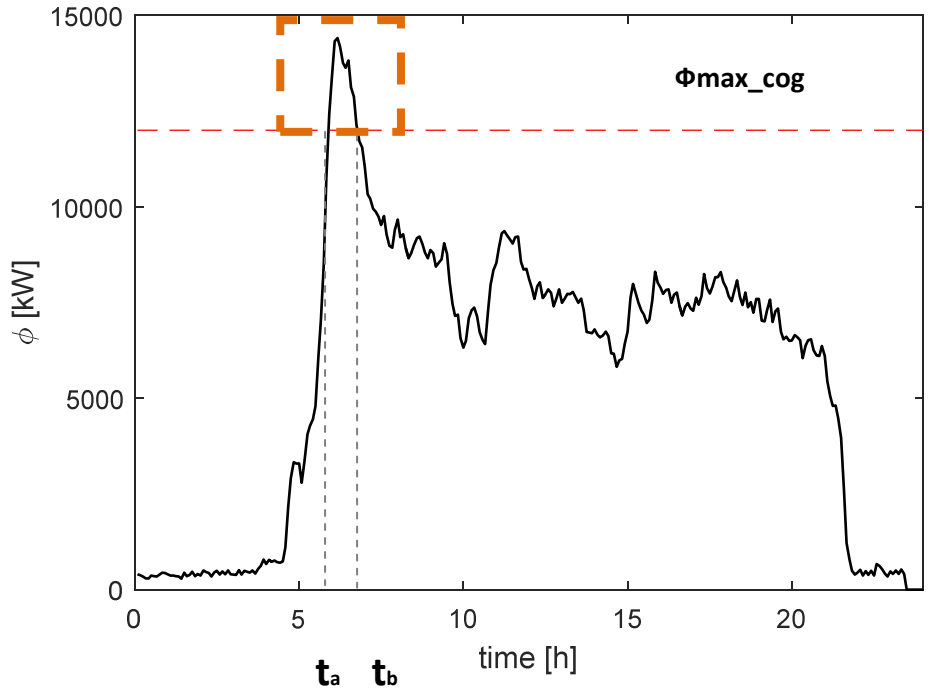

Figure 5.22. Thermal power evolution and, in evidence, the area to minimize as the objective function

2. In the second case the optimizer allows one minimizing the maximum peak value. It can be used when the thermal peak do not necessarily exceed the cogeneration maximum production and the goal is to reduce the peak in order to check the potential advantages in connecting additional buildings to the network . It can also be useful when the cogeneration fraction is not fixed in advance and the aim is to guarantee a thermal profile that is as flat as possible. This can be used for instance to check the possibility to decrease the electricity production. The objective function is:

$$\Phi_{max} = \max(\Phi_{BCT_{414}}(t)) \quad (5.6)$$

where

$$\Phi_{BCT_{414}}(t) = G_{TOT\_BCT_{414}}(t)\, c_p\, (T_{supply} - T_{ret\_nodeBCT_{414}}(t)) \quad (5.7)$$

In all the cases $T_{ret\_nodeBCT414}$ is evaluated through the thermal fluid-dynamic model

5.8.4 Optimization Results

Distances between the various users and the barycentre node have an effect on the temperature evolution in the network; this means that an optimization conducted at a district level is not just the summation of optimizations of single buildings. Figure 5.6 reports the curve obtained by

summing the thermal requests of all the users (dashed line) and the total thermal request at the barycentre (plain line); the latter takes into account the effects due to the delay time associated with the network topology and the heat losses. In particular, the dashed line assumes higher values before 6 a.m, and lower values in the following period, due to the fact that the time for water flow to reach the barycentre point is not considered. Furthermore, the integral of the plain curve is larger than the integral of the dashed curved, which is due to the fact that the power plants provide not only the heat required by the buildings but also the heat necessary to rise water temperature in the distribution network..

This proves that knowledge of the thermal request of users is not sufficient for studying the network behavior. Therefore, a thermo-fluid dynamic model is necessary in order to analyze peak shaving strategies properly.

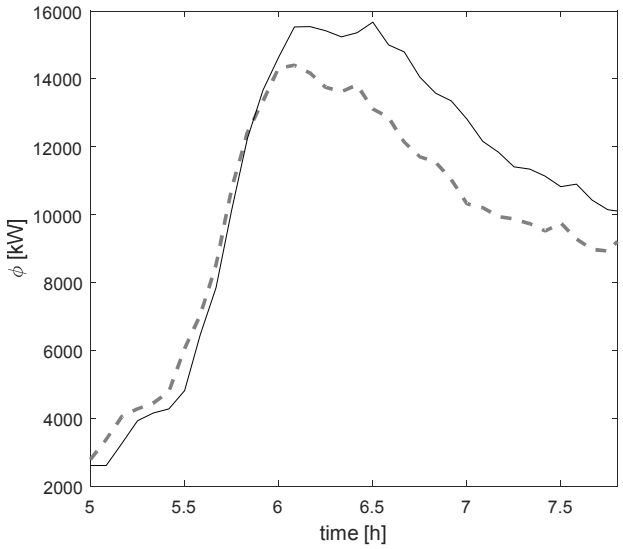

Figure 5.23. Thermal request evolution at the barycentre node (plain line) and sum of the user thermal requests (dashed line)

In Figure 5.24 the optimized thermal load evolution obtained respectively with the boiler production minimization and the peak minimization are depicted. The curve obtained with the optimized strategy is shifted with respect to that corresponding with current scenario because of the switching on anticipation of the heating systems. The grey horizontal line represents the maximum cogeneration power that can be provided to the distribution network.

As regards the first optimization approach, the integral above the grey horizontal line has been minimized. The figure clearly shows that, when the optimization is performed, the area corresponding to the heat produced trough boilers is reduced with respect to the one obtained with the current strategy. The maximum peak value instead is not significantly reduced.

When the second optimization approach is applied, the maximum value of the peak is clearly reduced, while the boiler production it is not significantly different with respect to that in the current scenario.

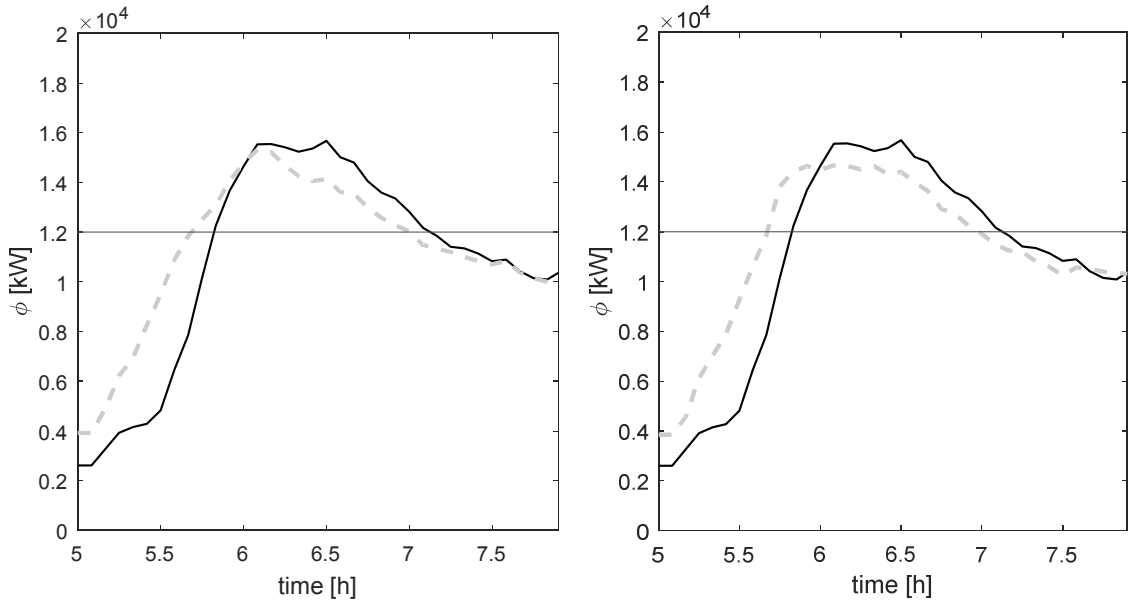

Figure 5.24. Optimized results (dark dashed line) compared to the current strategy (continuous lines): a) CASE A :Boiler production minimization b) CASE B: Thermal peak minimization

To make the comparison more clear the total heat required and the type of heat generation in the various cases is shown in Figure 5.24. The total thermal consumption corresponding with the optimized cases is clearly higher than in the current case, due to the additional consumption associated with anticipated starting of the heating system, which is only partially recovered during the day. In fact, the anticipated switching leads to an increase of the time period when the heating system is operating. In CASE A, the total energy increase is about 4% while in CASE B is about 4.4%. The total heat generation is provided in two different ways: trough cogeneration and trough boiler systems. Clearly the amount of heat produced in a cogeneration system allows to better exploit the use of fossil fuel due to the possibility of combine production of heat and electricity. In both the optimized cases the fraction of heat produced with a cogeneration system is larger than in the current scenario. In CASE A, the cogeneration fraction is about 93 %, in CASE B about 92% and in the current scenario about 90% (all the percentage refers to the considered barycentre). As a consequence, the use of heat produced through boilers is reduced (CASE A 7 %, CASE B 8%, current scenario 10%)

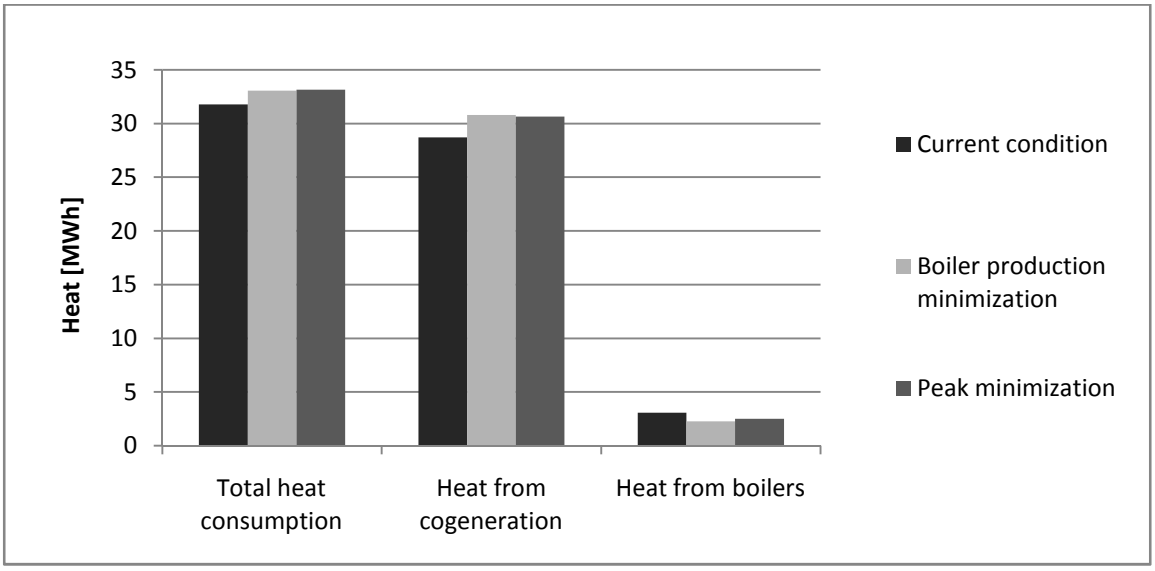

Figure 5.25. Amount of heat required in the current condition and in the optimized cases

Figure 5.26a reports the results in terms of primary energy consumption required in the different cases. The ratio between primary energy consumption and heat produced is considered 1.11 for the boilers and 0.36 for the cogeneration system. As regards the CASE A, even if the total energy request increases of about 1.27 MWh/day, the overall primary energy consumption decreases because of the higher performances of cogeneration with respect to the boilers. The energy savings obtained with the best set of anticipation is about 0.17 MWh/day. This correspond to the primary energy savings of about 1.25 % of the fuel consumption for the distribution network. As regards CASE B, an increase of the primary energy consumption is verified. This result warns to the use of the second optimization approach for primary energy reduction when the maximum production of cogeneration is not known. Nevertheless, this approach is very effective with respect to the minimization of the peak. In addition, the analysis should be properly combined with the opportunities such as the possibility to produce an additional amount of electricity(operating scenario) or the connection of additional users (design scenario). Figure 5.26b reports the maximum values assumed to the thermal evolution in the three considered cases. The peak reduction in the CASE B is about 900 kW; that means that the peak is reduced of about the 6% with respect to the current scenario.

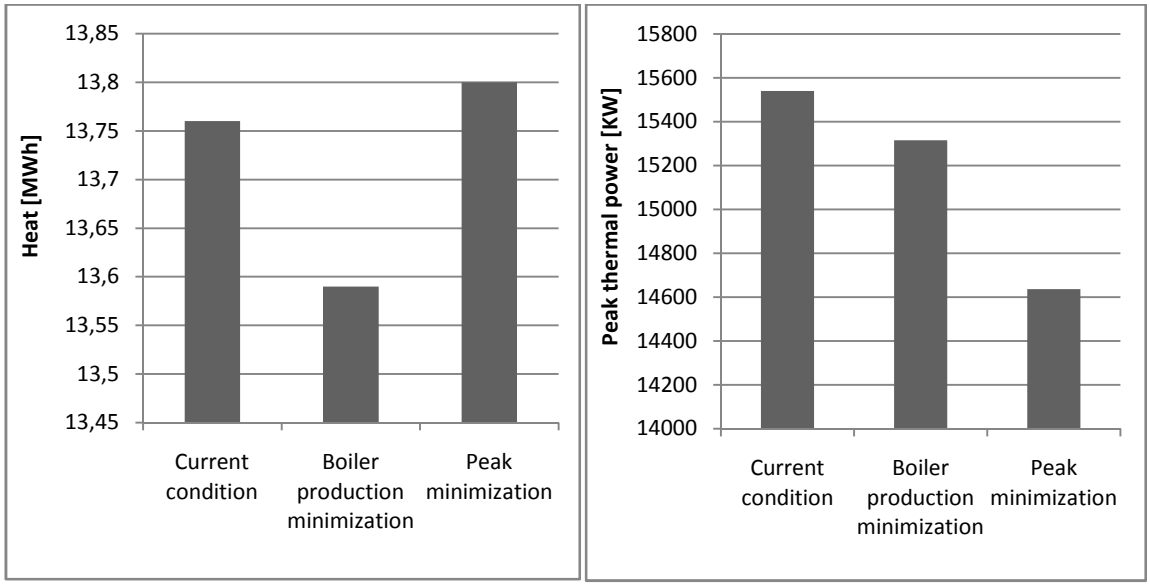

Figure 5.26. Current condition and in the optimized cases comparison: a) Primary energy consumption b) Maximum peak value

As regards the computational cost, the optimization tool provides the optimum set of anticipation using a single 3.3 GHz CPU in about 2 hours. This is a crucial feature to allow optimal operation in real networks. It is worth mentioning the fact that the approach corresponding with peak minimization has been implemented in March 2016 in the Turin district heating network, in the examined barycentre.

5.8.5 Optimization in the real case

The model has been used in order to reduce the thermal peak in March 2016 in the distribution network BCT 414 of the Turin district heating network. The results of the modified schedule have been collected through the monitoring system. A comparison between some results obtained in various days, before and after the use of the peak shaving strategy are reported in Figure 5.27. The figure depicts the evolution of the thermal load for the different days and the corresponding environmental temperature. The reported evolutions have all quite similar shapes and in particular it is possible to notice that the amount of heat request is not clearly related with the external temperature. Therefore the external temperature is just one of the parameters that affect the thermal load. For instance the thermal load may be affected to the temperature of the previous days due to thermal capacity of the buildings. The two curves indicated with MOD correspond to the application of the peak shaving strategy, while the curves labeled with OLD correspond to the strategy without changes. In the examined period, the following schedule changes have been applied.

1. Scenario MOD T_{env}=3.9°C: for 23 buildings an anticipation of 20 minutes has been applied , for 2 buildings an anticipation of 10 minutes has been applied; 7 buildings have not been modified in the schedule despite the possibility to do it.
2. Scenario MOD T_{env}=9.1°C: for 17 buildings an anticipation of 20 minutes has been applied , for 3 buildings an anticipation of 10 minutes has been applied; 14 buildings have not been modified in the schedule despite the possibility to do it.

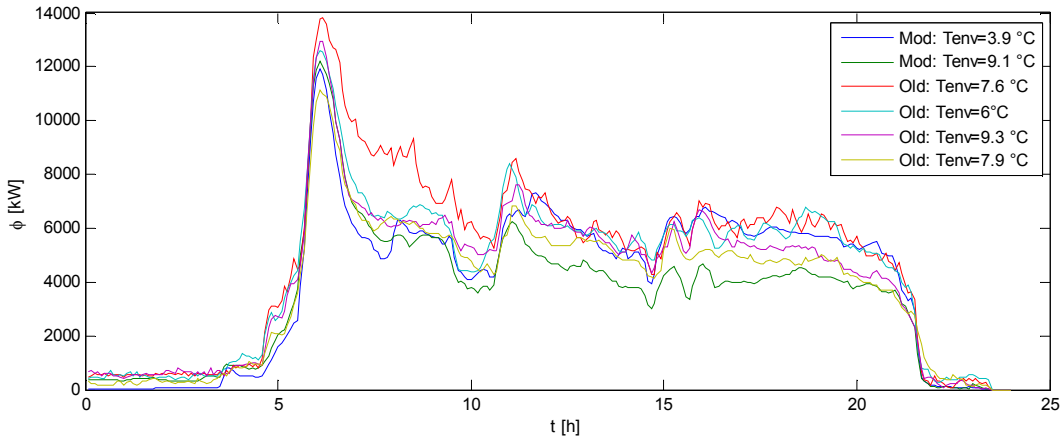

Figure 5.27. Measured thermal consumption of the BCT 414 in several cases. Mod= with peak reduction tool. Old= without peak reduction tool

In order to better compare the effects of the peak reduction tool it is worth to consider only the users that, in all the considered days, had the data transfer system able to deliver data. In fact the data transmission system may not be always able to deliver data due to absence of signal. The sums of the users always communicating for the days previously selected are reported in Figure 5.28. Only the period when the peak takes place has been considered. To better distinguish the different curves the two curves obtained after the tool use are reported through dashed lines. Furthermore a detail of the more interesting zone is also reported in Figure 5.29. The figure shows that the thermal peaks obtained with the fluid-dynamic tool are more flat than the others. This can be noticed, in particular, by comparing the green (MOD) line and the yellow (OLD) line. The thermal request associated to the green line increases faster than the yellow line, but the maximum value of the green line (10245 kW) is lower than the one of the yellow line (10584 kW). The obtained peak reduction is almost 340 kW, which corresponds to more than 3%, despite the limited number of buildings which schedule could be modified.

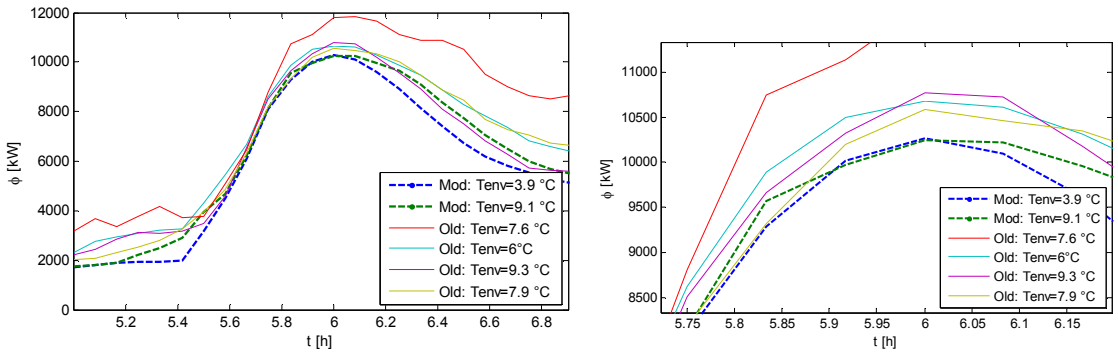

Figure 5.28. Sum of the communicating user thermal requests during: left) all the peak period; right) a detail.

5.9 Optimizer improvements

In order to make the optimizer more effective some further developments have been performed. In particular the possibility of increasing the anticipation range is investigated in order to make the peak shaving more effective. To explore such opportunities a model for the user heating must be applied in order to account for the internal temperature evolution when changes in the start-up time are applied. This analysis guarantees that the changes in the strategy do not produce significant effects on the building temperatures. In such way the comfort standard can be preserved. In particular the user simulator carried out consists of a building model based on the data available at the heat exchangers, which means that no indoor temperature sensors should be applied. This is a requirement to make the procedure applicable on a large scale. In addition it should be considered that the model does not aim to accurately predict the values of internal temperatures, but only to account for the possible changes.

5.9.1 Building physical model

The building model includes the thermal substation and the "macro heating device" which represents the ensemble of the heating system and the building envelope. A schematic of the system considered to simulate the buildings is shown in Figure 5.29.

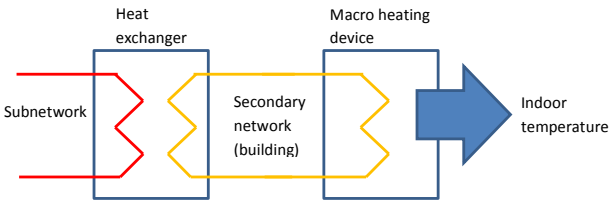

Figure 5.29. Schematic of the heating system in the buildings

An energy balance of the building is written including the unsteady term, the heat provided by the heating system Φ_{syst} and the losses Φ_{losses} with the environment, namely

$$\Phi_{syst} + \Phi_{losses} = Mc\frac{dT}{dt} \quad (5.8)$$

Where Mc is the thermal capacity of the building and T is the average indoor temperature. This means that a single average temperature T is considered in the building. For the purpose of the analysis proposed in this work, this does not represent a limitation of the model as it is further discussed in the next section. Losses can be expressed through a global dispersion coefficient per unit volume U_{vol}:

$$\Phi_{losses} = U_{vol}V(T - T_{outside}) \quad (5.9)$$

Both parameters Mc and U_{vol} are evaluated trough the analysis of measurement data available at each heat exchanger. These are the four temperatures at the heat exchanger, the mass flow rate on the primary network and the external temperature ($T_{outside}$). The term U_{vol} is evaluated using data collected when the system is operating in pseudo steady-state conditions, which typically take place in the afternoon, ,as shown in Figure 5.30.This figure shows the temperature difference between the flow at the outlet section and the inlet section of the heat exchanger. In particular, in the left part of the figure, the daily evolution is depicted while the second plot shows in detail the last part of the temperature decrease.

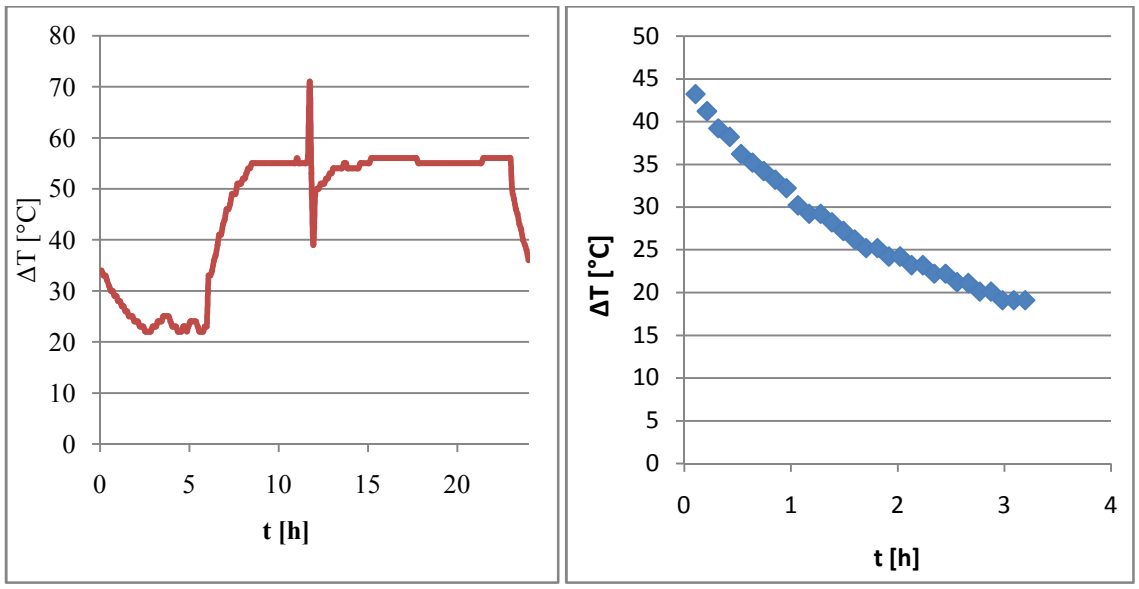

Figure 5.30. Model validation. Heat request at the heat exchanger comparison.

In these conditions, equation (1) is rewritten as:

$$U_{vol}V = \frac{\Phi_{syst}}{(T - T_{outside})} \quad (5.10)$$

The term Mc has been evaluated considering the transient operation after the heating system is switched off. In this case, it is assumed that, when the temperature of water exiting the heat exchanger on the secondary side of the heating system is approaching the indoor temperature, these two temperatures tend to decrease in a similar way. Therefore, data collected during the last

stage of the water cooling can be used to evaluate the decrease in the internal temperature and thus the thermal capacity of the building:

$$\frac{dT}{dt} Mc = U_{vol} V (T - T_{outside}) \quad (5.11)$$

Temperatures of the water exiting the DHS heat exchangers at the secondary side, T_{out_sec}, and heat flow exchange at the users, Φ_{syst}, are evaluated using the substation model.

The heating system of each building has been modeled considering the two heat exchangers shown in Figure 5.28. The first heat exchanger is the one in the substation where district heating network water flows on the primary side and the water of the building heating system flows on the secondary side. The second heat exchanger simulates all the heating devices in the building as a single component exchanging heat with the indoor environments (assumed at an homogeneous time dependent temperature T). The heat exchangers are modeled using a effectiveness-NTU method. A time delay is considered in order to account for the average time requested for water circulation on the secondary network. This is a third parameter that characterizes the building and it is calculate through comparison of the calculated thermal request profile and the registered evolution.

Temperatures on the secondary network have been calculated at each time step, since these values vary during operation. In contrast, the mass flow rate on the secondary network is constant when the heating system is operating, since typically no variable speed pumps are installed in the buildings. The mass flow rate on the secondary network is zero when the heating system is not operating.

The user model has been tested through data collected during a winter day in order to verify its capability to simulate the buildings indoor temperature evolution.

5.9.2 Building model results

In this section, results of the building model validation are reported. A specific building where four indoor temperature sensors were installed has been considered. Results in terms of indoor temperature evolution and heat flux measured at the heat exchangers are evaluated and compared with available measurements. In Figure 5.31, the temperature evolution computed through the building model (in black) is compared to the temperature evolutions measured in four different rooms. A winter day with an average external temperature of 8 °C is considered. The evolution is well captured by the model both in the heating-on and heating-off stages. During the heating stage the temperature increases of 4.5 degrees, the same of the temperature detected using the thermocouple installed in the building. Also, the time at which the maximum internal temperature is reached in simulations and measured data is similar. It is worth noticing that the model does not consider any contribution due to unpredictable contributions, such as solar radiation, but this is not considered in the currently applied control strategies.

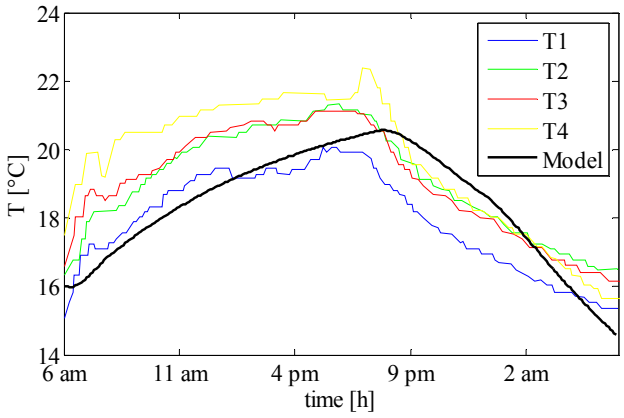

Figure 5.31Model validation. Indoor temperature comparison

Figure 5.32 illustrates a comparison of the heat request at the heat exchanger evaluated using the building model and the experimental data. It is possible to notice that the heat flux exchanged at the thermal substation is very large when the heating system is switched on. This is due to the fact that temperature on the secondary circuit drops significantly at night, reaching a temperature close to the internal building temperature. The average temperature difference between primary and secondary side is thus much larger than at design and so the heat flux. After the peak, the heat flux decreases due to the temperature increase on the secondary circuit. This decreasing trend is affected by the characteristic time requested to complete the secondary circuit. From Figure 5.31 it can be concluded that the model is able to capture the heat flow evolution at the heat exchanger both in transient and steady state conditions.

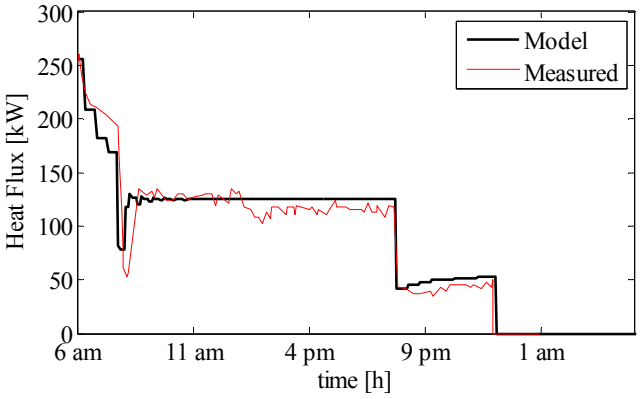

Figure 5.32 Model validation. Heat request at the heat exchanger comparison.

In addition, six buildings connected with the selected distributed networks are considered (Note that the analysis is performed considering a wider area than just the single distribution network adopted in the previous sections, because the building where indoor temperature were available is located on a different distribution network). For these buildings it is possible to compare the calculated temperature of water exiting the heat exchanger on the primary network

with the experimental values. These buildings are also used in order to show the effects of the rescheduling on the internal temperatures. The criteria to select the buildings are their volume and the distance between the building and the connection node with the transport network. These pieces of information are reported in Table 5.1, where model coefficients are also shown. These coefficients have been evaluated using the approach described above. Last term (t_c) is the characteristic time considered in the simulation of each building.

Building	Volume (m^3)	Distance (m)	U_{vol} V (W/K)	Mc (kJ/K)	tc (s)
1	3127	169	3752	70357	150
2	3000	856	2880	69005	150
3	6930	200	6029	169785	320
4	7019	769	5755	176176	300
5	14470	313	10418	393584	560
6	16725	750	19233	460773	660

Table 5.1. User model coefficients

A comparison between the calculated and measured temperatures of water exiting the selected heat exchangers is shown in Figure 5.33, which shows that the model is able to capture the behavior of buildings, with the exception of building C.

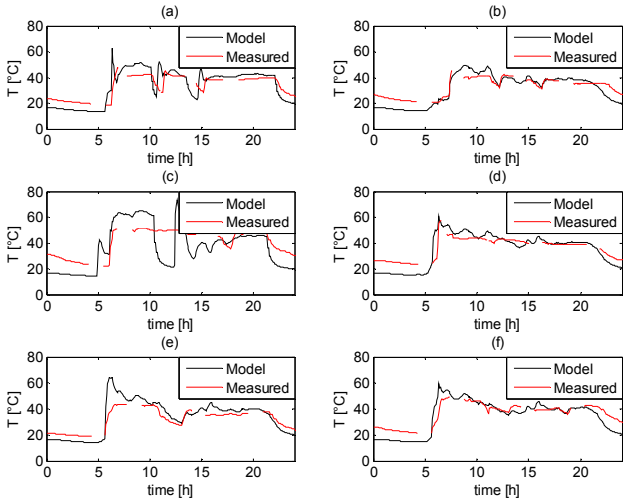

Figure 5.33. Temperature of water exiting the heat exchanger on the primary side for six selected buildings.

On the basis of the results presented in this section it is possible to conclude that the model is suitable for evaluating the acceptability, in terms of comfort level, of possible changes in the thermal request.

5.9.3 Thermal profile changes

Two scenarios corresponding with different changes in the thermal request profiles have been analyzed, as reported in Table 5.2. In both cases it has been considered that only 50% of the buildings accept to modify their thermal request profiles. The two cases differ in terms of the maximum anticipation in the start-up time of the heating system. The energy demand of the selected users has been modified in the following way:

1) a simulation corresponding with a scenario with no changes operated on the thermal request profiles is performed. This simulation allows one obtaining the thermal load curve and the internal temperature in each building as the function of time;

2) the time at which the heating system is switched on is anticipated of a period between 0 and the maximum value indicated in Table 5.2;

3) when the indoor temperature of a building reaches a desired value, during the first half of the morning, the heating system is switched off until the internal temperature profile crosses the curve corresponding to the scenario with no changes.

For each building, a temperature evolution curve is obtained. This curve is above the original curve in the first part of the morning. When the two curves cross each other, the thermal request profile continues in the same way as the scenario with no changes. It is important here to stress the fact that the use of an average temperature for the building is not a limitation since the criterion for acceptability of the new request profile is based on the comparison of the curves with and without changes. It is assumed that if the average temperature for the scenario with no changes was acceptable for the end-users, the fact that the same temperature is reached with the new profile guarantees the same comfort conditions.

The modified profile generally involves a larger thermal consumption for the building, nevertheless, this consumption takes place in off-peak hours, when cogeneration is available, while the thermal request in peak hours is reduced. The primary energy cost of these two amounts of heat is thus different: the off-peak heat request has a primary energy production cost of about 0.36 MWh/MWh (cost of heat produced through cogeneration), while the avoided heat consumption in peak hours has a primary energy cost of about 1.11 MWh/MWh (avoided cost of heat produced through boilers). In fact, cogenerated heat is produced by combined cycles characterized by an electrical efficiency of 58%. When these plants operate in maximum

cogeneration mode, electricity production decreases of about 50 MW, while heat production increases of about 240 MW. Therefore the cost of a unity of heat production is that of 0.21 unities of electricity. In contrast, the avoided heat production in peak hours allows reducing the use of industrial boilers which are characterized by an average efficiency of about 90%.

	Fraction	Maximum anticipation
CASE 1	50%	20min
CASE 2	50%	30min

Table 5.2. User request modification analyzed

5.9.4 Current thermal request

A first simulation of the distribution networks and the buildings connected with the network is performed in order to reconstruct the scenario "as-is". Thermal request of the buildings is set on the basis of measurements available using a time step of 5 minutes. The peak request of each building and the time at which it occurs are registered. These pieces of information are illustrated in Figure 5.34, where the various contributions and the total summation in each timeframe are presented. It is apparent that, as expected, there are many users requiring the highest amount of thermal power between 5.40 am and 6.40 am. The peak thermal power required from most of the buildings is below 1 MW. It can also be noticed that a large user presents a peak thermal request of 2750 MW at 8.45 am, which is an uncommon behavior. This type of user does not need any thermal request variation since its start-up peak occurs when most users are in off-peak conditions. As expected, the peak thermal power presents a maximum at 6.20 am. The peak value obtained in Figure 5.34 is not the maximum thermal request of the distribution network, because this only accounts for the peak request of each user. Users characterized by earlier peak request may have already reached the pseudo steady-state request, as shown in Figure 5.30, therefore the instant request may be different in shape and values.

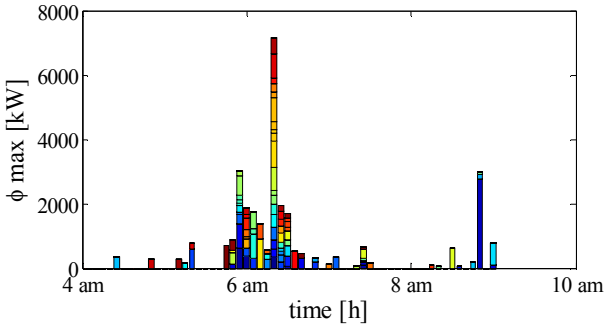

Figure 5.34. Current situation. Summation of the thermal peaks of the various buildings.

Figure 5.35 depicts the current total thermal load registered at the end nodes of the distribution networks of the considered area i.e. at the nodes linking the distribution network with the transport network. The thermal request between 0 a.m. and 5 a.m. is close to 0 MW, due to the absence in the considered network of users requiring heat also during the night, i.e. hospitals. A peak load of about 42 MW occurs at about 6.10 a.m., which means about 10 minutes before the maximum value reported in Figure 5.32. This is mainly due to the shape of the heat flux curves of the buildings, which is typically characterized by a thinner peak than that shown in figure 6 (which refers to a large building) and a slighter increase towards the pseudo steady state.

Then the thermal load reduces to values which vary between 10 MW and 20 MW. The red dashed line, represents the amount of thermal power that can be provided in cogeneration mode to this network. Such value has been obtained by distributing the total cogeneration capacity among the various distribution network according with their specific nominal request. As already discussed in this thesis, the presence of the morning peak does not allow proper exploitation of the cogeneration plants.

In the following section, possible strategies obtained by modifying the thermal request of the buildings are analyzed.

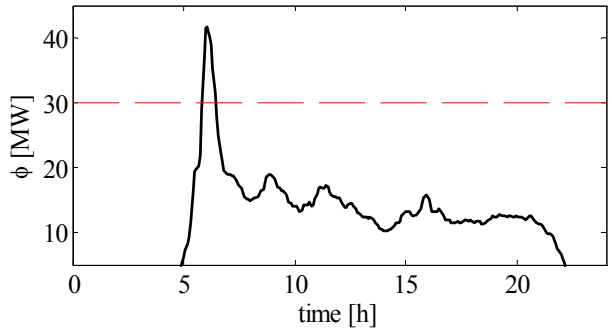

Figure 5.35 Current thermal power request evolution in the considered distribution network.

5.9.5 Thermal request modifications

Two different request profiles that are alternative to the current operational strategy have been defined have been defined according with the requirements defined in Table 2. The corresponding distributions of peaks are shown in Figure 5.36. In the first strategy the maximum peak summation is reduced to about 5 MW, but the main variation refers to the anticipation of peaks that in the current strategy occur before 6.10 a.m.: all peaks are made more homogeneous than that shown in figure 8 and are all below 2 MW. In the case of the modified strategy 2, the opportunity to anticipate up to 30 minutes is used to create a sort of alternation between "high" peaks of about 1-2 MW and small peaks.

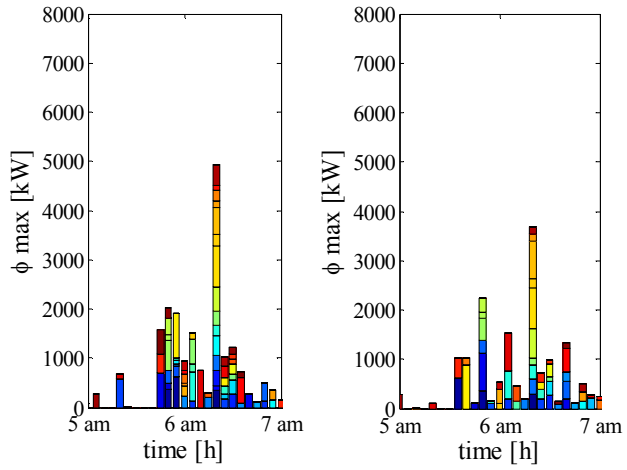

Figure 5.36. Modified strategies 1 (left) and 2 (right).
Summation of the thermal peaks of the various buildings.

The time profiles of the total heat load for the distribution network obtained by applying the current operational strategy and two alternative strategies are illustrated in Figure 5.37. Clearly, when the request of buildings is anticipated the total thermal request presents an anticipated increase. Both modified strategies 1 and 2 provoke a remarkable reduction in the peak load. Before the peaks, the alternative strategies require an additional amount of heat, but this is mainly supplied by cogeneration plants. In contrast, load is reduced after the peak, even if not of the same quantity, therefore a partial heat recovery is obtained. In the case of modified strategy 1, the additional thermal energy supplied to the network through cogeneration is 0.8 MWh/day, but the avoided production of thermal energy through boilers is about 1.4 MWh/day. This results in a reduction of primary energy consumption of more than 1.2 MWh/day. In the case of the second strategy, the additional thermal energy supplied to the network through cogeneration is about 1.2 MWh/day, but the avoided production of thermal energy through boilers is about 2.5 MWh/day. This results in a reduction of primary energy consumption of more than2.3 MWh/day.

If this result is extrapolated to the entire network, assuming that 50% of the request of buildings is rescheduled, the primary energy savings could be about 4-5% of the annual fuel consumption.

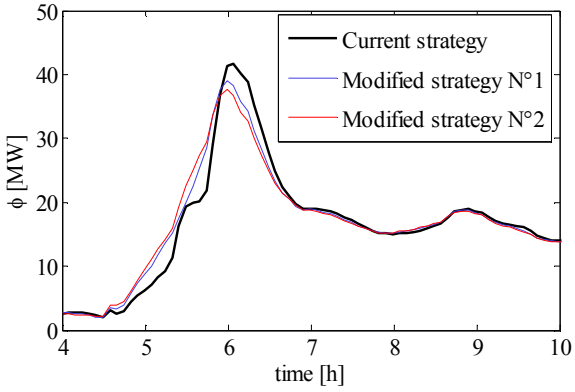

Figure 5.37 Thermal power request evolution in the considered distribution network with different user request variation strategy

The analysis of the indoor temperature using the building model is presented in Figure 5.38 for the six selected buildings. For each building, the curves, corresponding with the current strategy and the modified strategy are shown. Only the strategy 2 is shown, since it is the one involving the largest possible deviation in the startup schedule. In all cases the heating system is stopped at night, therefore internal temperature decreases, reaching a minimum at about 5-6 a.m. then the heating system is turned on and the internal temperature starts increasing. In the case of building (a) and (c), it is possible to notice that the heating system is stopped during the day (at 10.05 and 10.30, respectively), therefore the average internal temperature calculated using the compact model presents one or more oscillations above 20 °C. In contrast, the other buildings reach a plateau after an initial steep increase, which involves a reduction in the thermal request in the second part of the morning (after about 10 am) and a modulation during the day.

When the modified strategy is applied, the indoor temperature presents an anticipated increase, therefore the internal temperature curve stays above that corresponding with the current strategy. In the second part of the morning, between 9 and 11 depending on the examined building, the recovery is applied. This is obtained through partial anticipation of the first planned stop in the case of buildings (a) and (c) or by introducing such stop in the other cases. Stop duration is calculated so that the indoor temperature curve corresponding with the modified request crosses that corresponding with the current request. From this point on the thermal request profile follows the current one and so the indoor temperature. The fact that the indoor temperature is always maintained above or coincident with that corresponding with the application of the current strategy guarantees the fact that the modified strategies are acceptable for the end-users.

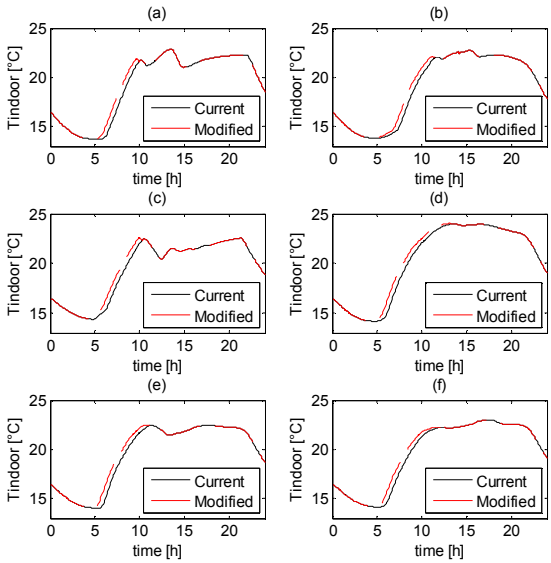

Figure 5.38. Indoor temperature evolution with the current and the modified users thermal requests.

5.10 Concluding Remarks

In this chapter presents a thermo fluid-dynamic model for the analysis of possible optimum for peak shaving in district heating systems is presented. The model has been built for performing unsteady simulation of large district heating networks and it has been applied to the largest district heating network in Italy, located in Turin, for the analysis of start-up transient operation.

The model is based on a steady state fluid-dynamic model and a transient thermal model of the network. The fluid-dynamic model evaluates the mass flow rates in branches using the SIMPLE algorithm. The thermal model determines the temperature in the nodes using an Upwind scheme. The models have been applied to the transport pipeline as well as to distribution networks. In order to keep low computational cost a different approach has been used: the transport and distribution networks have been simulated separately. In particular results provided to each distribution network simulation have been used as the input of the transport pipeline model. The time required by the thermo fluid-dynamic model to simulate 13 hours of the whole return network behaviour on a single 3.3 GHz CPU is about 2 hours

The model provides the temperature in all the nodes and the mass flow rates in all the branches. Results are compared with experimental data to prove model effectiveness. The model is able to detect the thermal power required to the plants with good approximation. Prediction of heat power required in different periods is useful as decisional support in operational strategies (e.g.

electricity production by the cogeneration systems) and for thermal peak shaving through installation of storage systems as well as the promotion of night attenuation or variation in the thermal request profile of the users. The model has been applied to examine the effects of network enlargement and to find optimal users switching on changes. In fact at first in particular the model is used to analyze the effect of local storage installation in a new portion of the network. Secondly a tool for optimizing changes of user thermal request strategy has been developed and applied to the minimization of the primary energy consumption. This tool has been applied to one of the Turin DHS distribution network and it is currently under testing in the real network. Results allow one quantifying the possible reduction of the non-cogeneration heat request during peak hours, with the current control technology. The possible reduction of the non-cogeneration heat is about 27%, while the maximum value of the peak can be reduced of the 6%. Results show that a primary energy reduction of about 0.17 MWh/day can be achieved, with a consequent energy saving of about 1.25% with respect to the current strategy. The tool provides results in about 2 hours, therefore it is sufficiently fast for application to the management of large networks. Further developments regards the full integration of the users model in the anticipation optimizer in order to make the peak shaving more effective without affect the indoor comfort level, as well as the implementation of the strategies involving larger changes in the start-up time of the various users. In particular reduction techniques can also be applied to more complex building models.

6

Wildfire application

6.1 Introduction

This chapter aims at proposing the reduction of a physical model through proper orthogonal decomposition. This means that with respect to the applications considered in Chapters 4 and 5 here the POD technique is directly applied to the model equation. An application to the wildfire prediction field is proposed, using a simple physical model as test case. The selected model is a one-dimensional model based on the energy conservation equation, which was applied to a real scenario with no-slope but variable wind velocity. The data necessary for the estimation of the parameters of the physical model have been obtained from field fire experiments. Data from additional field experiments have been used to check the model effectiveness in fire behaviour prediction. It is worth stressing that experimental data in this work are used with the only aim of checking that the full model is able to predict fire behaviour evolution correctly. In contrast, the goal of this analysis is to demonstrate that the POD reduction technique allows one to obtain results close to that of the full model but using a much smaller computational time. This means that the POD model should be checked against the full model, while the full model should be checked against the experimental data. In the followings paragraphs, after a literature overview,

the physical model is first tested using experimental data, the reduced model is compared to the full one and finally results were discussed. A 2D model is used to obtain the fire landscape propagation.

6.2 Literature overview

Reliable and computationally fast prediction of wildland fire behavior (e.g., rate of spread, energy release, perimeter and area growth) is crucial for operational purposes such as fire risk analysis, strategic fuel treatment planning, or support to incident management (Cruz and Alexander 2013). This goal is challenging for the fire scientist community since the early XX^{th} century (e.g., Fons 1946) due to difficulties related to the understanding and representation of complex fire spread processes, the involvement of multiple length and time scales and the presence of various sources of uncertainty (Sullivan 2009a, b, c; Cruz and Alexander 2013; Finney *et al* 2015).

Fire models currently used in operational modeling systems (e.g., Rothermel 1972; Coleman and Sullivan 1996;Canadian Forest Service 2004) are mainly empirical or quasi-empirical (Sullivan 2009a) because these models are pragmatic, straightforward to implement, and are computationally effective (Sullivan 2009b; Cruz and Alexander 2013). Although useful, these models suffer of many limitations such as uncertainty and imprecision, calibration needs and a condition of non-uniqueness (Morvan and Dupuy 2004; Cruz and Alexander 2013; Finney *et al.* 2013). Physical and quasi-physical fire models (Sullivan 2009a) attempt to overcome these limits by representing both the physics and chemistry of fire spread (Sullivan 2009a; Morvan 2011; Finney *et al.* 2015). Comparative analyses between empirical and physical models have shown that the development of fire operational tools based on physical approaches is a promising research field (Hanson *et al.* 2000;Morvan *et al.* 2009). Some of the most used tools based on physical models (Morvan 2011) are FIRESTAR (Morvan and Dupuy 2004), FIRETEC (Linn and Harlow 1997), FIRELES (Tachajapong *et al.* 2008), and WFDS (Mell *et al.* 2007). However, the physical mechanisms that occur in wildfires are very complex and involve large domains. Therefore, even when some simplifications are considered, such as two dimensional models (Morvan and Dupuy 2004), very high computational resources are required. This currently precludes their use as operationally-oriented tool (Sullivan 2009c), especially when the analysis of multiple scenarios is required. In this framework, a reduction technique is proposed for testing its capability on making physical models applicable to super real time fire prediction.

6.3 Model Description

With the aim described in the previous paragraph a simple physical model has been selected. This is a one-dimensional model which considers the energy equation (6.1) for the fuel array and imposes the local rate of burning fuel as proportional to the current amount of fuel where

combustion takes place (6.2). Similar models have been adopted in various works available in the literature (Balbi *et al.*1999; Simeoni *et al.* 2001):

$$\rho c\frac{\partial T}{\partial t}+k_v v\frac{\partial T}{\partial x}=k\frac{\partial^2 T}{\partial x^2}-h(T-T_e)-\frac{H}{s}\frac{dM}{dt}+\Phi_{RAD} \tag{6.1}$$

$$\frac{dM}{dt}=-aM \tag{6.2}$$

The first term in the energy equation is the storage term. This depends on the average density ρ of the mixture of fuel and air, the specific heat per unit volume, c, and the time variation of temperature. The second term is the convective term. This depends on the air velocity v along the fire propagation direction x and the derivative of temperature with respect to x. As fluid flow in not solved, velocity is assumed as constant throughout the domain, which is a limitation of the model.

The empirical coefficient k_v, which value is obtained through experiments, is used in order to allow substituting the upwind velocity to the local velocity.

The first term on the right hand side is the diffusive term, which accounts for heat conduction. Quantity k is an equivalent thermal conductivity associated with the mixture of fuel and air. The second term accounts for the convective heat losses towards the environment, which is assumed at a constant temperature T_e. The quantity h is a convective heat transfer coefficient per unit volume and is evaluated on the basis of available experiments, as shown below. The third term is a source term which accounts for the heat released due to fuel combustion. The quantity H is the heat content of the fuel, while s is the fuel array depth. These are multiplied times the rate of mass variation, which is evaluated through equation (6.2).

Last term accounts for the net radiation heat transfer with the other portions of fuel array (j). This term is computed as:

$$\Phi_{RAD}=\sum_j rF_{ij}\varepsilon\sigma\left(T_j^{\,4}-T^4\right) \tag{6.3}$$

where r is the radiative coefficient accounting for the surface per unit volume emitting thermal radiation, F_{ij} is the view factor of the surface with respect to the surrounding areas, ε is the emissivity and σ is the Stefan-Boltzmann coefficient. The presence of the radiative term (6.3) make the energy equation non-linear.

The mass variation rate due to fuel combustion is assumed as directly proportional to the local fuel mass, according to Balbi *et al.* 1999. The parameter a assumes a positive constant value only

if the cell temperature at the previous time step is higher than the ignition temperature, otherwise it is zero. In order to limit the possible impact of the assumptions related with the combustion model, the parameter *a*, which value depends on fuel type and humidity, is evaluated experimentally.

Despite being simple, the selected physical model presents two important features that need to be tested to prove the applicability of POD to wildfire science: 1) possible propagation of the fire front over large domains and 2) physical phenomena modeled through non-linear terms (the radiative term in this specific case). In this framework, the previously mentioned limitations of the physical model do not affect significantly the outcomes of such POD application. Once proved POD applicability to this model, more detailed models can be considered, such as two dimensional models, or models including continuity and momentum equations, radiative transfer equation and complex combustion models.

In order to solve the energy equation, a numerical approach has been used. Energy equation has been discretized with a finite difference central scheme (Ferziger and Peric 2002) and a Newton-Raphson algorithm has been used in order to solve it. The energy equation of the full model can be written in matrix form and, after the opportune rearrangements, becomes:

$$\boldsymbol{C}\dot{\boldsymbol{T}} = \boldsymbol{A}\boldsymbol{T} + \boldsymbol{D}\boldsymbol{T}^4 + \boldsymbol{f} \tag{6.4}$$

where matrix **C** includes the coefficients of the storage term, matrix **A** the coefficients of the convective term, diffusive term and unknown part of the heat loss, matrix **D** the radiative term and vector **f** the known part of the heat loss term and the source term.

Dirichlet boundary conditions have been imposed at both the boundaries. A sinusoidal temperature distribution with a maximum of 700 K has been imposed as initial condition in the first 0.4 m of the domain in order to represent the fuel ignition while the environmental temperature is set at t=0 in all the other regions. The initial mass condition per unit area is 0.39 kg/m^2 everywhere. For the effect of the radiation o the unburned fuel the flame is considered to be 50 cm height.

The model has been applied to the system shown in Figure 6.1. The domain is 50 m long. This system is the one dimensional description of the domain used for the experimental data collection necessary to parameterize the physical model. A partition of the domain is also reported in the figure in order to better display the results and compare them with the measurements from field experiments.

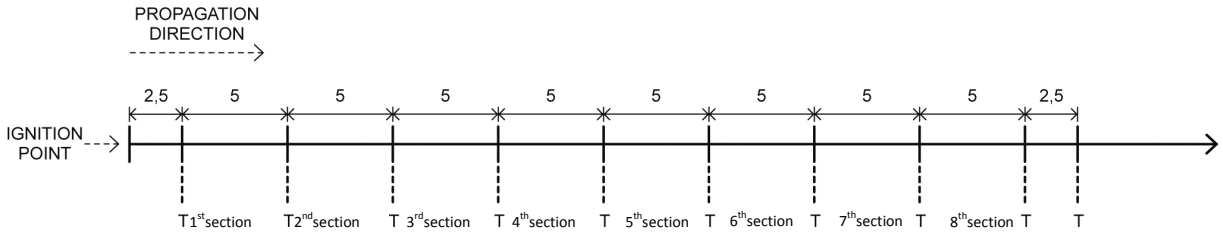

Figure 6.1 Experimental and model domain

The various parameters necessary in the full model have been obtained using measured data and information on fuel characteristics, weather and fire behavior collected during field fire experiments on grassland fuels, dominated by *Molinia arundinacea* Shrank (Figure 6.2). The analysis has been carried out under controlled conditions in winter 2009 in North-West Italy (Ascoli *et al.* 2009).

The values of the fuel energy content, H, the density of the mixture of fuel and air, ρ, and the fuel height, s, have been computed by assessing the grass fuel structure and load in the field soon before burning. At each experimental site, fuels were harvested in six 1-m^2 quadrats and oven-dried in the laboratory at 90°C to determine the load (t ha^{-1}) on a dry basis. The fuel depth has been assessed every 0.5 m along six linear transects (length =10 m) at each fire site. Fuel load and bulk density range between 4.29 to 5.50 t ha^{-1}, and 2.2 to 7.1 kg m^{-3}, respectively. Flammability parameters (surface area to volume ratio, moisture of extinction, heat content) have been derived from published values for similar grass fuels as provided by the Fuel Characteristics Classification System (USDA 2015).

Figure 6.2 Field fire experiment

Four fire experiments have been conducted through a collaboration with the Università di Torino. The data have been collected under moderate dry weather on the same day in the winter dry season, when the grass fuel was fully cured. Fuels have been thus entirely constituted by dead grasses with a diameter smaller than 6 mm (i.e., dead fine fuels) with a cover of 100% at each experimental site.

Fuel moisture has been assessed soon before each fire experiment by collecting five samples of dead *Molinia* leaves. Fresh samples have been weighed in the field using a portable scale, and then oven dried in the laboratory at 90°C to constant weight. Fuel moisture has been computed on a dry weight basis and ranged between 11% and 19%. To let the fire front spread freely through grasses, each fire experiment has been ignited by a 25 m line ignition, and the fire was allowed to spread for 50 m before being suppressed along a fuel break.

At each fire experiment, the fire spread has been assessed by measuring the arrival time of the fire front by using K-thermocouples (0.4 mm in diameter) positioned at fixed points (asterisk symbols in Figure 6.1) along a 50 m transect parallel to the spreading fire front. K-thermocouples have been placed within the fuel bed (5-10 cm from the soil surface) and the environmental (air-gas-fuel) temperature has been measured at intervals of 1 second. Consequently, at each sampling point the maximum temperature and the temperature-time profile have been obtained (6.3). During each fire experiment, air temperature and moisture, and wind speed and direction have assessed every 10 seconds by two weather stations positioned at a height of 2 m upwind the experimental plot.

Time since last rain was 19 days. Air temperature and moisture, and wind speed during the four experiments ranged between 20 to 27%, 19 to 25°C, and 2.8 to 7.1 km h^{-1}, respectively. The coupling of weather data with fire behavior data has allowed to separate thermocouple data recorded during no-wind conditions, backfire and head fire phases (i.e., against and with the wind respectively).

Both no-wind conditions and head fire conditions have been considered for the model parameters evaluation. In total, 32 rate of spread observations have been collected (8 each experiment, as shown in Figure 6.1), each associated with fuel characteristics (load; bulk density; moisture), environmental conditions (slope; wind speed), fire behavior (rate of spread; no-wind, back or head fire phase) and effects (fuel consumption). Rate of spread ranges between 0.8 to 14.2 m min^{-1}. Fuel consumption has been assessed soon after the fire by collecting remaining charred fuels in six 1 m^2 quadrats at each fire site and ranged between 75 and 90% of the pre-fire mean fuel load. In total, 40 experimental temperature-time profiles have been collected (10 each experiment, as shown in Figure 6.3). Maximum flame temperature ranges between 244°C and 733°C. Average residence time above 60°C and 300°C are 183 and 21 seconds, respectively.

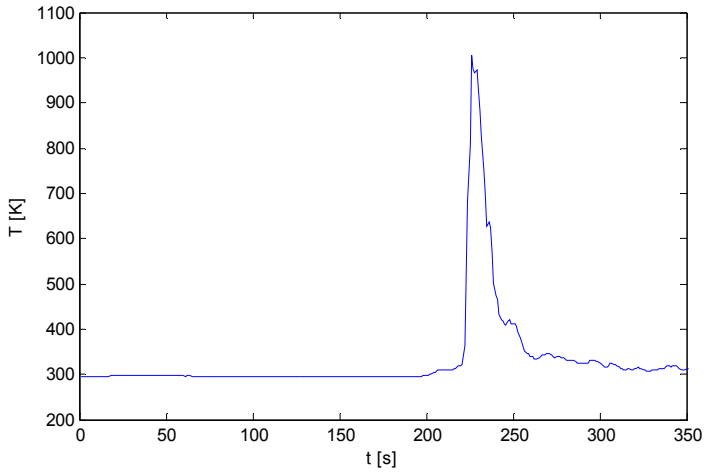

Figure 6.3 Temperature-time profile collected to a thermocouple

The values of the diffusive coefficient k, the convective losses coefficient h, the linearized reaction rate a, the radiative coefficient r and the convective coefficient k_v have been determined using a comparison between simulations and experimental data. A genetic algorithm has been applied in order to parameterize the set of coefficients to simulate the fire front spread. Indeed, genetic algorithms have been successfully used to calibrate coefficients of wildfire prediction models (Wendt *et al.* 2013, Ascoli *et al.* 2015). The relative errors in terms of burning period, $Err_{burning}$, arrival time, $Err_{arrive,}$ maximum temperature, $Err_{maxT,}$ and integral of the temperature in time, $Err_{integral,}$ have been computed. The sum of these deviations has been considered as the indicator of the error performed to the model respect to experimental data in fire behavior prediction, as indicated in (6.5).

$$Err = w_1 * Err_{maxT} + w_2 * Err_{integral} + w_3 * Err_{arrive} + w_4 * Err_{burning} \quad (6.5)$$

The weight factors (w1, w2, w3, w4) have been added in order to select the importance of each error. In particular, the weight factors associated with temperature measurements (w1, w2) have been selected as smaller than the others with the intent of filtering the effects due to the errors in field measurements.

The genetic algorithm has been used to find an optimal set of coefficients that minimizes the error, keeping it below a threshold level (5%). To limit premature convergence towards local optima, a crossover probability of 0.8 and an average mutation of 0.3 (this latter value changes during the optimization process) have been set (Srinivas and Patnaik 1994) and a large initial population (Pandey et al. 2014) equal to 60 random cases. The optimization has been conducted in 40 generations.

In order to determine k_v, the optimization has been carried out considering 3 of the 32 available segments where 3 different values of wind velocity were registered: 0 m s^{-1}, 1.4 m s^{-1} and 2.0 m s^{-1}. The same set of coefficients has been then used to simulate fire propagation depending on the wind velocity, as registered during the experiments. Results have been compared with experimental results collected in presence of the same wind velocity. The average value of the three error indicators, obtained with the three different wind speeds, has been computed and the set of coefficients that minimize the error has been evaluated; in this way the physical model has been parameterized. The coefficient evaluation strategy is summarized in Table 6.1.

Symbol	Explanation	Evaluation
P	Mixture air fuel density	Laboratory Analysis
C	Specific heat	(Campbell, Norman 2012)
k_v	Advective coefficient	GA usingThermocouple Measurements
K	Diffusive coefficient	GA usingThermocouple Measurements
H	Losses coefficient	GA using Thermocouple Measurements
H	Energy content	Laboratory Analysis
S	Fuel height	Field Analysis
A	Mass rate variation coefficient	GA using Thermocouple Measurements
R	Radiative coefficient	GA using Thermocouple Measurements

Table 6.1. List of the model coefficients and the related evaluation strategy.

6.4 Full Model results

In this first part of the section, the outcomes of the coefficients setting are analyzed. At first, a discretization analysis has been performed in order to select the time step and the grid size that provide an acceptable error. Results are plotted in Figure 6.4. Time step and spatial discretization have been selected in order to keep both errors, due to time and space, below 10%. Simulations have been performed considering a time step 0.1 s and a resolution of 0.02 m.

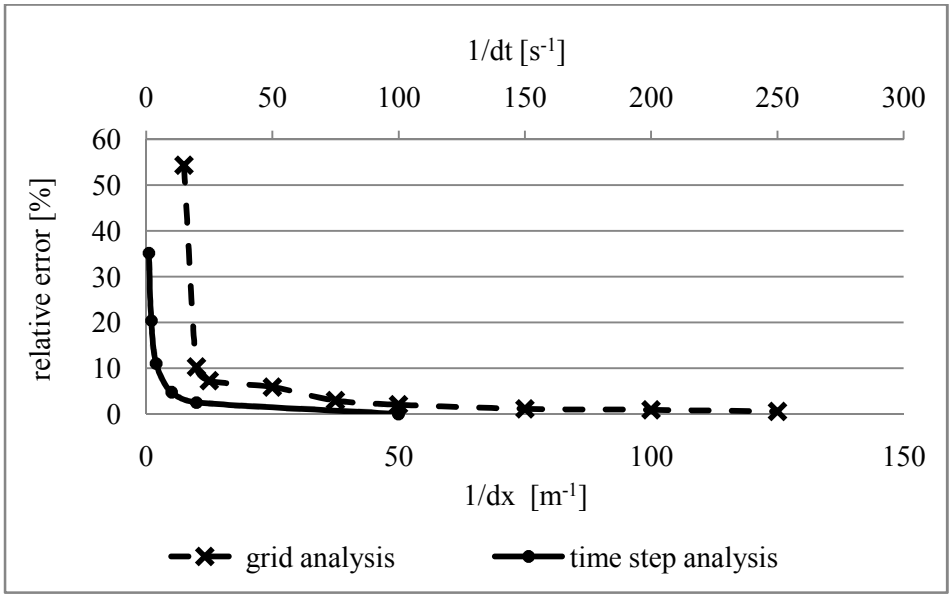

Figure 6.4 Time step and Grid analysis results

After defining the space and time discretization, the model coefficients have been set through genetic algorithm optimization. The values of the coefficients evaluated with the genetic algorithm are: a=0.034962 s^{-1}, k_v=798.576 J $m^{-3}K^{-1}$, k=0.89455 $Wm^{-1}K^{-1}$, h=1191.608 W $m^{-3}K^{-1}$, r=2.6610 m^{-1}.

A comparison of the rate of spread (ROS) obtained with the physical model and the experimental ROS is shown in Figure 6.5 for three different wind velocities. These results show that the physical model is able to capture the behavior of the experimental fire front evolution. A small error of about 0.01-0.02 m/s is committed for each wind speed. Deviations are due to the inaccuracy of the model but also the uncertainties in the parameters and in the measurements, such as the non-homogeneous fuel characteristics, humidity, wind velocity, etc.

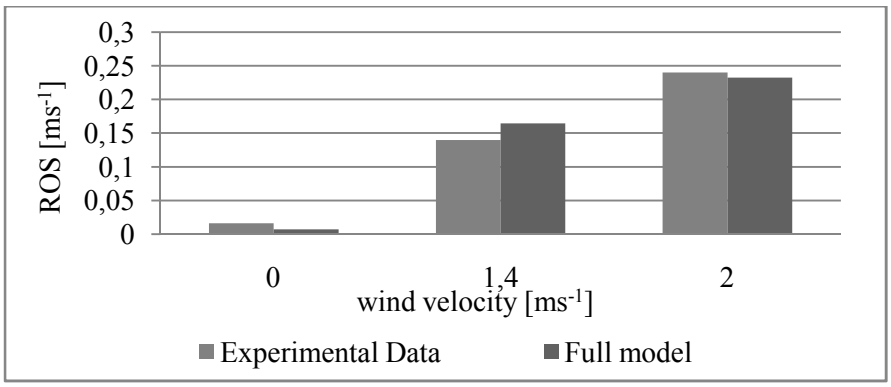

Figure 6.5 ROS obtained with the set full model and the ROS obtained during the experiments

In order to further comment these deviations, a collection of the relevant rate of spread data gathered during the experiments are reported in Figure 6.6, expressed as the function of wind velocity. A general trend of the fire evolution can be noticed, but an average deviation of 15% is registered with respect to the expected linear trend (Sullivan, 2009b). The maximum difference in the ROS is about 0.075 m s^{-1}.

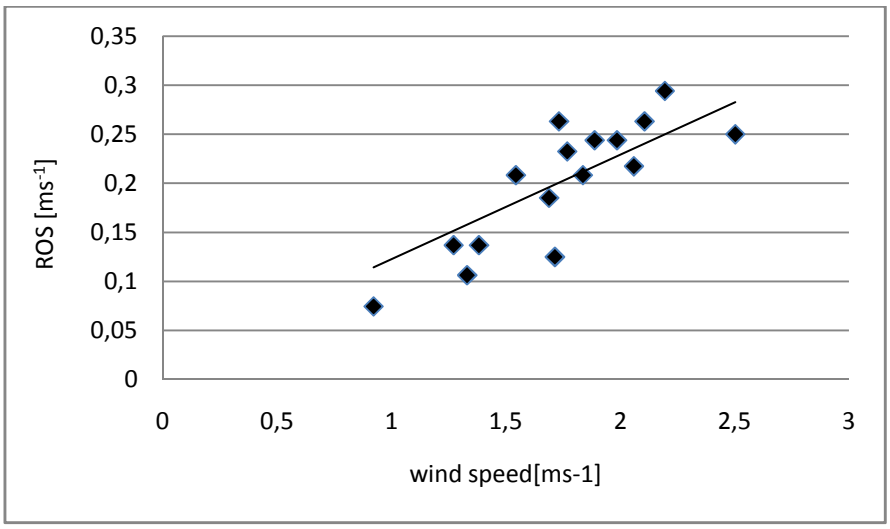

Figure 6.6 Collection of ROS obtained during all the experiments in different wind conditions

6.5 POD approach to wildfire modeling

As discussed in paragraph 2.5 POD technique (Sirovich 1987) is based on the main idea that a physical field can be expressed as a linear combination of the mode eigenfunctions, which describe the spatial aspects, and amplitude coefficients, which account for time dependence. Therefore, using POD procedure it is possible to split the contribution of spatial coordinate and time contribution, and considering just the first k mode, as reported in equation (6.1).

$$\mathbf{T}(x,y,z,t) \cong \widetilde{\mathbf{B}}(x,y,z)\boldsymbol{\alpha}(t) \tag{6.6}$$

Therefore, rewriting (6.4) using (6.6) and multiplying by $\widetilde{\mathbf{B}}^{T}$, the energy equation becomes:

$$\widetilde{\mathbf{C}}\boldsymbol{\alpha}' = \widetilde{\mathbf{A}}\boldsymbol{\alpha} + \widetilde{\mathbf{B}}^{\mathrm{T}}\mathbf{D}(\widetilde{\mathbf{B}}\boldsymbol{\alpha})^{4} + \widetilde{\mathbf{B}}^{\mathrm{T}}\mathbf{f} \tag{6.7}$$

where

$$\widetilde{\mathbf{C}} = \widetilde{\mathbf{B}}^{\mathrm{T}}\mathbf{C}\widetilde{\mathbf{B}} \qquad \text{and} \qquad \widetilde{\mathbf{A}} = \widetilde{\mathbf{B}}^{\mathrm{T}}\mathbf{A}\widetilde{\mathbf{B}} \tag{6.8}$$

A smaller set of equation is then solved with a consequent decrease of computational cost. The obtained ODEs have been discretized through Backward Euler scheme and solved using the Newton-Raphson method. The time step and the resolution of the POD model have to be the same as the physical model it is derived from.

In order to find an appropriate number of snapshots to be considered in the snapshot matrix, a parametric analysis has been conducted varying the number of snapshots. The analysis has been performed for various values of the ROS. Results of the POD model show that no significant differences in the fire front propagation are registered if the time gap among the snapshots is selected according the following inequality:

$$\Delta t_{snap} < \frac{1}{ROS_{predicted}\left[\frac{m}{s}\right]_*^2} \tag{6.9}$$

For the application presented in this work, a maximum acceptable gap of 1.5 s between two consecutive snapshots has been obtained and no significant differences were noticed comparing results obtained using one snapshot per second or more. A total of 60 snapshots have been collected every second performing a single simulation using the full model and assuming homogeneous fuel characteristics and constant wind speed. This means that no computationally expensive simulations are necessary to obtain the snapshots, even in the case of applications to large domains.

Once the snapshots are collected and the correlation matrix is built, just a small fraction of eigenfunctions, 7%, is sufficient in order to simulate fire propagation. This produces the reduction of computational cost.

An additional aspect, which is specific for the application of POD to forest fire engineering, should be pointed out. Fire front propagation at a certain time involves a very limited portion of the full domain, which could be instead quite vast. A conventional approach, involving definition of the snapshots on the entire domain, would result inefficient from the computational viewpoint. An alternative approach has been adopted in this work: snapshots have been defined only on a limited portion of the domain, where the phenomena related with the presence of fire front take place (e.g. radiation heat transfer). The length of this portion should be therefore calibrated according with the flame high. The eigenfunctions have been set to zero outside this portion of domain. Eigenfunctions built in this way have been then moved with the fire front during its propagation. This technique allows one to apply the model also to very large domains with small computational costs.

In this application, a 50 m full domain has been considered, in order to compare results with the available experimental data. Eigenfunctions have been obtained collecting the snapshots in a

portion of the domain of 20 m, while they have been set to zero outside. The portion of domain has been then moved, through change of the coordinates, after few iterations.

The input of the POD model are the fuel parameters, the wind speed and the boundary conditions, as for the full model. The model calculates the temperature distribution as the function of time and the rate of spread.

6.6 POD model results

In this section, results obtained using the POD model are reported and analyzed with the aim of providing information on its effectiveness in predicting the wildfire field. A comparison with both the full model results and experimental data is performed.

Temperature distributions at different time frames obtained with the full model and the POD model considering 2 ms^{-1} wind speed are reported in Figure 6.7. These results show that the evolution predicted by the full model rapidly reaches a shape that tends to a pseudo steady state, which does not change with time. The temperature profile in the combustion region varies only in the first part of the simulation then the rate of spread is constant. Figure 6.7 indicates that a good agreement between full model and POD model is achieved, although the POD model slightly over-predicts the fire front velocity. The differences that can be observed in Figure 6.7 are due to the fact that only a part of the total amount of eigenfunctions is used, in order to reduce the computational cost.

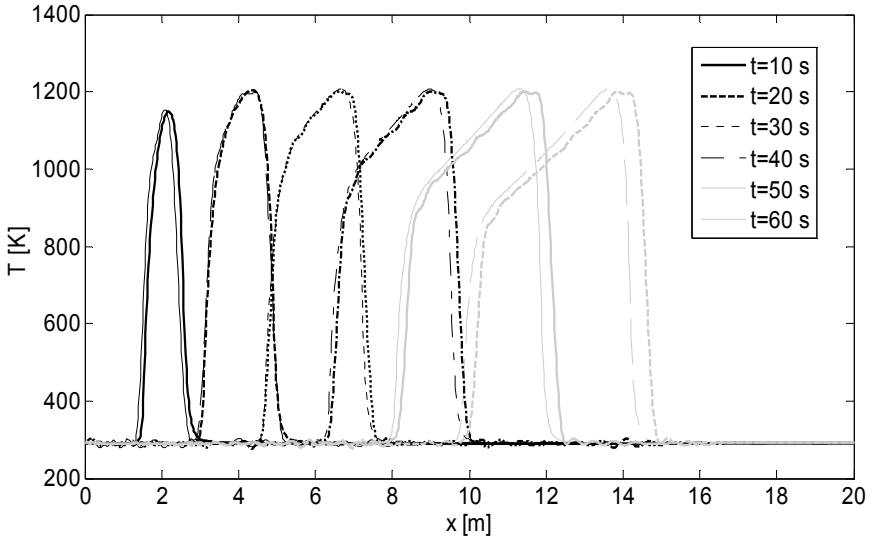

Figure 6.7 Temperature distribution at different times Full model (plain line)and POD model (bold lines)

In order to better compare the results obtained with the full and the POD model, a comparison of the rates of spread is reported in Figure 6.8a. This indicates that a good agreement between experimental ROS and the rate of spread calculated with the proposed model is achieved.

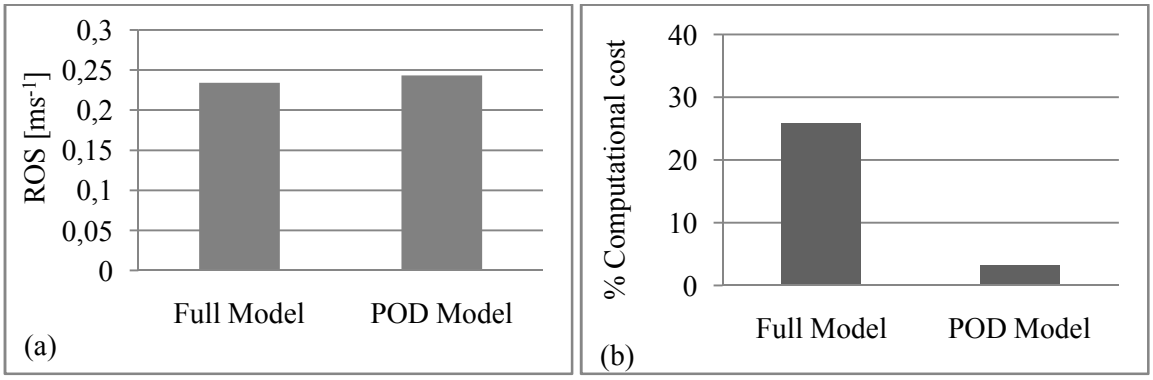

Figure 6.8.Comparison between Full and POD model in terms of relative error and computational cost

In figure 6.8b, a comparison of computational time requested to solve the problem using the two models in the same portion of domain (20 m) is shown. The computational cost is expressed as the ratio between the computational time for the simulation and the fire propagation time. A reduction of 85% in the computational time is obtained using the POD model. This result suggests that model reduction can be an useful approach to be used in order to make physical models more suitable for fast (or faster) simulations. It is worth noticing that comparison on the 20 m domain is fair, since both the mesh of the physical model and the eigenfunctions are defined on this portion. In the case a larger domain were considered, the advantage of POD model would be even larger. In fact, the number of nodes of the physical model would increase and so its computational cost per time step, while the number of eigenfunctions would remain the same and so the computational cost per time step of the POD model.

The error, as previously indicated in Figure 6.8a, depends on the number of eigenfunctions used to evaluate the results. The higher the number of eigenfunctions, the higher the accuracy of results, but also the higher the computational cost. Therefore is necessary to find a trade-off between accuracy and computational cost.

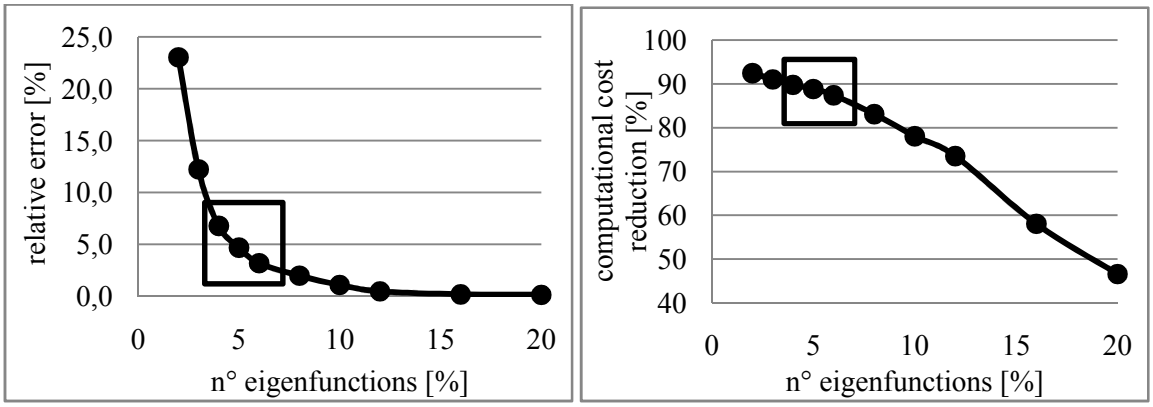

Figure 6.9 Relative error and computational cost reduction performed to the POD model with different number of eigenfunctions

In order to select a proper number of eigenfunctions, an error analysis has been performed. Results are reported in Figure 6.9. The square in the figures represents the number of eigenfunctions that is interesting to select due to the low relative error performed and the high reduction in computational cost.

6.7 POD model application

6.7.1 POD for simulation in the experimental domain (different wind speeds)

Once the POD model is obtained, it can be used for fast simulation of scenarios obtained by varying the model parameters, such as the fuel characteristics or wind speed, without need of any additional snapshots. This means that no additional full model simulations are necessary. The POD model has been applied to the prediction of the fire evolution in two particular experiments carried out on the entire domain (see Figure 6.10). During the experiments, wind speed had changed, varying from 0,9 m s^{-1} to 2.5 m s^{-1}. It is worth remarking that the POD model was created considering the snapshots corresponding to a single wind velocity, 2.0 m s^{-1}. Therefore only a single full model simulation is required in order to obtain a reduced model which is then used in a wide range of wind speeds. The values of ROS obtained with the POD model in the different domain sections are compared with the full model results and the experimental values. Each domain section is characterized by a particular wind velocity, due to the variations that were registered during the experiments. Results are reported in Figure 6.10.

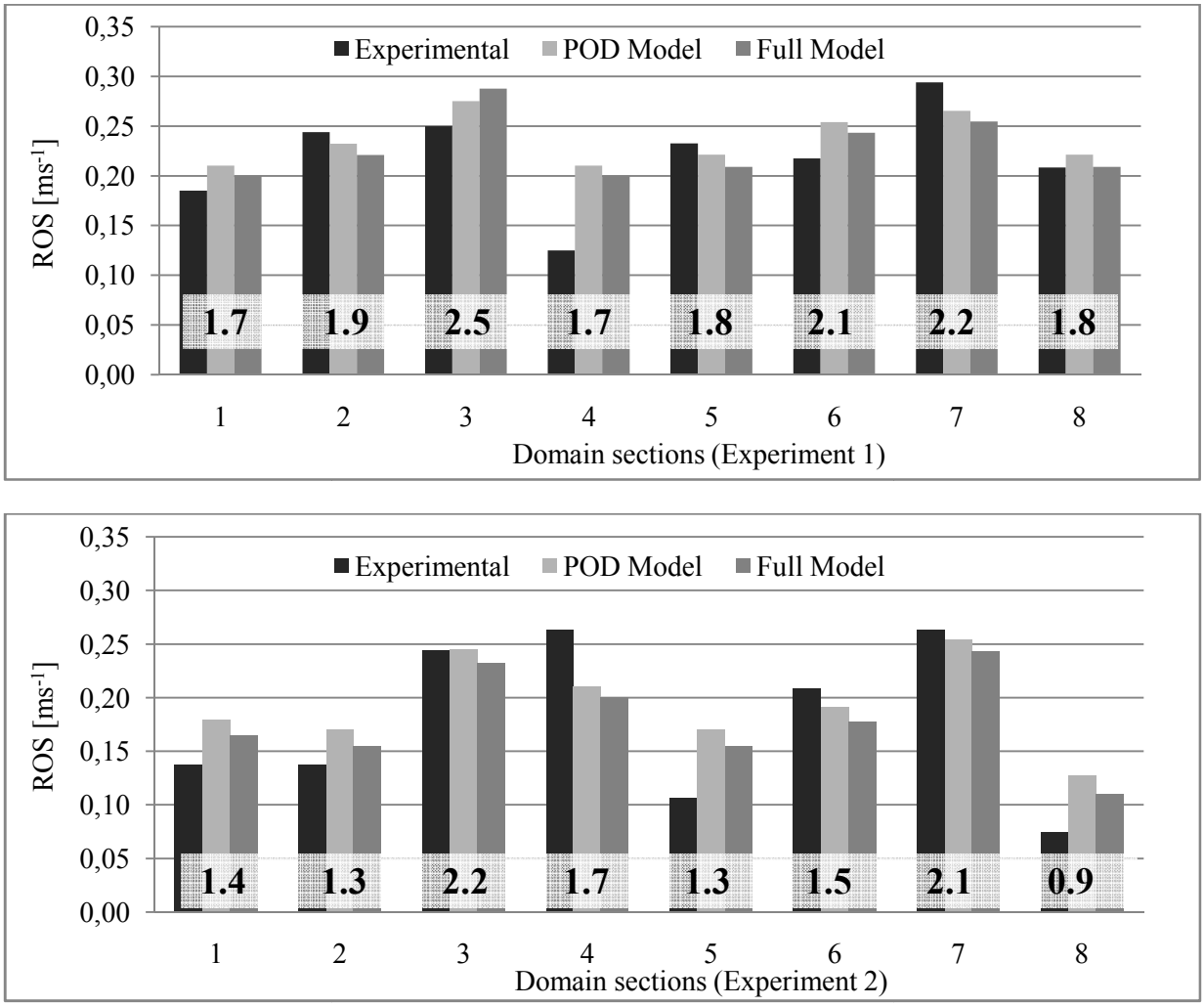

Figure 6.10 ROS results: comparison simulations vs experiments(in bold the corresponding wind speeds).
1st and 2nd experiments

Having in mind the goal of testing the performance of the POD model, the most interesting comparison is that with the full model results. In this regard, it is possible to notice that the average deviation of the two models in the 18 sections is about 6.4%, with an average difference in the ROS of about 0.013 m s^{-1}, while the maximum difference is about 0.017 m s^{-1}. Deviations are slightly larger in the sections characterized by smaller velocity (0.9-1.3 m s^{-1}), since the snapshots that have been used in model reduction corresponds to a larger velocity (2.0 m s^{-1}). In general, these results prove that POD method can be used as a model reduction technique for wildfire evolution physical model.

Comparison between both models and experimental results is performed with the purpose of showing that the physical models (both the full and the reduced ones) are suitable for representing the events. The average deviations of the two models with respect to the experiments is about 20%, with an average difference in the ROS of about 0.03 m s^{-1}.

In some cases, the level of accuracy is smaller, with a maximum difference in the ROS of about 0.09 m s-1. As already discussed, this is due to the non-homogeneities in fuel characteristics, humidity and wind (which value was read each 10 s), as shown by the not precise relation between wind speed and rate of spread (Figure 6.6). For instance with the same wind speed (1.7 m s-1) two very different experimental rates of spread were obtained.

6.7.2 POD for simulation with different fuel

The main strength of the POD projection approach is the ability to reproduce the behavior of the system with some different characteristics, using snapshots provided to an experiment or simulation executed in other conditions. It can be useful for carrying out simulations with different fuel conditions or developing sensitivity or parametric analysis using a reduced model built from a single reference scenario. In particular, it is possible to assess the effects of the fuel parameters using small computational resources. In this paper the effect of uncertainties in the evaluation of the reaction rate are investigated using the POD model. In particular, a +/- 30% variation of a (Eq. 6.2) has been considered. The resulting variation of ROS are illustrated in Fig. 6.11. The rate of spread evaluated with the full and POD model are very similar; the maximum error obtained is less than 6%. Furthermore the considered case is characterized by a low propagation velocity, therefore the deviation has a very small value, of the order of 0.0006 m/s. Figure 6.11 shows that an higher value of *a* correspond to a slower propagation, while ROS decrease with smaller value of *a*.

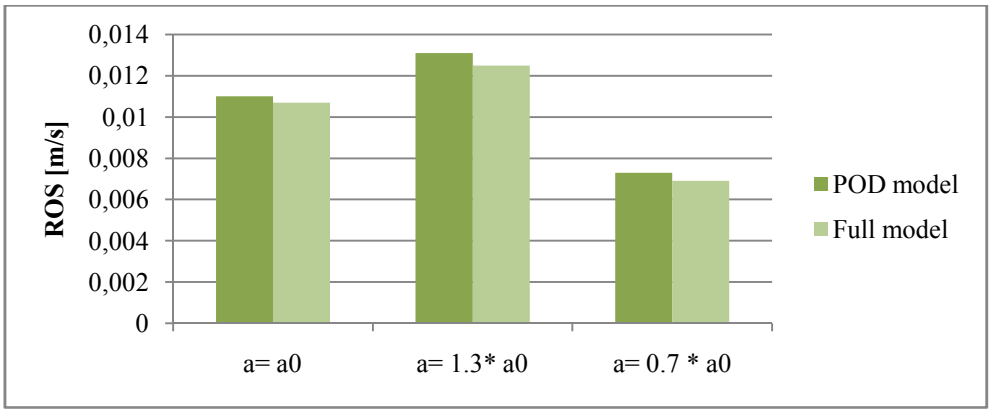

Figure 6.11 ROS with different mass loss rate coefficient (Guelpa et al 2014)

6.8 Discussion about POD applied to wildfire problems

On the basis of the results, it is possible to state that the application of POD technique to physical models is suitable for fast prediction of wildfire behavior, since large reduction in computational

efforts is accompanied by sufficiently small deviations in the ROS. This advantage is expected to be strengthened when the model complexity or the domain size increases.

A crucial aspect is that the POD model is built using snapshots collected from a very small number of simulations or experiments. Simulations or experiments do not need to refer to the entire event development, but may refer to a limited portion of domain. As an example, in the application presented here a single simulation has been conducted for 60 seconds considering constant wind speed (2.0 m/s) and homogeneous fuel. Once the snapshots are obtained, it is possible to perform simulations where the fuel characteristics (density, height, humidity, etc.) and wind speed vary with space and/or time, using the same POD model, i.e. no additional simulations using the full physical model or experiments are requested. Figure 6.10 is an example of POD application to scenarios corresponding with different wind speeds. An example of application to different fuel characteristics is available in Figure 6.11, where the POD model has been applied to a +/- 30% variation of the parameter *a* in a scenario without wind. The maximum relative error in the ROS was less than 6% (i.e. within the acceptable accuracy according to the number of snapshots, as highlighted in Figure 6.9), while the total variation in the ROS is about 50%.

The POD approach proposed in the present work is not limited to the selected physical model, but can be extended in the future to more complex models. Various works in the literature show that most of the phenomena considered in complex physical models can be reduced through POD, as discussed below:

2D propagation. Different techniques can be adopted to extend POD models to 2D propagation. As a first option, a 1D model can be combined with a simulation models (Sullivan 2009a) in order to obtain a landscape propagation (see for instance Anderson *et al* (1982) model or Glasa and Halada 2008). Section 6.9 shows an application of the simulator approach with experimental validation. A second option consists in dividing the fire-front during its evolution into multiple sectors and perform the POD simulation (always using the same basis) for each sector, so that the new fire-front can be obtained. Another choice is the creation of a 2D POD model that solves the conservation equations in a two-dimensional domain as described in Du *et al* 2013. The initial position of the fire front does not affect the POD model and when the initial point changes, there is no need to re-compute a new POD basis.

Large domain extension. The analysis developed in this work is applied to a small domain (50 m). This choice was forced by the need of referring to field experiments, which data are necessary for tuning the model coefficients and for validation purpose. The POD approach proposed here calculates the basis on a limited portion of the domain (20 m), which is moved with the fire front during the simulation. In this way, it is not necessary to define the eigenfunctions on the full

domain where propagation may occur, which would require a large number of eigenfunctions and high computational costs. The proposed approach, instead, allows one defining the eigenfunctions on a limited portion of domain with an extension depending on the fire size and then using it for possible propagations on large domains.

Fluid flow and turbulence. Various applications of POD to fluid dynamic problems are available in the literature. In Cazemier e*t al.* 1998 and Frouzakis, *et al.* 2000, the proper orthogonal decomposition has been successfully applied to a DNS formulation of fluid flow. The Galerkin method has been combined with POD in order to reduce turbulence models (Sirovich 1987; Berkooz e*t al.* 1993), such as RANS models (Rambo and Yoshi 2005) or LES models (Ullmann and Lang 2010). In the case of LES, which is the model adopted in various CFD codes such as WFDS and FIRELES, POD allows one reducing significantly the computational resources requested for the turbulence model. This issue is clearly presented in a recent paper (Keskinen *et al.* 2016) where the application to the simulation of an internal combustion engine is proposed.

Coupled fluid flow and heat transfer. POD modeling, mainly in the form of Galerkin-POD, has been applied to combined fluid flow and heat transfer problems. In Du *et al*. 2013b, a POD model is used for fast prediction of the air side velocity and temperature fields in an air-cooled condenser, which shows complex non-linear behavior, dependent on the meteorological conditions and operational configuration. In Ghosh and Joshi 2013 a POD model is used to predict transient air temperatures in an air-cooled data center. As a third example, it worth citing the work by Han *et al*. 2015, where a POD model is applied to the reduction of a natural convection problem considering radiation heat transfer at the boundaries.

Combustion models. Various papers in the literature present the application of POD to chemical kinetics (Danby and Echekki 2005) or to the simulation of chemical reactors (Yuan *et al*. 2005; Bizon, Continillo 2012). POD was successfully used also to solve combustion problems involving fluid flow, heat transfer and chemical reactions, such as in (Pyta *et al*. 2014; Iudiciani 2012).

The proposed approach has allowed to successfully deal with two specific features of the POD application to wildfire propagation. This overview shows that the approach has large potential to be applied to complex physical models.

6.9 Landscape evolution

6.9.1 Huygens Principle applied to fire propagation

In order to obtain the landscape propagation, when a 1D model is used, it is necessary to use mathematical models that transform the one-dimensional result in a two-directional propagation, as discussed in the previous section. Many interesting mathematical model have been developed out to morph the shape of a fire front as it advances in all the directions. In particular, it is necessary to represent the burning zone perimeter and to perform a suitable method for changing the perimeter position with time. The delimitation of the burning or not burning zone is usually represented using one of the following approaches: 1) perimeter considered as a curve or 2) perimeter defined as the boundary of different types of cells.

In this analysis, an approach based on Huygens principle, that was first used by Anderson *et al.* (1982 for wildfire evolution) has been applied to the POD model. The idea is to consider that fire propagates with an elliptical spread at each point of the fire front with the main axis directed along the main propagation direction. Therefore the fire front at the time step t grows as the envelope of all the ellipses built at each point of the fire front at the time t-1 (Figure 6.12).

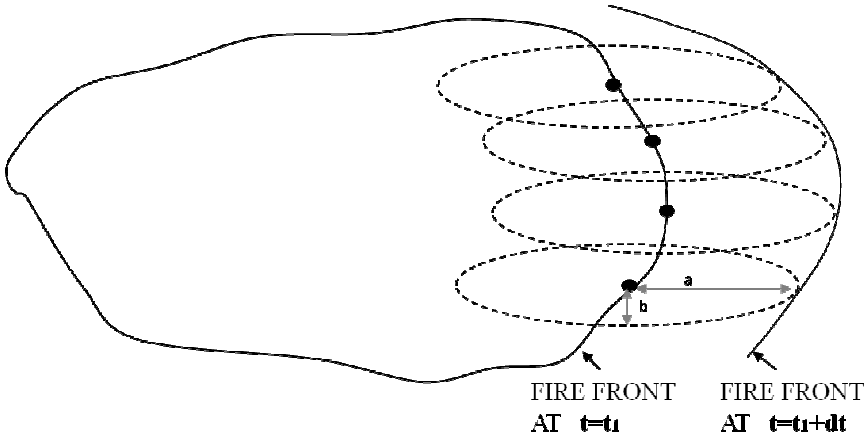

Figure 6.12 Huygens Principle applied to forest fire

The Huygens principle has been applied, in this case considering the main propagation direction as coincident with the direction of the wind. Therefore the major semi-axis length is given by the ROS with a certain wind speed times the time step. The length of the minor axis is the ROS when no wind occurs times the time step. Therefore:

$$a = ROS(wind\ velocity = v) \cdot dt \tag{6.10}$$

$$b = ROS(wind\ velocity = 0) \cdot dt \tag{6.11}$$

6.9.2 Fire evolution

The capability of the 2D model to detect the fire spread evolution has been tested using experimental data. Figure 6.13 reports a schematic of the experimental domain, about 30 m large and 50 m long. The orange line is the ignition line. The arrival time of the fire front at the points indicated with black circles was collected during the experiment. Therefore the set of 10 values (t_th_1, th_2, ..., t_th_n) has been compared with the results obtained using the 2D model

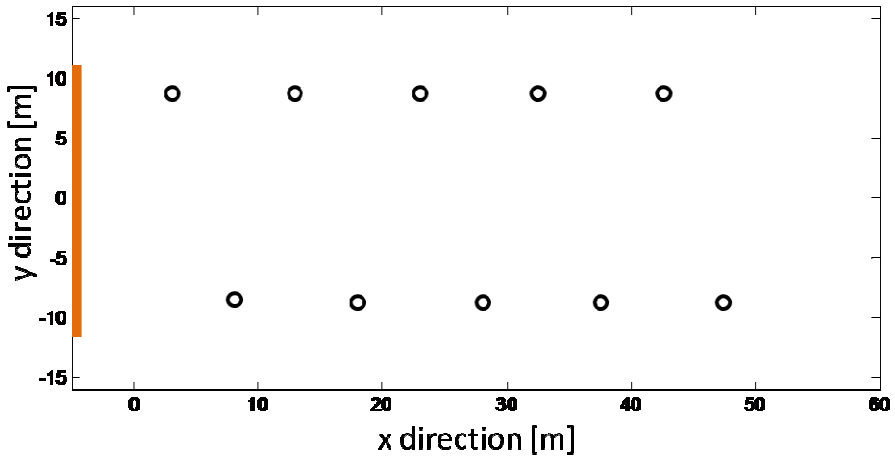

Figure 6.13 Experimental domain

Figure 6.14 reports the fire fronts at each time t_th_i evaluated using the 2D model and the wind velocity and direction detected at each time period between t_th_i and t_th_{i+1} . During the experiments, wind direction was mainly between SW and SSW. Accordingly, the fire front reaches higher distances in the lower part of the domain (where $y<0$) due to the higher wind component in the west direction.

The distance measured along the x direction between the blue points and the black circles is the error associated with the 2D model perform. The error values have been depicted in Figure 6.15.

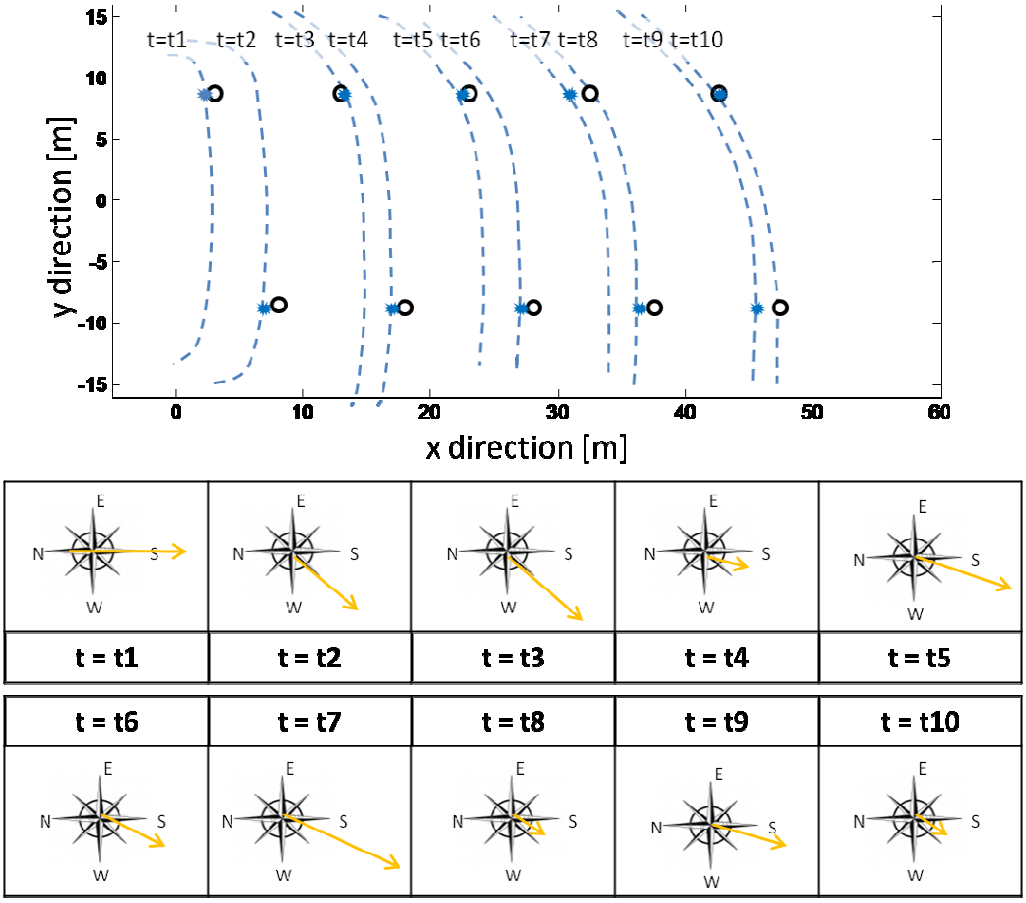

Figure 6.14 2D model fire front at t=t_th$_i$. In the table the wind speed and direction at each time period.

The 2D model fire front differ from the experimental fire front of a maxim of 2.2 m, while the mean difference is about 1 m and the relative error about 5%. Therefore a good agreement is obtained between the model results with the 2D experimental fire propagation.

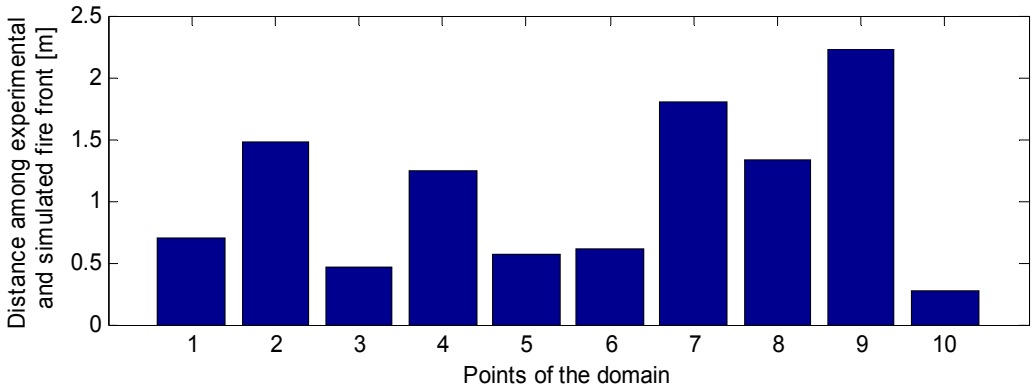

Figure 6.15 2D model fire front at t=t_th$_i$. In the table the wind speed and direction at each time period.

6.9.3 Fast 2D Landscape propagation model including wind and slope contribution

When both wind and slope affect the rate of spread, a different approach should be used in order to obtain landscape propagation. This necessity is due to the fact that these two contributions may have different orientations. A fast propagation approach has been obtained computing the fire evolution towards the principal propagation directions. This means that the 2π radians have been divided into a limited number of sectors. In each direction, the contributions slope and wind are computed and the corresponding rate of spread is obtained. In order to test the 2D propagation model, the Rothermel model has been used to evaluate the 1D rate of spread in each selected direction. The Rothermel model has thus been implemented using a Matlab® code and tested trough data obtained with the Behave software that includes a Rothermel model. In Figure 6.16,an example with 4 main propagation directions (indicated with I,II,III,IV) is reported. The components of the vector wind (w) and slope (s) are evaluated in each propagation direction and the rate of spread is evaluated accordingly.

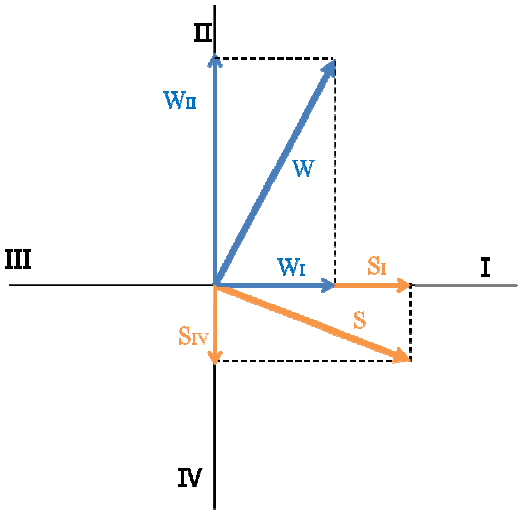

Figure 6.16 Main propagation direction approach

In the examined application, at each time step the fire front in divided into a number of portions of fixed length (in the simulations, a maximum length of 1m has been set). For the central point of each portion, the propagation is then evaluated as discussed here above. In particular, 16 main directions have been selected for each point of the fire front.

An up-slope terrain (23°), with variable wind speed, is considered. The slope in oriented towards East while wind is oriented towards north-east. The wind speed velocity varies between 5 and 15 km/h. Figure 6.17 shows the corresponding 2D propagation results. In black the initial burning area is reported, while red curves represent the fire front at different time frames. The red thick line is the fire front at the end of simulation, after 65 minutes. The figure shows that wind and

slope contributions are of primary importance in the fire spread. This is clear from the comparison of the distance between the ignition area and the final fire front in the same direction of wind and slope (E, N-E) respect to the distance in the S-W direction where no wind and slope contribution occur. Propagation in the S-W direction is negligible respect to the propagation in the N-E direction. Furthermore between 45 and 60 minutes, when the wind speed is higher, the distance among the red lines is larger.

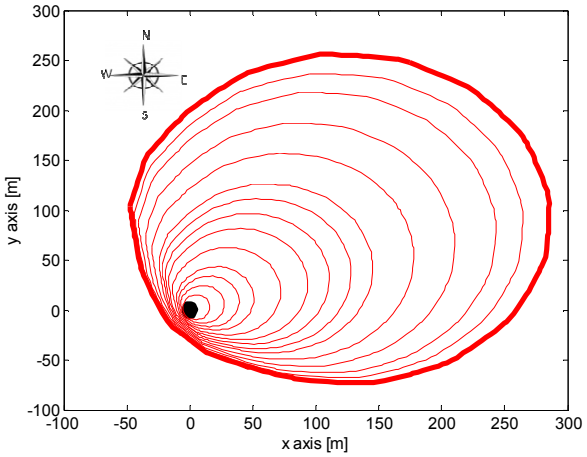

t	wind speed	wind direction	Slope	slope direction
[min]	***[km/h]***	**-**	***[rad]***	**-**
0	5,00	N-E	0,4	E
5	5,00	N-E	0,4	E
10	5,00	N-E	0,4	E
15	5,00	N-E	0,4	E
20	10,00	N-E	0,4	E
25	10,00	N-E	0,4	E
30	8,00	N-E	0,4	E
35	8,00	N-E	0,4	E
40	8,00	N-E	0,4	E
45	15,00	N-E	0,4	E
50	15,00	N-E	0,4	E
55	15,00	N-E	0,4	E
60	10,00	N-E	0,4	E
65	10,00	N-E	0,4	E

Figure 6.17 Main propagation direction approach results.
left: result obtained through the simulator; right: data used as inputs

6.10 Concluding remarks

The work carried out is the first application of POD technique to wildland fire physical models, with the aim of significantly reduce the computational time requested for simulation. A simple 1D problem, which parameters were obtained from field experiments, has been selected to develop a suitable strategy for the application of POD to wildfire engineering.

POD model is able to provide results very similar to the full model with significant reduction in the computational cost. As an example, using 6% of the available eigenfunctions, an average deviation of 6.4% in the results is obtained, while the computational time to solve the energy equation is reduced of 85% with respect to the full model.

Snapshots provided by the full model in a single wind condition (2.0 m s^{-1}) have been used to create the reduced model, which has been then applied to the simulations in different wind conditions (0.9-2.5 m s^{-1}). Results show that POD model is able to estimate the ROS with good accuracy, even when the wind speed differs from that used to obtain the snapshots. The average

deviation in the ROS prediction by the two models is of about 0.013 m s^{-1}, while the maximum difference is about 0.017 m s^{-1}. Similarly, the same POD model can be applied to non-homogeneous fuel distributions.

These are promising results, which encourage a further application of the POD technique to more complex and multi-dimensional physical models in order to reduce their computational cost and make their use for operational purposes more feasible. Furthermore a model for 2D fire propagation that takes into account the difference between wind and slope direction has been carried out. Further development will be focused on the inclusion of the moisture and slope contribution in the physical model. The contribution of the moisture will be considered modifying the term related to the mass consumption and the unsteady term, while the slope contribution is taking into account through the adjustment of the radiative and convective terms. The model will be included in the 2D landscape propagation tool with the aims of obtaining a very fast physical simulator that can be used as evolution prediction, real time risk analysis and preventive risk analysis. Furthermore, future plans include an analysis aiming at the evaluation of the preferential paths for the prediction of the fire evolution by means of an entropy generation analysis.

7

Conclusions and future developments

The work presented in this thesis is related to the modeling of energy transfer in systems involving large domains and long evolution time. In particular, various approaches to make simulations of such types of systems fast have been developed and applied. Three different applications have been analyzed:

- The thermal plume evolution in the subsurface due to groundwater heat pumps installation is analyzed with the aim of determining the effects of a newly installed heat pump on possible downstream installations. This is a possible future scenario in urban areas. The system involves spaces of the order of kilometers and times of the order of years. It cannot be considered stationary because of the changes in the operating conditions of the heat pump as well as the propagation of the thermal plume in the ground. A multi-level modeling approach has been used to make the computational cost to solve a multi-year simulation acceptable. The model consists in coupling a 3D model

in the near field (near the extraction and re-injection wells) where the velocity and temperature gradients are higher and a network model in the far field, where the effect of the velocity profile becomes close to the undisturbed profile and the temperature gradients small. The approach proposed here is not new but here it has been applied for the first time to the analysis of groundwater resources. The main novelty is thus related with the application, which can be used to create a tool for the analysis of large territories where multiple installations of heat pumps are planned.

- The Turin District Heating Network has been considered as an application with the idea of producing fast tools for the analysis of possible improvements in the operating conditions. The Turin DHN is one of the largest in Europe and the largest in Italy therefore a high computational time is required to solve the thermal fluid dynamic problem in the whole network. Two different aspects have been analyzed. At first, a tool for the optimization of pumping strategies has been built with the aim of minimizing the electricity consumption requested to pump water to the various users. Secondly some methods for the thermal peak shaving have been investigated. In particular storage installation have been considered and changes in user thermal requests have been optimized, with the purpose of increasing the cogeneration exploitation and, as a consequence, reduce the primary energy consumption. The DHN description is based on a graph approach and the model solve the conservation equation for the network. In both the analyzed cases a POD-RBF technique has been applied to the model to ensure a major simulation velocity. The main novelties related to this part consists in the development of a fast tool for the analysis of district heating networks. The tool is able to integrate measured data coming from the thermal substations in order to evaluate the opportunities for operation improvements or optimization. In addition the approach is suitable for multi-level analysis, which involves the use of the fluid-dynamic model for the main transport network and reduced models for the distribution networks. A carefully validation has also conducted in order to make it possible to use the tool in the real plant, where the tool is currently under tests.
- A wildfire prediction model has been developed with the aims of showing the potential for the use of POD to such kind of systems. This work is based on the main idea to make wildfire physical models, which are currently characterized by very high computational costs, suitable for fast simulation and risk analysis purposes. A simple 1D model based on energy and mass conservation equation has been implemented and its capability to predict real fire spread on grassland has been tested through experimental data. A fast landscape propagation tool has been performed with the purpose of producing a two-dimensional fire evolution predictor. The POD reduction technique has never been applied to simulate forest fire propagation and this work represents the starting point for a

more complete use of this technique addressing wildfire related problems. The approach has been currently integrated in an industrial prototype tool for risk analysis within an European Integrated Project (AF3). To apply POD to wildfire a novel approach has been proposed in order to limit the analysis only to the domain where fire propagates. The domain is then moved with time as the fire front advances.

The work shows that often, in different fields, high computational costs become a severe limitation to perform simulations or, in some cases, to use models as operational tools. Often these restrictions can be overcame trough the choice of a suitable reduction technique. For instance the groundwater application can be solved in high, but reasonable, computational cost, only trough a reduction approach. In this particular case the multi-level technique allows the model to provide results in a much smaller time. The solution of the full 3D model on a single 3.3 GHz CPU is performed in about 2 days for a domain 600x500x100 and considering 3 years operation for the heat pumps. On the other hand, the network model requires about 2 hours to complete the simulation in a domain 300x2000 m long. The multi-level method allows one to significantly reduce the computational cost and to obtain results in an acceptable amount of time. If the 3D model were applied to the entire domain a computational cost of more than a week would be expected. The expected computational cost reduction is more than 70%. This results become more important if examined from a more complex point of view as indicated in this section later on.

In some cases the computational cost required for the simulation is not a limitation for researches purposes; however it constitutes an inadequate characteristic for real time purposes. This is the case of simulations in case of large DHSs and wildfire system propagation.

In these two cases the full models have been reduced trough different techniques. In both applications the present work reports the capability of the proposed methods to avoid high computational complexity and the corresponding reduction in accuracy. As reported in the Chapter 4, the POD interpolation approach (POD-RBF technique) allows a reduction of more than 95% of the computational cost with a maximum deviation of about 8% with respect to the full model. The POD projection approach reduces the computational time of about the 85% with respect to the full model about 6% average deviation. However the robustness of the POD projection approach allows to apply the reduced model also in case that are far from the case used for the snapshots construction. Therefore when the model has to be more general as possible, it would be better to adopt a more robust approach even if a higher computational cost is required. As an example in the two proposed applications the POD model is able to detect the fire behaviour also when an extrapolation with respect to the input data is required, while the POD-RBF methods only allows one to interpolate quickly the system behaviour within the domain for scenarios where snapshots are obtained. In the case of the POD model, it is difficult to define a

unique precision that characterizes this model reduction technique, because it essentially depends on the deviation between the simulated scenario and that considered for creating the snapshots. As an example when a difference in the fuel type occurs as a variation of ±30% in the coefficients values the maximum relative error detected was about 6%, a low value respect to the uncertainties related to the different conditions. In particular for the aims of the DHN simulation, both the optimal pumping operation and the thermal load prediction are evaluated in various representative scenarios and for the considered applications the is no significant need for extrapolation. Therefore the POD-RBF is a suitable method for this particular application, a remarkable reduction in the computational cost with small deviations can be obtained. In the future, the possible application of the method to the analysis of network expansion or malfunctioning operation may require using an approach able to allow extrapolations such as the POD model.

Considering the results obtained, in the author's opinion the proposed methods and applications deserve further developments. Various ideas that should be considered as future work are discussed below:

- As regards the ***groundwater*** analysis, the present work provides the basis for the future elaboration of a simulator able to include more heat pump installations in a large domain. Such composite model will be able to perform a simulation of an entire urban area, providing results of possible interactions between the heating systems. These scenarios present potential issues as documented in various analyses performed for the towns of London and Turin among others (Fry 2009). Two different pieces of information can be made available by means of the composite model: 1) The combined effects of more heat pump installations can be significantly different than the global effects of just one; in fact it is possible that a certain amount of water is extracted from or re-injected in the thermal plume created by an heat pump located up-stream. In the case the downstream installation is operating in cooling mode and the water temperature results as modified by the winter operation of an upstream system, the second pump reduces the effects produced by the first one. The opposite occurs when the two systems, despite the time requested for water to flow and reach the second installation, are in phase (e.g. warmer water resulting from summer mode operation extracted from a heat pump operating in summer mode). 2) Secondly such analysis gives useful details useful to predict the changes in heat pumps performances that can be not negligible. In fact from the study reported in Chapter 3 an installation 400 m from the test case would have a non negligible increase in the heat pump winter performances. On the other hand the thermal plume would produce, in the heat pump far 700 m from the test case, a decrease in the performances of more than 30%. Clearly the analysis would be more accurate if all the groundwater heat pump installed in the cities (that nowadays are usually not a low number) would be considered.

Furthermore an experimental analysis for the model validation will be developed when the experimental data collected in some points of the groundwater domain will be available. The tool could be also applied in order to analyze possible thermal storage in aquifer that could be designed even in the case of smooth water flow.

- About ***DHS,*** different further steps have been planned:
  - The inclusion of all the distribution networks through a GIS based input is one of the main improvement considered; this information allows one considering the evolutions of the network including connection of additional users or installations of additional portions of the network. Such global model including the main network and all the distributions networks allows one to have a more complete view of the network behaviour and constitutes a valuable tool for operations and system improvement decisions.
  - Another important improvement regards the optimizer for the best time schedule for the various users. At present, the full model is used as the fluid-dynamic solver in the optimization tool installed on the real network and currently applied to a single barycentre (BCT-414). This is time consuming and it is not possible to directly extend it on the global network. Different approaches can to be considered in order to overcome such limitation. The POD-RBF technique could be applied to each single barycentre in order to make the optimum evaluation faster. At present the computational time required for running the optimization of a single barycentre is about 2.5 hours. The inclusion of the reduced POD-RBF is supposed to accelerate the simulation and allows to obtain the results in about 15 minutes.
  - The application of POD-RBF to operating conditions with malfunctions has been tested but not fully exploited. The analysis of possible malfunctions in pipes requires a significant increase in the number of free variables. The proposed approach might not be suitable for the solution of such problem. As a possible future development the POD approach could be used in order to reduce the momentum equation similarly to what has been proposed for the fire propagation. Another possible approach that is worth considering is the analysis of sensitivities to malfunctions through application of topological optimization. This option is currently under development within a different doctoral thesis.
  - Furthermore a more detailed user model will be developed in order to allow better exploitation of the opportunities for primary energy savings. In fact, increasing the anticipation range can be performed only trough a user model that guarantees that the changes in the start-up time strategy do not produce

significant effects on the building temperatures, so that the comfort standards can be preserved. A user model by means of the commercial software "Energy Plus" will be built. This model could be then reduced using for instance neural network in order to obtain fast simulation of the buildings behaviour as a function of the heating scheduling. This would allow to perform an optimization that includes, for each test case, a check of the indoor comfort level.

- Regarding the ***wildfire prediction simulator*** various contributions will be included in the physical model in order to make it capable to reproduce fire evolution in several conditions.
    - At first the moisture content have to be included in the model. In fact it is a very important characteristic that can significantly vary the fire propagation. This contribution will be included in the mass variation coefficient term of the energy conservation equation in order to take into account the differences in the combustion when a moisture content varies. Furthermore also the unsteady term has to be modified in order to take into account the presence of the water.
    - The slope contribution should be included when the fire propagate in an up-slope terrain. In this case the spread is faster due to main aspects: the different view factor and buoyancy contribution. Therefore both the radiation and the convective terms have to be properly modified. This part of inclusion is currently in progress.
    - The obtained model will be included in the 2D tool for landscape propagation in order to use it as a fire evolution simulator. In particular the contribution of retardant substances and other extinguish procedure will be studied through the model. This aspect has the aim of proposing a simple and fast physical model for estimation of the real time risk analysis and the evaluation of the preventive risk. Only a very fast model can in fact be used for such purposes because of the suitability to perform in a short time many simulation taking into account the input data uncertainty and, in case of preventive analysis, the ignition point.
    - Furthermore another kind of analysis has been planned and it is currently under elaboration. It has the aims of determining the main propagation direction in case of different directional contribution. In fact the fire spread direction is mainly due to wind direction, slope direction and position of the fuel with less level of moisture and lower ignition point. When all these contributions appear at the same time the fire propagate according a preferential path. The future work will be focused on the use of the entropy generation analysis to identify preferential paths for fire propagation analysis. In such works the effects due to

the fuel type, fuel characteristics (e.g. humidity), wind and slope as well as the heat transfer mechanisms, including radiation, have to be taken into account.

- The POD model has proven to be very effective in reducing the computational time requested for multiple simulations. As the approach has been applied to a simple physical model, it is worth further developing it in order to allow its application to more complex physical models.

References

Ancona, M. A., Melino, F., & Peretto, A. (2014). An Optimization Procedure for District Heating Networks. *Energy Procedia*, *61*, 278-281.

Anderson, D. H., Catchpole, E. A., De Mestre, N. J., & Parkes, T. (1982). Modelling the spread of grass fires. *The Journal of the Australian Mathematical Society. Series B. Applied Mathematics*, *23*(04), 451-466.

Angayarkkani, K., & Radhakrishnan, N. (2010). An intelligent system for effective forest fire detection using spatial data. *arXiv preprint arXiv:1002.2199*.

Antoulas, A. C. (2005). *Approximation of large-scale dynamical systems* (Vol. 6). Siam.

Arad, N., Dyn, N., Reisfeld, D., & Yeshurun, Y. (1994). Image warping by radial basis functions: application to facial expressions. *CVGIP: Graphical models and image processing*, *56*(2), 161-172.

Aringhieri, R., & Malucelli, F. (2003). Optimal operations management and network planning of a district heating system with a combined heat and power plant. Annals of Operations Research, 120(1-4), 173-199.

Ascoli D., Vacchiano G., Motta R., Bovio G. (2015) Building Rothermel fire behaviour fuel models by genetic algorithm optimisation. *International Journal of Wildland Fire* 24, 317-328

Ascoli, D., Beghin, R., Ceccato, R., Gorlier, A., Lombardi, G., Lonati, M., ... & Cavallero, A. (2009). Developing an adaptive management approach to prescribed burning: a long-term heathland conservation experiment in north-west Italy. *International Journal of Wildland Fire*, *18*(6), 727-735.

Balbi J., Santoni P., Dupuy J. (1999) Dynamic modelling of fire spread across a fuel bed. *International Journal of Wildland Fire* 9, 275–284

Barelli, L., Bidini, G., & Pinchi, E. M. (2006). Implementation of a cogenerative district heating: Optimization of a simulation model for the thermal power demand. *Energy and buildings*, *38*(12), 1434-1442.

Benner, P & Heike Faßbender (2015). Model Order Reduction: Techniques and Tools. Springer London, 10.1007/978-1-4471-5102-9_142-1

Benonysson A., Bohm I.B., Ravn H.F. (1995). Optimization in a District Heating System. *Energy Conversion and Management* 36: 297-314.

Benonysson, A., Bøhm, B., & Ravn, H. F. (1995). Operational optimization in a district heating system. *Energy conversion and management*, *36*(5), 297-314.

Berkooz G., Holmes P., Lumley J.L. (1993). The proper orthogonal decomposition in the analysis of turbulent flows. *Annual review of fluid mechanics* 25, 539-575

Berkooz, G., Holmes, P., & Lumley, J. L. (1993). The proper orthogonal decomposition in the analysis of turbulent flows. *Annual review of fluid mechanics*, *25*(1), 539-575.

Białecki, R. A., Kassab, A. J., & Fic, A. (2005). Proper orthogonal decomposition and modal analysis for acceleration of transient FEM thermal analysis. *International journal for numerical methods in engineering*, *62*(6), 774-797.

Bizon, K., & Continillo, G. (2012). Reduced order modelling of chemical reactors with recycle by means of POD-penalty method. *Computers & Chemical Engineering*, *39*, 22-32.

Blanco, P. J., Pivello, M. R., Urquiza, S. A., & Feijóo, R. A. (2009). On the potentialities of 3D–1D coupled models in hemodynamics simulations. *Journal of Biomechanics*, *42*(7), 919-930.

Bojic, M., & Trifunovic, N. (2000). Linear programming optimization of heat distribution in a district-heating system by valve adjustments and substation retrofit. *Building and Environment*, *35*(2), 151-159.

Booij, N., Ris, R. C., & Holthuijsen, L. H. (1999). A third-generation wave model for coastal regions: 1. Model description and validation. *Journal of geophysical research: Oceans*, *104*(C4), 7649-7666.

Brenner, T. A., Fontenot, R. L., Cizmas, P. G., O'Brien, T. J., & Breault, R. W. (2012). A reduced-order model for heat transfer in multiphase flow and practical aspects of the proper orthogonal decomposition. *Computers & Chemical Engineering*, *43*, 68-80.

Buchan, A. G., Pain, C. C., Fang, F., & Navon, I. M. (2013). A POD reduced-order model for eigenvalue problems with application to reactor physics.*International Journal for Numerical Methods in Engineering*, *95*(12), 1011-1032.

Buchan, A. G., Pain, C. C., Fang, F., & Navon, I. M. (2013). A POD reduced-order model for eigenvalue problems with application to reactor physics.*International Journal for Numerical Methods in Engineering*, *95*(12), 1011-1032.

Buhmann, M. D. (2000). Radial basis functions. *Acta Numerica 2000*, *9*, 1-38.

Buljak V (2011). Inverse analyses with model reduction: proper orthogonal decomposition in structural mechanics. Springer Science & Business Media

Burgan, R. E., & Rothermel, R. C. (1984). BEHAVE: fire behavior prediction and fuel modeling system--FUEL subsystem.

Calì M., Borchiellini R. (2002). District Heating Network Calculation and Optimization. *Encyclopedia of Life Support Systems*, UNESCO (paper 3.19.3.8).

Campbell, G. S., & Norman, J. M. (2012). An introduction to environmental biophysics. Springer Science & Business Media.

Canadian Forest Service (2004). Prometheus User Manual v. 3.0.1.

Cazemier, W., Verstappen, R. W. C. P., & Veldman, A. E. P. (1998). Proper orthogonal decomposition and low-dimensional models for driven cavity flows.*Physics of Fluids (1994-present)*, *10*(7), 1685-1699.

Chinesta, F., Ammar, A., Leygue, A., & Keunings, R. (2011). An overview of the proper generalized decomposition with applications in computational rheology. *Journal of Non-Newtonian Fluid Mechanics*, *166*(11), 578-592.

Chinesta, F., Leygue, A., Bordeu, F., Aguado, J. V., Cueto, E., González, D., ... & Huerta, A. (2013). PGD-based computational vademecum for efficient design, optimization and control. *Archives of Computational Methods in Engineering*, *20*(1), 31-59.

Colella, F. (2010). Multiscale Modelling of Tunnel Ventilation Flows and Fires.

Colella, F., Rein, G., Verda, V., & Borchiellini, R. (2011). Multiscale modeling of transient flows from fire and ventilation in long tunnels. *Computers & Fluids*,*51*(1), 16-29.

Coleman, J. R., & Sullivan, A. L. (1996). A real-time computer application for the prediction of fire spread across the Australian landscape. *Simulation*, *67*(4), 230-240.

Cosentino, S., Guelpa, E., Melli, R., Sciacovelli, A., Sciubba, E., Toro, C., & Verda, V. (2014, November). Optimal Operation and Sensitivity Analysis of a Large District Heating Network Through POD Modeling. In *ASME 2014 International Mechanical Engineering Congress and Exposition* (pp. V06AT07A027-V06AT07A027). American Society of Mechanical Engineers.

Cosentino, S., Guelpa, E., Melli, R., Sciacovelli, A., Sciubba, E., Toro, C., & Verda, V. (2014). Identification of the optimal operational strategy of a large district heating networks through POD modeling. *Proceedings of ECOS*, 15-19.

Cross, H. (1936). Analysis of flow in networks of conduits or conductors.*University of Illinois. Engineering Experiment Station. Bulletin; no. 286*.

Cruz M.G., Alexander M.E. (2013). Uncertainty associated with model predictions of surface and crown fire rates of spread. *Environmental Modelling & Software* 47, 16-28.

Danby, S. J., Echekki, T. (2005). Proper orthogonal decomposition analysis of autoignition simulation data of nonhomogeneous hydrogen–air mixtures. Combustion and Flame144, 126–138.

D'Angelo, C., & Quarteroni, A. (2008). On the coupling of 1d and 3d diffusion-reaction equations: Application to tissue perfusion problems. *Mathematical Models and Methods in Applied Sciences*, *18*(08), 1481-1504.

Diao, N., Li, Q., & Fang, Z. (2004). Heat transfer in ground heat exchangers with groundwater advection. *International Journal of Thermal Sciences*, *43*(12), 1203-1211.

Dietrich, J. C., Zijlema, M., Westerink, J. J., Holthuijsen, L. H., Dawson, C., Luettich, R. A., & Stone, G. W. (2011). Modeling hurricane waves and storm surge using integrally-coupled, scalable computations. *Coastal Engineering*,*58*(1), 45-65.

Dotzauer, E. (2002). Simple model for prediction of loads in district-heating systems. *Applied Energy*, 73(3), 277-284.

Du J., Fang F, Pain C.C., Navon I.M., Zhu J., Ham D.A. (2013). POD reduced-order unstructured mesh modeling applied to 2D and 3D fluid flow.*Computers & Mathematics with Applications* 65, 362-379

Du X., Hu H., Shen Y., Yang L., Yang Y. (2013b). Reduced order analysis of flow and heat transfer for aircooled condenser of power generating unit, *Applied Thermal Engineering* 51, 383–392.

Fang, T., & Lahdelma, R. (2014). State estimation of district heating network based on customer measurements. *Applied Thermal Engineering*, *73*(1), 1211-1221.

Fang, T., & Lahdelma, R. (2015). Genetic optimization of multi-plant heat production in district heating networks. *Applied Energy*, *159*, 610-619.

Fatouh, M., & Elgendy, E. (2011). Experimental investigation of a vapor compression heat pump used for cooling and heating applications. *Energy*,*36*(5), 2788-2795.

Finney, M. A., Cohen, J. D., Forthofer, J. M., McAllister, S. S., Gollner, M. J., Gorham, D. J., ... & English, J. D. (2015). Role of buoyant flame dynamics in wildfire spread. *Proceedings of the National Academy of Sciences*, *112*(32), 9833-9838.

Finney, M. A., Cohen, J. D., McAllister, S. S., & Jolly, W. M. (2013). On the need for a theory of wildland fire spread. *International journal of wildland fire*,*22*(1), 25-36.

Fons W., 1946. Analysis of fire spread in light forest fuels . J. Agr. Res. 72, 93-121

Formaggia, L., Gerbeau, J. F., Nobile, F., & Quarteroni, A. (2001). On the coupling of 3D and 1D Navier–Stokes equations for flow problems in compliant vessels. *Computer Methods in Applied Mechanics and Engineering*, *191*(6), 561-582.

Fornberg, B., & Flyer, N. (2005). Accuracy of radial basis function interpolation and derivative approximations on 1-D infinite grids. *Advances in Computational Mathematics*, *23*(1-2), 5-20.

Fry, V. A. (2009). Lessons from London: regulation of open-loop ground source heat pumps in central London. *Quarterly Journal of Engineering Geology and Hydrogeology*, *42*(3), 325-334.

Freedman, V. L., Waichler, S. R., Mackley, R. D., & Horner, J. A. (2012). Assessing the thermal environmental impacts of an groundwater heat pump in southeastern Washington State. *Geothermics*, *42*, 65-77.

Freno, and Cizmas, P. G. (2014). A proper orthogonal decomposition method for nonlinear flows with deforming meshes. *International Journal of Heat and Fluid Flow*, *50*, 145-159.

Freno, B. A., Brenner, T. A., & Cizmas, P. G. (2013). Using proper orthogonal decomposition to model off-reference flow conditions. *International Journal of Non-Linear Mechanics*, *54*, 76-84.

Frouzakis, C. E., Kevrekidis, Y. G., Lee, J., Boulouchos, K., & Alonso, A. A. (2000). Proper orthogonal decomposition of direct numerical simulation data: Data reduction and observer construction. *Proceedings of the Combustion Institute*, *28*(1), 75-81.

Ghosh, R., & Joshi, Y. (2013). Error estimation in POD-based dynamic reduced-order thermal modeling of data centers. *International Journal of Heat and Mass Transfer*, *57*(2), 698-707.

Glasa J., Halada L. (2008). On elliptical model for forest fire spread modeling and simulation. *Mathematics and Computers in Simulation,* 78, 76-8

Golberg D.E. Genetic algorithms in search, optimization, and machine learning. Addionwesley; 1989.

Guelpa, E., Sciacovelli, A., Verda, V., & Ascoli, D. (2014). Model reduction approach for wildfire multi-scenario analysis. *Parte: http://hdl. handle. net/10316.2/34013*.

Guelpa, E., Toro, C., Sciacovelli, A., Melli, R., Sciubba, E., & Verda, V. (2016). Optimal operation of large district heating networks through fast fluid-dynamic simulation. *Energy*, *102*, 586-595. doi:10.1016/j.energy.2016.02.058

Gustafsson, J., Delsing, J., & van Deventer, J. (2010). Improved district heating substation efficiency with a new control strategy. *Applied Energy*,*87*(6), 1996-2004.

H.-J.G. Diersch, Reference Manual for FEFLOW®.WASY GmbH Berlin Germany, 2005, p. 292. http://www.feflow.info/

Haaland, S.E. (1983) "Simple and Explicit Formulas for the Friction Factor in Turbulent Flow" Journal of Fluids Engineering, Vol. 103 (5), pp. 89–90.

Han, D., Yu, B., Chen, J., Wang, Y., & Wang, Y. (2015). POD reduced-order model for steady natural convection based on a body-fitted coordinate.*International Communications in Heat and Mass Transfer*, *68*, 104-113.

Hanson, H. P., Bradley, M. M., Bossert, J. E., Linn, R. R., & Younker, L. W. (2000). The potential and promise of physics-based wildfire simulation.*Environmental Science & Policy*, *3*(4), 161-172.

Harary F.,Graph Theory.Narosa Publishing House, New Delhi;1995.

Helbing, D., Farkas, I. J., Molnar, P., & Vicsek, T. (2002). Simulation of pedestrian crowds in normal and evacuation situations. *Pedestrian and evacuation dynamics*, *21*(2), 21-58.

Berkooz, G., Holmes, P., & Lumley, J. L. (1993). The proper orthogonal decomposition in the analysis of turbulent flows. *Annual review of fluid mechanics*, *25*(1), 539-575.

Horowitz, L. W., Walters, S., Mauzerall, D. L., Emmons, L. K., Rasch, P. J., Granier, C., ... & Orlando, J. J. (2003). A global simulation of tropospheric ozone and related tracers: Description and evaluation of MOZART, version 2. *Journal of Geophysical Research: Atmospheres*, *108*(D24).

Hotelling, H. (1933). Analysis of a complex of statistical variables into principal components. *Journal of educational psychology*, *24*(6), 417.

Irwin, G. W., Warwick, K., & Hunt, K. J. (1995). *Neural network applications in control* (No. 53). Iet.

Iske, A., & Sonar, T. (1996). On the structure of function spaces in optimal recovery of point functionals for ENO-schemes by radial basis functions. Numerische Mathematik, 74(2), 177-201.

Iudiciani P. (2012). Swirl stabilized premixed flame analysis using LES and POD. Ph.D dissertation, Lund University.

Jiang, X. S., Jing, Z. X., Li, Y. Z., Wu, Q. H., & Tang, W. H. (2014). Modelling and operation optimization of an integrated energy based direct district water-heating system. *Energy*, *64*, 375-388.

Jokinen E, Kontu K, Rinne S, Lahdelma R. Demand side management in District Heating buildings to optimize the heat production. Proceedings of ECOS 2014. Turku, Finland, June 15-19.

Karplus, M., & Kuriyan, J. (2005). Molecular dynamics and protein function. *Proceedings of the National Academy of Sciences of the United States of America*, *102*(19), 6679-6685.

Kerckhoffs, R. C., Neal, M. L., Gu, Q., Bassingthwaighte, J. B., Omens, J. H., & McCulloch, A. D. (2007). Coupling of a 3D finite element model of cardiac ventricular mechanics to lumped systems models of the systemic and pulmonic circulation. *Annals of biomedical engineering*, *35*(1), 1-18.

Keskinen J-P., Vuorinen V., Kaario O. (2016). Nonlinear time series analysis from large eddy simulation of an internal combustion engine. *International Journal of Heat and Fluid Flow,* 57, 79–90

Koiv, T. A., Mikola, A., & Palmiste, U. (2014). The new dimensioning method of the district heating network. *Applied Thermal Engineering*, *71*(1), 78-82.

Krysl, P., Lall, S., & Marsden, J. E. (2001). Dimensional model reduction in non-linear finite element dynamics of solids and structures. *International Journal for numerical methods in engineering*, *51*(4), 479-504.

Laajalehto T., Kuosa M., Mäkilä T., Lampinen M., Lahdelma R. (2014) Energy efficiency improvements utilising mass flow control and a ring topology in a district heating network. *Applied Thermal Engineering*, 69: 86-95.

Larsen, H. V., Pálsson, H., Bøhm, B., & Ravn, H. F. (2002). Aggregated dynamic simulation model of district heating networks. *Energy conversion and management*, *43*(8), 995-1019.

Lefschetz, S. (1937). On the fixed point formula. *Annals of Mathematics*, 819-822.

Ormsbee, L. E. (2006, August). The history of water distribution network analysis: The computer age. In *8th Annual Water Distribution Systems Analysis Symposium* (pp. 27-30).

Lindenberger, D., Bruckner, T., Groscurth, H. M., & Kümmel, R. (2000). Optimization of solar district heating systems: seasonal storage, heat pumps, and cogeneration. *Energy*, *25*(7), 591-608.

Linn, R. R., & Harlow, F. H. (1997). *FIRETEC: a transport description of wildfire behavior* (No. LA-UR--97-3920; CONF-980121--). Los Alamos National Lab., NM (United States).

Lumley J.L., Yaglom A.M., Tatarski V.I. (1967). Atmospheric turbulence and radio wave propagation. *Journal of Computational Chemistry,* 23, 1236-1243

Lund H., Moller B., Mathiesen B.V., Dyrelund A, The role of district heating in future renewable energy systems. Energy 2010; 35: 1381–1390.

Marcotte, D., Pasquier, P., Sheriff, F., & Bernier, M. (2010). The importance of axial effects for borehole design of geothermal heat-pump systems. *Renewable Energy*, *35*(4), 763-770.

McKeown, C., Haszeldine, R. S., & Couples, G. D. (1999). Mathematical modelling of groundwater flow at Sellafield, UK. *Engineering Geology*, *52*(3), 231-250.

Mell, W., Jenkins, M. A., Gould, J., & Cheney, P. (2007). A physics-based approach to modelling grassland fires. *International Journal of Wildland Fire*,*16*(1), 1-22.

Miller, A. S., & Blott, B. H. (1992). Review of neural network applications in medical imaging and signal processing. *Medical and Biological Engineering and Computing*, *30*(5), 449-464.

Molina-Giraldo, N., Bayer, P., & Blum, P. (2011). Evaluating the influence of thermal dispersion on temperature plumes from geothermal systems using analytical solutions. *International Journal of Thermal Sciences*, *50*(7), 1223-1231.

Morvan D. (2011) Physical Phenomena and Length Scales Governing the Behaviour of Wildfires: A Case for Physical Modelling. *Fire Technology*, 47, 437–460

Morvan D., Dupuy J.L. (2004) Modeling the propagation of a wildfire through a Mediterranean shrub using a multiphase formulation. *Combustion and flame,* 138, 199-210

Morvan D., Méradji S., Accary G. (2009) Physical modelling of fire spread in grasslands. *Fire Safety Journal*, 44, 50-61

Nam, Y., & Ooka, R. (2010). Numerical simulation of ground heat and water transfer for groundwater heat pump system based on real-scale experiment. *Energy and Buildings*, *42*(1), 69-75.

Narain, R., Golas, A., Curtis, S., & Lin, M. C. (2009, December). Aggregate dynamics for dense crowd simulation. In *ACM Transactions on Graphics (TOG)*(Vol. 28, No. 5, p. 122). ACM.

Ni, L., Li, H., Jiang, Y., Yao, Y., & Ma, Z. (2011). A model of groundwater seepage and heat transfer for single-well ground source heat pump systems. *Applied Thermal Engineering*, *31*(14), 2622-2630.

Østergaard, P. A., Mathiesen, B. V., Möller, B., & Lund, H. (2010). A renewable energy scenario for Aalborg Municipality based on low-temperature geothermal heat, wind power and biomass. *Energy*, *35*(12), 4892-4901.

Ostrowski, Z., Bialecki, R. A., & Kassab, A. J. (2005). Advances in application of proper orthogonal decomposition in inverse problems. In *Proc. 5th Int. Conf. on Inverse Problems in Engineering: Theory and Practice, Cambridge, UK*.

Pálsson, H. (2000). *Methods for planning and operating decentralized combined heat and power plants*. Risø & DTU-Department of Energy Engineering (ET).

Pandey, H. M., Chaudhary, A., & Mehrotra, D. (2014). A comparative review of approaches to prevent premature convergence in GA. *Applied Soft Computing*, 24, 1047-1077.

Patankar SV. Numerical Heat Transfer and Fluid Flow; 1980.

Pearson, Karl. (1901) On lines and planes of closest fit to systems of points in space. *The London, Edinburgh, and Dublin Philosophical Magazine and Journal of Science,* 2, 559-572

Peric, M., & Ferziger, J. H. (1996). Computational methods for fluid dynamics.

Pirouti, M., Bagdanavicius, A., Wu, J., & Ekanayake, J. (2012). Optimisation of supply temperature and mass flow rate for a district heating network.*Proceedings of ECOS*, 26-29.

Piters, A. J. M., Boersma, K. F., Kroon, M., Hains, J. C., Van Roozendael, M., Wittrock, F., & Apituley, A. (2012). The Cabauw Intercomparison campaign for Nitrogen Dioxide measuring Instruments (CINDI): design, execution, and early results.

Pollandt, R. (1997). Solving nonlinear differential equations of mechanics with the boundary element method and radial basis functions. *International journal for numerical methods in engineering*, 40(1), 61-73.

Prato A. P., Strobino F., Broccardo M., & Giusino, L. P. (2012). Integrated management of cogeneration plants and district heating networks. *Applied Energy*, 97, 590-600.

Pyta, L., Hakenberg, M., & Abel, D. (2014, August). Model Reduction and Control of a Compressible Channel Flow with Combustion⋆. In *World Congress*(Vol. 19, No. 1, pp. 7001-7006).

Quarteroni, A., & Veneziani, A. (2003). Analysis of a geometrical multiscale model based on the coupling of ODE and PDE for blood flow simulations. *Multiscale Modeling & Simulation*, *1*(2), 173-195.

Quarteroni, A., Ragni, S., & Veneziani, A. (2001). Coupling between lumped and distributed models for blood flow problems. *Computing and Visualization in Science*, *4*(2), 111-124.

Quarteroni, A., Valli, A. (1999), "Domain Decomposition Methods for Partial Differential Equations", Oxford Science Publications, Oxford.

Rambo J, Joshi Y (2005). Reduced Order Modeling of Steady Turbulent Convection Flows Using the POD. *Proceedings of the ASME 2005 Summer Heat Transfer Conference*, 837-846

Romo, T. D., Clarage, J. B., Sorensen, D. C., & Phillips, G. N. (1995). Automatic identification of discrete substates in proteins: Singular value decomposition analysis of time-averaged crystallographic refinements.*Proteins: Structure, Function, and Bioinformatics*, *22*(4), 311-321.

Roos, A., Bohlin, F., Hektor, B., & Hillring, B. (2003). Woodfuel procurement strategies of district heating plants. *Energy*, *28*(2), 127-140.

Rosenfeld A, Kak AC (2014). Digital picture processing (Vol. 1). Elsevier

Rothermel, R. C. (1972). A mathematical model for predicting fire spread in wildland fuels.

Russo, S. L., Taddia, G., Baccino, G., & Verda, V. (2011). Different design scenarios related to an open loop groundwater heat pump in a large building: Impact on subsurface and primary energy consumption. *Energy and Buildings*,*43*(2), 347-357.

Samozino, M., Alexa, M., Alliez, P., & Yvinec, M. (2006). Reconstruction with Voronoi centered radial basis functions.

Schadschneider, A., Klingsch, W., Klüpfel, H., Kretz, T., Rogsch, C., & Seyfried, A. (2009). Evacuation dynamics: Empirical results, modeling and applications. In *Encyclopedia of complexity and systems science* (pp. 3142-3176). Springer New York.

Schilders, W. (2008). Introduction to model order reduction. In *Model order reduction: Theory, research aspects and applications* (pp. 3-32). Springer Berlin Heidelberg.

Sciacovelli A, Verda V, Borchiellini R, Numerical Design of Thermal Systems. Clut, Torino; 2013.

Sciacovelli, A., Guelpa, E., & Verda, V. (2013, November). Pumping Cost Minimization in an Existing District Heating Network. In *ASME 2013 International Mechanical Engineering Congress and Exposition* (pp. V06AT07A066-V06AT07A066). American Society of Mechanical Engineers.

Sciacovelli, A., Guelpa, E., & Verda, V. (2014). Multi-scale modeling of the environmental impact and energy performance of open-loop groundwater heat pumps in urban areas. Applied Thermal Engineering, 71(2), 780-789. doi:10.1016/j.energy.2016.02.058

Seaman, N. L. (2000). Meteorological modeling for air-quality assessments.*Atmospheric environment*, *34*(12), 2231-2259.

Shahin, M. A., Jaksa, M. B., & Maier, H. R. (2001). Artificial neural network applications in geotechnical engineering. *Australian Geomechanics*, *36*(1), 49-62.

Shvartsman S.Y., Theodoropoulos C., Rico-Martınez R., Kevrekidis I.G., Titi E.S.., Mountziaris T.J. (2000) Order reduction for nonlinear dynamic models of distributed reacting systems. *Journal of Process Control,* 10, 177-184

Simeoni A., Santoni P.A., Larini M., Balbi J.H. (2001) On the wind advection influence on the fire spread across a fuel bed: modelling by a semi-physical approach and testing with experiments. *Fire safety journal,* 36, 491-513

Sirovich L. Turbulence and the dynamics of coherent structures, Parts I, II and III, Q. Appl. Maths XLV, 1987; 561-590.

Srinivas M., Patnaik L.M. (1994). Adaptive probabilities of crossover and mutation in genetic algorithms. *IEEE Transactions on Systems, Man and Cybernetic,s* 24, 656-667.

Stevanovic, V. D., Zivkovic, B., Prica, S., Maslovaric, B., Karamarkovic, V., & Trkulja, V. (2009). Prediction of thermal transients in district heating systems.*Energy Conversion and Management*, *50*(9), 2167-2173.

Stevanovic, V. D., Prica, S., Maslovaric, B., Zivkovic, B., & Nikodijevic, S. (2007). Efficient numerical method for district heating system hydraulics.*Energy Conversion and Management*, *48*(5), 1536-1543.

Sullivan AL (2009a) Wildland surface fire spread modelling, 1990–2007.1 Physical and quasi-physical models. International Journal of Wildland Fire 18, 349–368

Sullivan AL (2009b) Wildland surface fire spread modelling, 1990–2007. 2: Empirical and quasi-empirical models. International Journal of Wildland Fire18, 369-386

Sullivan AL (2009c) Wildland surface fire spread modelling, 1990–2007. 3: Simulation and mathematical analogue models. International Journal of Wildland Fire 18, 387-403

Tachajapong W., Lozano J., Mahalingam S., Zhou X., Weise D.R (2008). An Investigation of Crown Fuel Bulk Density Effects on the Dynamics of Crown Fire Initiation in Shrublands. *Combustion science and technology*, 180, 593-615.

Tol H.I., Svendsen S. (2012) Improving the dimensioning of piping networks and network layoutsin low-energy district heating systems connected to low-energy buildings: A case study in Roskilde, Denmark. *Energy*, 38: 276-290

Tripodi C. Evolution of the Turin District Heating System and the Design of North-West District Network. Energethica. 24-26 May 2012, Turin, Italy (In Italian). http://www.fiper.it/fileadmin/user_upload/news/energethica2012/tripodi.pdf

U.S. Department of Energy, Energyplus Energy Simulation Software, Energy Efficiency and Renewable Energies, 2008. http://apps1.eere.energy.gov/buildings/energyplus.

Ullmann S, Lang J (2010). A POD-Galerkin reduced model with updated coefficients for Smagorinsky LES. In V European conference on computational fluid dynamics, ECCOMAS CFD.

USDA (2015). US Forest servicehttp://www.fs.fed.us/pnw/fera/fccs/inferred_variables/table2_metric/table2_metric.htm . Accessed on May 2015

Verda V, Baccino G. Primary energy reductions in District Heating Networks through variation of the thermal load profile of the users. Proceedings of ECOS 2014. Turku, Finland, June 15-19.

Verda V., Ciano C. (2005). Procedures for the Search of the Optimal Configuration of District Heating Networks. *Int. J. of Thermodynamics* 8: 143-153

Verda, V., & Colella, F. (2011). Primary energy savings through thermal storage in district heating networks. *Energy*, 36(7), 4278-4286.

Verlaan, M. (1998). *Efficient Kalman filtering algorithms for hydrodynamic models* (Doctoral dissertation, PhD thesis, Delft University of Technology).

Wang H, Yin W, Zhou Z, Lahdelma R. Optimizing the design of a district heating network. Proceedings of ECOS 2015, Pau, France June 30-July 3.

Wang, Y., Yu, B., Cao, Z., Zou, W., & Yu, G. (2012). A comparative study of POD interpolation and POD projection methods for fast and accurate prediction of heat transfer problems. *International Journal of Heat and Mass Transfer*,*55*(17), 4827-4836.

Wendt K., Cortes A., Margalef T. (2013) Parameter calibration framework for environmental emergency models. *Simulation Modelling Practice and Theory*, 31, 10–21

Wong, B.K., Bodnovich, T.A., & Selvi, Y. (1997). Neural network applications in business: A review and analysis of the literature (1988–1995). *Decision Support Systems*, *19*(4), 301-320.

Yuan T., Cizmas P.G., O'Brien T.O. (2005). A reduced-order model for a bubbling fluidized bed based on proper orthogonal decomposition. *Computers and Chemical Engineering*, 30, 243–259.

Zhou, Y. Z., & Zhou, Z. F. (2009). Simulation of thermal transport in aquifer: a GWHP system in Chengdu, China. *Journal of Hydrodynamics, Ser. B*, *21*(5), 647-657.